

1 Scenario set-up and the new CMIP6-based climate-related forcings provided within the  
2 third round of the Inter-Sectoral Model Intercomparison Project (ISIMIP3b, group I and II)

3  
4 Katja Frieler<sup>1,2</sup>, Stefan Lange<sup>1</sup>, Jacob Schewe<sup>1</sup>, Matthias Mengel<sup>1</sup>, Simon Treu<sup>1,2</sup>, Christian Otto<sup>1</sup>, Jan  
5 Volkholz<sup>1</sup>, Christopher P.O. Reyer<sup>1</sup>, Stefanie Heinicke<sup>1</sup>, Colin Jones<sup>3</sup>, Julia L. Blanchard<sup>4</sup>, Cheryl S. Harrison<sup>5</sup>,  
6 Colleen M. Petrik<sup>6</sup>, Tyler D. Eddy<sup>7</sup>, Kelly Ortega-Cisneros<sup>8</sup>, Camilla Novaglio<sup>4</sup>, Ryan Heneghan<sup>9</sup>, Derek P.  
7 Tittensor<sup>10</sup>, Olivier Maury<sup>11</sup>, Matthias Büchner<sup>1</sup>, Thomas Vogt<sup>1</sup>, Dánnell Quesada-Chacón<sup>1</sup>, Kerry  
8 Emanuel<sup>12</sup>, Chia-Ying Lee<sup>13</sup>, Suzana J. Camargo<sup>13,14</sup>, Linn Hamester<sup>1</sup>, Jonas Jägermeyr<sup>14,15,1</sup>, Sam Rabin<sup>16,a,b</sup>,  
9 Jochen Klar<sup>1</sup>, Iliusi D. Vega del Valle<sup>1</sup>, Lisa Novak<sup>1</sup>, Inga J. Sauer<sup>1</sup>, Gitta Lasslop<sup>17</sup>, Sarah Chadburn<sup>18</sup>, Eleanor  
10 Burke<sup>19</sup>, Angela Gallego-Sala<sup>20</sup>, Noah Smith<sup>21</sup>, Jinfeng Chang<sup>22</sup>, Stijn Hantson<sup>23</sup>, Chantelle Burton<sup>19</sup>, Anne  
11 Gädeke<sup>1</sup>, Fang Li<sup>24</sup>, Simon N Gosling<sup>25</sup>, Hannes Müller Schmied<sup>17,26</sup>, Fred Hattermann<sup>1</sup>, Thomas Hickler<sup>17</sup>,  
12 Rafael Marcé<sup>27</sup>, Don Pierson<sup>28</sup>, Wim Thiery<sup>29</sup>, Daniel Mercado-Bettín<sup>27</sup>, Robert Ladwig<sup>30</sup>, Ana I. Ayala<sup>28</sup>,  
13 Matthew Forrest<sup>17</sup>, Michel Bechtold<sup>31</sup>, Robert Reinecke<sup>32</sup>, Inge de Graaf<sup>33</sup>, Jed O. Kaplan<sup>34</sup>, Alexander  
14 Koch<sup>35</sup>, Matthieu Lengaigne<sup>11</sup>, Rohini Kumar<sup>36</sup>, Maryna Strokhal<sup>37</sup>

15  
16  
17 Affiliations:

18 <sup>1</sup>Potsdam Institute for Climate Impact Research, 14473 Potsdam, Germany

19 <sup>2</sup>University of Potsdam, Institute for Environmental Science and Geography, 14476 Potsdam, Germany

20 <sup>3</sup>National Centre for Atmospheric Science and School of Earth and Environment, University of Leeds,  
21 Leeds, LS29JT, UK

22 <sup>4</sup>Institute for Marine and Antarctic Studies, University of Tasmania, Hobart, Tasmania, Australia

23 <sup>5</sup>Department of Ocean and Coastal Science and Center for Computation and Technology, Louisiana State  
24 University, Baton Rouge, Louisiana, USA

25 <sup>6</sup>Scripps Institution of Oceanography, University of California San Diego, CA, USA

26 <sup>7</sup>Centre for Fisheries Ecosystems Research, Fisheries & Marine Institute, Memorial University, St. John's,  
27 NL, Canada

28 <sup>8</sup>Marine and Antarctic Research for Innovation and Sustainability, Department of Biological Sciences,  
29 University of Cape Town, Rondebosch, Cape Town, 7701, South Africa

30 <sup>9</sup>School of Environment and Science, Griffith University, Brisbane, Queensland, Australia

31 <sup>10</sup>Department of Biology, Dalhousie University, Halifax, Nova Scotia, Canada, B3H 4R2

32 <sup>11</sup>IRD, Univ Montpellier, CNRS, Ifremer, INRAE, MARBEC, Sète, France

33 <sup>12</sup>Lorenz Center, Massachusetts Institute of Technology, Cambridge, MA, USA

34 <sup>13</sup>Lamont-Doherty Earth Observatory, Columbia University, Palisades, New York, USA

35 <sup>14</sup>Columbia Climate School, Columbia University, New York, NY 10025, USA

36 <sup>15</sup>NASA Goddard Institute for Space Studies, New York, NY 10025, USA

37 <sup>16</sup>Climate and Global Dynamics Laboratory, National Center for Atmospheric Research Boulder, CO 80302,  
38 USA

39 <sup>17</sup>Senckenberg Leibniz Biodiversity and Climate Research Centre (SBIK-F), Frankfurt am Main, Germany.

40 <sup>18</sup>Department of Mathematics, University of Exeter, Exeter UK

41 <sup>19</sup>Met Office Hadley Centre, Fitzroy Road, Exeter, UK

- 42 <sup>20</sup>Geography Department, University of Exeter, Exeter, UK
- 43 <sup>21</sup>College of Engineering, Mathematics and Physical Sciences, University of Exeter, Exeter EX4 4QF, UK.
- 44 <sup>22</sup>College of Environmental and Resource Sciences, Zhejiang University, Hangzhou, China
- 45 <sup>23</sup>Faculty of Natural Sciences, Universidad del Rosario, Bogotá, Colombia
- 46 <sup>24</sup>International Center for Climate and Environment Sciences, Institute of Atmospheric Physics, Chinese  
47 Academy of Sciences, Beijing, China
- 48 <sup>25</sup>School of Geography, University of Nottingham, Nottingham, UK
- 49 <sup>26</sup>Institute of Physical Geography, Goethe University Frankfurt, Frankfurt am Main, Germany
- 50 <sup>27</sup>Blanes Centre for Advanced Studies (CEAB-CSIC), Blanes, Spain
- 51 <sup>28</sup>Department of Ecology and Genetics, Uppsala University, Norbyvägen 18 D, 752 36 Uppsala, Sweden
- 52 <sup>29</sup>Vrije Universiteit Brussel, Department of Water and Climate, Brussels, Belgium
- 53 <sup>30</sup>Department of Ecoscience, Aarhus University, C.F. Møllers Allé 3, 8000 Aarhus C, Denmark
- 54 <sup>31</sup>KU Leuven, Department of Earth and Environmental Sciences, Leuven, Belgium
- 55 <sup>32</sup>Johannes Gutenberg-University Mainz, Mainz, Germany
- 56 <sup>33</sup>Earth Systems and Global Change Group, Wageningen University and Research, Wageningen, The  
57 Netherlands
- 58 <sup>34</sup>Department of Earth Sciences and Institute for Climate and Carbon Neutrality, The University of Hong  
59 Kong, Hong Kong
- 60 <sup>35</sup>Simon Fraser University, Burnaby, British Columbia, CA
- 61 <sup>36</sup>Department of Computational Hydrosystems, Helmholtz Centre for Environmental Research—UFZ,  
62 Leipzig 04318, Germany
- 63 <sup>37</sup>Wageningen University & Research, Wageningen, Netherlands
- 64 <sup>a</sup>formerly at: Institute of Meteorology and Climate Research / Atmospheric Environmental Research,  
65 Karlsruhe Institute of Technology, Garmisch-Partenkirchen, Germany
- 66 <sup>b</sup>formerly at: Department of Environmental Sciences, Rutgers University, New Brunswick, New Jersey, USA
- 67
- 68 *Correspondence to:* Katja Frieler ([katja.frieler@pik-potsdam.de](mailto:katja.frieler@pik-potsdam.de))
- 69

70 **Abstract.** This paper describes the climate-related forcings (CRFs) provided within the ‘b’ part of the third  
71 simulation round of the Inter-Sectoral Impact Model Intercomparison Project (ISIMIP3b). While ISIMIP3a  
72 comprises historical impact models simulations forced by observational CRF and direct human forcings  
73 (DHF), the ISIMIP3b CRFs are based on climate model simulations generated within the sixth phase of the  
74 Coupled Model Intercomparison Project (CMIP6). In a first set of experiments (ISIMIP3b, group I) the  
75 CMIP6-based CRFs for the historical period are combined with historical observation-based DHF also  
76 considered in ISIMIP3a (e.g. land use patterns, water and agricultural management, and fishing efforts).  
77 These group I simulations allow for the quantification of impacts of historical climate change by  
78 comparison to simulations where the observational DHF are combined with simulated pre-industrial CRFs.  
79 In addition, the impacts of observed changes in CRFs can be compared to the impacts of simulated  
80 changes in CRFs by comparing the ISIMIP3a simulations to the ISIMIP3b, group I simulations. The second  
81 group of experiments (ISIMIP3b, group II) comprises future projections assuming constant observational  
82 direct human forcings at 2015 levels to estimate the impact of climate change given today’s direct human

83 influences for the low emission scenario SSP1-2.6, the high and the very high emission scenarios SSP3-7.0,  
84 SSP5-8.5, respectively. The very high emissions scenarios and the assumption of fixed present day direct  
85 human forcings particularly allow for testing the scalability of impacts in terms of global temperature  
86 change. The provided CRFs comprise atmospheric CO<sub>2</sub> and CH<sub>4</sub> concentrations, atmospheric and oceanic  
87 climate data, coastal water levels, tropical cyclone tracks and their associated wind speed and  
88 precipitation fields. In addition to the CRFs data, this paper describes the experiments belonging to group  
89 I and II and the rationale behind them. Another set of future projections accounting for changing DHFs  
90 (ISIMIP3b, group III) is in preparation and will be described in another paper.

91  
92

### 93 **Introduction**

94 This is the second paper of a series of three papers describing the experiments of the third simulation  
95 round of the Inter-Sectoral Impact Model Intercomparison Project ISIMIP (isimip.org). The project  
96 provides a common scenario framework for cross-sectorally consistent climate impact simulations.  
97 **Currently, operational simulation protocols exist for the following sectors: Agriculture, Biomes, Energy,**  
98 **Fire, Food security and nutrition, Groundwater, Labour, Lakes global, Lakes regional, Fisheries and marine**  
99 **ecosystems global, Fisheries and marine ecosystems local, Peatland, Permafrost, Water global, Water**  
100 **regional. Additional protocols for Coastal systems, Regional forests, Temperature-related mortality,**  
101 **health indicators, Terrestrial biodiversity and Water quality sectors are under development.** In its third  
102 round it covers i) model evaluation and climate impact attribution experiments based on observation-  
103 based climate and direct human forcings (DHF) (ISIMIP3a, first paper, (Frieler et al., 2023)), ii) climate  
104 impact simulations driven by simulated climate-related forcings (CRF) based the sixth phase of the  
105 Coupled Climate Model Intercomparison Project (CMIP6) assuming ISIMIP3a observational DHF in the  
106 historical period and fixed 2015 DHF for the future simulations (ISIMIP3b, group I+II, this paper), and iii)  
107 an upcoming set of CMIP6-based future projections where DHF vary according to given Shared  
108 Socioeconomic Pathways (SSPs) (no adaptation scenarios) and in response to climate change impacts  
109 (adaptation scenarios) (ISIMIP3b, group III). So while this paper only describes the ISIMIP3b CRF, the third  
110 paper will only address the DHFs that are still under development while the CRF of the group III simulations  
111 will be identical to the future CRF described here.

112

113 Similar to the Coupled Model Intercomparison Project (CMIP) (Eyring et al., 2016) all simulations will be  
114 freely available (<https://data.isimip.org/>) to allow for follow-up analysis. The consistent design of the  
115 simulations does not only allow for the comparison of climate impact simulations within each sector, but  
116 also enables the bottom-up integration of impacts across sectors. Thus, it provides a unique basis for the  
117 estimation of the effects of climate change on, e.g., the economy, displacement and migration, health, or  
118 water quality resolving the mechanisms along different impact channels and fully exploiting the process-  
119 understanding represented in the biophysical impact models.

120

121 Compared to ISIMIP2b, the ISIMIP3b CRF represent the following updates: i) climate forcing data based  
122 on phase 6 of the Coupled Model Intercomparison Project (CMIP6) (Eyring et al., 2016) and post-processed  
123 by an improved bias adjustment and statistical downscaling method (see section 3.2), and ii) large

124 ensembles of potential realisations of tropical cyclone tracks, wind and precipitation fields derived from  
125 two different modelling approaches assuming CMIP6 boundary conditions, while in ISIMIP2b only one  
126 approach was used and precipitation fields were not included. In addition, we plan to provide coastal  
127 water levels at high temporal resolution (upcoming). The approach to generate the data is also described  
128 here.

129  
130 The development of the ISIMIP3b protocol was coordinated by the ISIMIP-Cross-Sectoral Science Team  
131 (CSST) at the Potsdam Institute for Climate Impact Research (PIK) along the same decision process as for  
132 ISIMIP3a (Frieler et al., 2024a).

133  
134 This paper is accompanied by a simulation protocol (*ISIMIP3b Simulation Protocol*, 2023) providing all  
135 technical details such as file and variable naming conventions, as well as sector-specific output variables  
136 to be reported by the participating modelling teams. This paper refers to the protocol version of December  
137 21st, 2023. However, as the protocol may still be updated due to addition of new variables, correction of  
138 errors, or the inclusion of new sectors, contributors to ISIMIP should always refer to [protocol.isimip.org](http://protocol.isimip.org)  
139 for the most up to date reference for planned impact model simulations.

140  
141 The ISMIP3a and ISIMIP3b protocols have been jointly developed and participation in ISIMIP3 requires  
142 contribution to both ISIMIP3a and ISIMIP3b, using the same impact model versions in order to allow for  
143 the evaluation of the impact models future projections in ISIMIP3b.

144  
145 In the following, we describe the rationale behind the individual scenario set-ups (section 1). We then  
146 introduce the individual climate-related forcing data sets in the second section covering atmospheric  
147 climate data including lightning and tropical cyclones tracks, wind and precipitation fields; ocean data;  
148 coastal water levels; and atmospheric CO<sub>2</sub> as well as CH<sub>4</sub> concentrations.

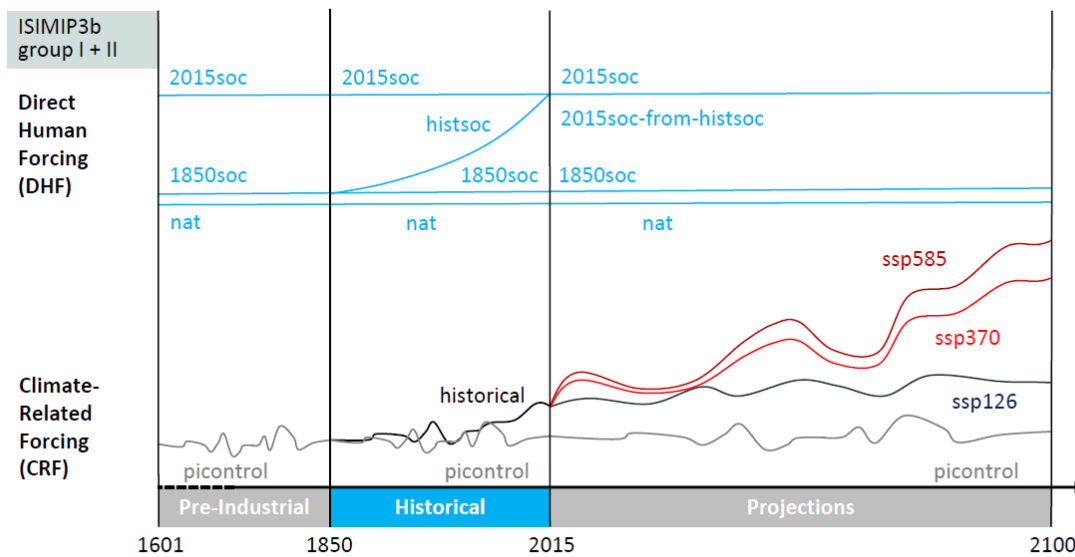
## 150 **1 Experiments and underlying rationale**

151  
152 The selection of the scenarios is a community-driven process constrained by the availability of climate  
153 model simulations (multi-GCM ensemble per scenario) and socio-economic background information (such  
154 as land use patterns, populations and GDP data etc. additionally required as 'Direct Human Forcing' for  
155 the ISIMIP3b, group III impact model simulations that will be introduced in an upcoming paper). These  
156 criteria have made CMIP6-ScenarioMIP the reference point for the selection (O'Neill et al., 2016). The  
157 selection of ISIMIP3b scenarios (see **Figure 1**) from the four ScenarioMIP Tier 1 scenarios was additionally  
158 driven by the aim to capture a wide range of possible futures from low to high emission scenarios and to  
159 provide of a long baseline simulation assuming pre-industrial climate conditions that allows for a robust  
160 estimation of reference return levels of extreme events. This is why the original selection comprised the  
161 pre-industrial baseline ('picontrol'), the historical simulations ('historical'), SSP1-2.6 representing the 'low  
162 end of the range of future forcing pathways in the IAM literature' (O'Neill et al., 2016), and SSP5-8.5  
163 representing the 'high end of the range of future pathways in the IAM literature' (O'Neill et al., 2016).  
164 Given recent mitigation efforts, some estimates of recoverable coal reserves, and decreasing prices for

165 renewable energies the emissions underlying SSP5-8.5 have been criticised for being unplausibly high  
166 (Hausfather & Peters, 2020). Based on these discussions, the ‘medium to high end of the range of future  
167 forcing pathway’ SSP3-7.0 (O’Neill et al., 2016) has been added to the ISIMIP3b scenario set-up. While this  
168 scenario is described as ‘average no climate protection policy’ by (Hausfather & Peters, 2020), we highlight  
169 that we explicitly not describe it as a ‘business as usual scenario’ and that this was not the framing within  
170 ScenarioMIP either. Instead SSP3-7.0 is based on rather extreme assumptions about land use changes and  
171 aerosol emissions e.g. leading to a scaling of precipitation with global mean temperature that diverges  
172 from the scaling identified in the other scenarios (Shiogama et al., 2023). In addition, SSP5-8.5 is explicitly  
173 kept in the ISIMIP3b ensemble as its particularly strong warming signal allows testing to what degree the  
174 simulated impacts of climate may scale with global mean temperature, which could allow for a translation  
175 of impacts to other emission scenarios. In addition, even under lower emission scenarios, global warming  
176 levels as the ones reached under SSP5-8.5 in 2100 will eventually be reached later in time as long as  
177 emissions are not reduced to zero. These impacts of high warming levels would not be captured when  
178 only considering lower emission scenarios ending in 2100.

179  
180 All ISIMIP experiments are determined by the underlying set of CRFs and DHF, where each package of CRF  
181 and DHF has a specific label that will then be included in the output file names to allow for an identification  
182 of the experiments they belong to. The individual experiments are defined by the combination of both  
183 types of forcing data sets, where the associated specifiers are indicated in brackets in the subheadings  
184 naming the experiments (CRF specifier + DHF specifier). The different combinations of the default sets of  
185 ISIMIP3b CRFs (‘picontrol’, ‘historical’, ‘ssp126’, ‘ssp370’, and ‘ssp585’) and DHF (‘histsoc’, ‘2015soc’,  
186 ‘1901soc’, ‘1850soc’, ‘nat’, and ‘2015soc-from-histsoc’) are sketched in **Figure 1** and described in more  
187 detail below.

188  
189 The CRF data described in this paper are mandatory; i.e. if impact models consider this forcing, the  
190 specified dataset must be used; if an alternative input data set is used instead, the run cannot be  
191 considered an ISIMIP3b, group I + II simulation. The DHF for the historical period is identical to the  
192 ISIMIP3a DHF listed in **Table 1** of (Frieler et al., 2024a) where we also indicate whether the data set is  
193 mandatory or optional. Optional forcing data could be used but is not mandatory. In addition, the protocol  
194 includes a set of sensitivity experiments that are described as deviations from the default runs and labelled  
195 by the baseline CRF and DHF settings and a third specifier indicating the deviation from this default setting.  
196 The ISIMIP3b group I+II sensitivity runs include experiments with fixed levels of atmospheric CO<sub>2</sub>  
197 concentrations (‘2015co2’), high levels in CO<sub>2</sub> concentrations in combination with low levels of climate  
198 change (‘ssp585co2’), and runs with lightning data that vary in response to climate change (‘varlightning’),  
199 while lightning is fixed at present day levels in the default runs. These sensitivity experiment runs are not  
200 depicted in **Figure 1** but listed in **Table 2**.



203  
204  
205  
206  
207  
208  
209

**Figure 1:** Illustration of the default ISIMIP3b forcing data sets. Each ISIMIP3b experiment is defined by a combination of a CRF data set with a DHF data set. The considered combinations are listed in **Table 2** and the underlying rationale is described in section **1.1** and **1.2**. **Table 1** lists all data sets defining the considered CRFs while the DHFs are based on the same datasets as in ISIMIP3a. Potentially required spin-up procedures are not included in the Figure, but described in section **1.1**.

The ISMIP3b simulations are divided into two groups. Group I comprises the simulations from 1601 - 1849 (pre-industrial) and 1850 - 2014 (historical) assuming simulated pre-industrial and historical CRFs and different constant ('nat', '1850soc', and '2015soc') or varying ('histsoc') levels of DHF based on the same observational data used in ISIMIP3a (see **Figure 1**). Group II comprises the future projections assuming constant 2015 levels of DHF (see **Figure 1**) including a baseline with pre-industrial CRF (grey line in the future projections part of **Figure 1**). All experiments are introduced in more detail below (section **1.1** for group I and **1.2** for group II).

In contrast to ISIMIP3a, the CRFs provided for ISIMIP3b currently only comprise atmospheric (see section **2.1**) and oceanic climate data (see section **2.4**), tropical cyclone tracks with associated wind and precipitation fields (see section **2.2**), and CO<sub>2</sub> and methane concentration (see section **2.5**). We do not yet provide associated coastal water levels (see section **2.2.3** for planned work), and lightning data (see [Table 511](#)). Impact simulations that rely on the missing forcings cannot be generated within ISIMIP3b yet, but we are currently developing their setup and will provide the forcings as soon as possible. The ISIMIP3b atmospheric and oceanic climate data is derived from five different General Circulation Models (GCMs) generated within the Coupled Model Intercomparison project, phase 6 (CMIP6).

**Table 1: Climate-Related Forcing datasets for ISIMIP3b.**

Forcing	Status	Source, description
---------	--------	---------------------

Climate-related forcings ('picontrol', 'historical', 'ssp126', 'ssp370', 'ssp585')		
Atmospheric forcings ('picontrol', 'historical', 'ssp585', 'ssp370', 'ssp126')		
Gridded atmospheric climate forcing	mandatory	Bias-adjusted data (pre-industrial climate, historical climate, and future projections for the SSP1-2.6, SSP3-7.0, and SSP5-8.5 scenarios) generated by GFDL-ESM4, IPSL-CM6A-LR, MPI-ESM1-2-HR, MRI-ESM2-0, and UKESM1-0-LL within CMIP6 (Lange & Büchner, 2021), see section 2.1
Local atmospheric climate forcing for lakes	mandatory	Atmospheric data extracted from the data sets above for 72 lakes that have been identified within the lake sector as locations (grid cell of the ISIMIP 0.5° grid, <a href="#">ISIMIP3 local lake sites</a> ) where models can be calibrated based on observed temperature profiles and hypsometry within ISIMIP3b (depth and area) (Lange and Büchner 2021)
Tropical cyclone tracks with wind and precipitation fields	mandatory	<p><del>Available on request (see section 2.2)</del>, samples of synthetic tropical cyclone tracks derived from the five CMIP6 GCMs considered within ISIMIP generated by two different statistical downscaling approaches, see section 2.2.</p> <p>MIT approach (Emanuel et al., 2008, 2025):</p> <ul style="list-style-type: none"> <li>• <a href="#">pre-industrial climate from IPSL-CM6A-LR, MPI-ESM1-2-HR and MRI-ESM2-0 (all 1850-2014), and from UKESM1-0-LL (1950-2100)</a></li> <li>• historical climate from IPSL-CM6A-LR, MPI-ESM1-2-HR, UKESM1-0-LL and GFDL-ESM4 (all 1850-2014), and from MRI-ESM2-0 (1950-2014).</li> <li>• Future climate: <a href="#">ssp126 (2061-2100)</a>, <a href="#">ssp370 (2015-2100)</a> and <a href="#">ssp585 (2015-2100)</a> from IPSL-CM6A-LR, MPI-ESM1-2-HR, MRI-ESM2-0, UKESM1-0-LL, and <a href="#">ssp585 (2061-2100)</a> from GFDL-ESM4.</li> </ul> <p>Two different configurations (SD and CRH, see section 2.2) of the Columbia HAZard model (CHAZ, Lee et al., 2018, 2025):</p> <ul style="list-style-type: none"> <li>• <del>pre-industrial climate (1601-2100) from GFDL-ESM4, IPSL-CM6A-LR, MPI-ESM1-2-HR, MRI-ESM2-0, and UKESM1-0-LL.</del></li> <li>• historical climate (1850-2014) from GFDL-ESM4, IPSL-CM6A-LR, MPI-ESM1-2-HR, MRI-ESM2-0, and UKESM1-0-LL</li> <li>• future climate (2015-2100): <a href="#">ssp126</a>, <a href="#">ssp370</a>, <a href="#">ssp585</a> from GFDL-ESM4, IPSL-CM6A-LR, MPI-ESM1-2-HR, MRI-ESM2-0, and UKESM1-0-L</li> </ul>

		For tracks generated by the MIT approach, we also provide wind and precipitation fields (Quesada-Chacón et al., 2025)
Lightning	mandatory	Flash Rate Monthly Climatology <del>from (Cecil, 2006)</del> , not changing with climate change (Cecil, 2006)
Oceanic forcings ('picontrol', 'historical', 'ssp585', 'ssp370', 'ssp126')		
Oceanic climate forcing	mandatory	Uncorrected data (pre-industrial climate, historical climate, and future projections for the SSP1-2.6, SSP3-7.0, and SSP5-8.5 scenarios) generated by GFDL-ESM4, IPSL-CM6A-LR, MPI-ESM1-2-HR, and UKESM1-0-LL within CMIP6 (Büchner 2024), see section 2.4
Coastal water levels		
Coastal water levels	mandatory	In section 2.3 we describe a method to generate relative sea level projections that smoothly extend tide gauge observations into the future building on a Bayesian model (Perrette & Mengel, 2025). For ISIMIP3, we plan to extend the framework to all coastlines and directly use ISIMIP GCM output for the global thermodynamic and local stereodynamic components, adjusting the gridded simulations to associated observations to ensure a consistent transition from the historical period. Ice sheet and glacier contributions are incorporated through spatial fingerprints, while unresolved vertical land motion processes are estimated from residuals at tide gauges and extrapolated where no observations are available. We are also developing an approach to extend the sea level projections to daily maximum water levels derived from the ISIMIP3 atmospheric forcings (daily mean Surface Air Pressure and daily mean Near-Surface Wind Speed).
Atmospheric composition or fluxes		
Atmospheric CO <sub>2</sub> concentration	mandatory	(Büchner & Reyer, 2022) based on the following sources: 1850-2005: (Meinshausen et al., 2011); 2006-2014: Global annual CO <sub>2</sub> from NOAA Global Monthly Mean CO <sub>2</sub> (Lan et al., 2023); 2015-2100: (Meinshausen et al., 2020)
Atmospheric CH <sub>4</sub> concentration	mandatory	(Büchner & Reyer, 2022) based on the following sources: 1850-2014:(Meinshausen et al., 2017); 2015-2100: (Meinshausen et al., 2020)
Climate-Related Forcings for the sensitivity experiment 'varlightning', using above forcing data except for:		

Lightning data ('varlightning')		
Varying lightning according to climate change	mandatory	Lightning data has been generated for the ssp126, ssp370, and ssp850 climate projections from UKESM1-0-LL (Kaplan et al., 2023)
Climate-Related Forcings for the 'de-biased' sensitivity experiment		
Global oceanic forcings		
Oceanic forcings based on de-biased atmospheric forcings	mandatory	<u>In section 2.4.2 we describe an approach to de-bias the oceanic forcings based on the ocean biogeochemistry model NEMO-PISCES forced by a de-biased version of the IPSL-CM6A-LR-based atmospheric forcing as an option to fulfil the demand for de-biased ocean data we would like to follow.</u> <del>Not available yet, simulated by the ocean biogeochemistry model ocean biogeochemistry NEMO-PISCES forced by a de-biased version of the IPSL-CM6A-LR-based atmospheric forcing (see section 2.4.2)</del>
Regional oceanic forcings		
De-biased oceanic forcing based on observed oceanic data for individual variables and regions	mandatory	<u>The regional models of the fisheries and marine ecosystem sector have applied regional bias-adjustments within their impact simulations that are described in section 2.4.3 and that make these simulations part of the 'de-biased' sensitivity experiment in the sector (see Table 2) while the default experiments are based on the raw oceanic forcings.</u> <del>Not centrally provided, see section 2.4.3</del>

228

229

230

231

232

233

234

235

236

237

238

239

240

241

242

243

## 1.1 ISIMIP3b, group I: Climate-model based impact model simulations for the period from 1601 to 2015

The group I experiments cover the years 1601-1849 with pre-industrial CRFs ('picontrol') and fixed 1850 direct human forcings ('1850soc') described in the grey column 3 of the ISIMIP3b scenario **Table 2** as well as the subsequent years 1850-2014 considering pre-industrial and historical CRFclimate-related forcings ('picontrol' or 'historical') and different assumptions about DHFdirect human forcings ('histsoc', '2015soc', '1850soc', and 'nat') as described in the grey column 4 of **Table 2**. The reasoning behind the individual experiments are introduced below.

**Pre-industrial reference simulations (picontrol + histsoc, picontrol + 2015soc, picontrol + 2015soc-from-histsoc, picontrol + 1850soc, picontrol + nat; default):** To estimate the impacts of historical and future changes in the CRFs, the protocol includes reference simulations based on pre-industrial CRFs and DHF identical to those considered in the climate change scenario runs. In order to allow for the fitting of

244 extreme value distributions such as Gumble or Generalized Extreme Value (GEV) distributions to, e.g.  
245 annual maximum discharge to estimate reference 100 year return levels ~~of certain impacts~~, the runs are  
246 designed to ~~-include~~includes the generation of large samples (at least 250 years) of impact distributions  
247 distribution based on stable pre-industrial CRFs (picontrol) and constant DHFs (see ‘picontrol + 1850soc’,  
248 ‘picontrol + 2015soc’, and ‘picontrol + nat’ experiments in **Table 2**).

249 In addition, the protocol includes a reference experiment for the historical period (1850-2014) with DHF  
250 changing over time (histsoc) and 1850-2014 pre-industrial CRF (picontrol), while fixed 2015 DHF is  
251 considered afterwards (2015-2100) (‘picontrol + 2015soc-from-histsoc’). This run may be different from  
252 the ‘picontrol + 2015soc’ simulation for this time window because of the lagged effects of increasing DHF  
253 from 1850 to 2014. The ‘histsoc’ DHF is identical to ISIMIP3a (Frieler et al., 2024a).

254 The complete pre-industrial reference runs are divided in two parts. Only the first parts from the start  
255 until 2014 belong to group I (grey fields in Table 2~~the table~~), while the second parts covering the period  
256 2015-2100 belong to group II (red parts of ~~the t~~Table 2).

257  
258 Comparing these reference simulations to the scenario experiments using historical CRFs (historical +  
259 histsoc, historical + 2015soc, historical + 1850soc, historical + nat; default (see below)) allows for the  
260 estimation of the effects of simulated historical climate change conditional on the assumed DHF. The  
261 historical CRFclimate-related forcing (‘historical’) starts from the pre-industrial climate simulation in 1850,  
262 i.e. the ‘picontrol’ and ‘historical’ versions of the experiments have a common starting point. As some  
263 impact indicators may have ‘internal’ trends not necessarily forced by external drivers (e.g. re-growth of  
264 forests), the comparison of the 1850-2014 impact simulations forced by the ‘historical’ CRF to parallel  
265 simulations using the ‘picontrol’ CRF is more appropriate to estimate the effects of historical climate  
266 change than comparing an early period of the historical impact simulation to the end of the historical  
267 period.

268 For models requiring a spin-up, the ‘picontrol’ CRFs should be used in combinations with DHF i) at 1850  
269 levels to spin-up for the ‘1850soc’ and ‘histsoc’ experiments, ii) at 2015 levels to initialise the ‘2015soc’  
270 experiment, and iii) set to zero to start the ‘nat’ experiments. For the spin-up the ‘picontrol’ CRF should  
271 be copied as often as needed. The ‘picontrol + 1850soc’ run from 1601-1849 is part of the regular  
272 experiments that should be reported and hence the spin-up has to be finished before this pre-industrial  
273 period.

274 To allow for a quantification of the impacts of the anthropogenic CRFs, we also support historical  
275 reference simulation assuming only natural CRF (‘hist-nat’ simulations generated within the Detection and  
276 Attribution Model Intercomparison Project (DAMIP) as sub-MIP of CMIP6, (Gillett et al., 2016) by providing  
277 the associated bias-adjusted CRF as secondary climate input data (Lange et al., 2023). However, associated  
278 simulations are not an official part of ISIMIP3b and not described in the associated protocol.

279  
280 **Standard historical simulations based on historical climate-related forcing and observed changes in**  
281 **direct human forcing (historical + histsoc; default):** The historical simulations (1850-2014) are forced by  
282 historical (‘historical’) CRFs and DHFs evolving according to observations (ISIMIP3a ‘histsoc’ DHF). The  
283 ISIMIP3b ‘historical + histsoc’ experiment is comparable to the default ‘obsclim + histsoc’ run used in  
284 ISIMIP3a but based on simulated CRFs. The simulated climate is different from the observed realisation

285 due to differences in the internal variability of the observed and simulated historical climate and potential  
286 deficits in the climate model simulations. A comparison between the default ISIMIP3b ‘historical + histsoc’  
287 impact model simulations to the associated ISIMIP3a results allows for a quantification of the effects of  
288 the discrepancies between the observed and simulated CRFs on the considered impact indicators. This  
289 experiment can be initialised from the spin-up of the associated pre-industrial reference simulation in  
290 case a spin-up is needed.

291  
292 **Simulations with historical climate-related forcing and fixed 2015 direct human forcing (historical +**  
293 **2015soc; default):** This historical experiment is similar to the standard historical experiment except that  
294 it is forced by fixed 2015 DHF. It is introduced into the ‘first priority’ scenario-set-up to generate an  
295 ensemble of historical cross-sectorally consistent impact simulations that is as large as possible by not  
296 excluding impact models that are not able to handle varying DHF. If a spin-up is needed the experiment  
297 can be initialised from the spin-up of the associated pre-industrial reference simulation (picontrol +  
298 2015soc, default) described at the beginning of this section.

299  
300 **Simulations with historical climate-related forcing and fixed 1850 direct human forcing (historical +**  
301 **1850soc; default):** This historical experiment is also similar to the standard historical experiment but it is  
302 forced by the fixed 1850 DHFs. It corresponds to the ‘obsclim + 1901soc’ simulation of ISIMIP3a. Here in  
303 ISIMIP3b we consider the year 1850 instead of 1901 used in ISIMIP3a as this is the year where the  
304 ‘historical’ climate simulations with observed natural and human forcings start, i.e. a branch from the pre-  
305 industrial climate simulations assuming constant pre-industrial forcings (‘picontrol’). If a spin-up is  
306 required it does not have to be newly generated as it is identical to the spin-up for the default ‘picontrol  
307 + 1850soc’, ‘picontrol + histsoc’, and ‘historical + histsoc’ experiments and described in the beginning of  
308 this section.

309  
310 **Simulations with historical climate-related forcing and no direct human forcings (historical + nat;**  
311 **default):** Considering no ~~DHFdirect human forcings~~ (nature run) allows quantifying the effect of the  
312 simulated historical climate change conditional on otherwise natural conditions, i.e. no direct human  
313 influences on land use, water management etc.. This experiment is introduced as a companion  
314 experiment to the ‘obsclim + nat’ simulations of ISIMIP3a. The comparison with the three historical  
315 simulations with constant ~~DHFdirect human forcings~~ allows testing, to what degree the impact of climate  
316 change on the simulated natural or human systems is conditional on the underlying ~~DHFdirect human~~  
317 ~~forcing~~. This experiment is only included for the biomes and fisheries and marine ecosystems fisheries  
318 sectors as models from other sectors usually need some basic information such as vegetation patterns  
319 that are not available for natural-only conditions. The biomes models generate their own natural-only  
320 vegetation patterns based on their dynamic representation of vegetation. A spin-up does not have to be  
321 newly generated but is identical to the spin-up for the ‘picontrol + nat’ experiment described above.

322  
323 **‘De-biased’ sensitivity simulations within the marine ecosystems and fisheries sector (FishMIP) with de-**  
324 **biased historical oceanic forcings and no or histsoc direct human forcings (historical + nat, historical +**  
325 **histsoc; de-biased):** So far, the default oceanic forcing is not bias-adjusted as globally the observational

326 data are ~~too sparse~~ ~~to sparse~~ to be used in a similar empirical way as for the bias-adjustment of the  
327 atmospheric forcing. However, the biases in the forcing are expected to also induce biases in the historical  
328 and future impact simulations. To quantify these effects and to test a suggested bias-adjustment method  
329 based on comprehensive ocean-biogeochemistry model simulations forced by bias-adjusted atmospheric  
330 forcings we include a sensitivity experiment where the default [CRFclimate-related forcing](#) is replaced by  
331 input data generated by a dynamical de-biasing approach (Lengaigne et al., 2025) using the NEMO-PISCES  
332 physical-biogeochemical ocean model (Madec, 2015), which is the oceanic component of the IPSL-CM6A-  
333 LR climate model. Thus, the forcing data will first be generated for IPSL-CM6A-LR, but later extended to  
334 other ISIMIP-GCMs as described in subsection **2.4.2**.

335 In contrast, the oceanic forcing for the regional component of the marine ecosystems and fisheries sector  
336 have been bias-adjusted by regional observational oceanic data as described in subsection **2.4.3**. In this  
337 case most models only use the bias-adjusted inputs and not the raw ones. Nevertheless the experiments  
338 are labeled as ‘de-biased’ sensitivity experiments to ensure a consistent naming across scales.  
339

## 340 **1.2 ISIMIP3b, group II: Climate-model based future impact model simulations with** 341 **constant 2015 direct human forcings**

342  
343 The ISIMIP3b, group II simulations comprise a set of future impact projections (2015-2100) using fixed  
344 levels of [DHFdirect human forcings](#) as considered in the historical simulations (‘2015soc’, ‘1850soc’, and  
345 ‘nat’) or reached at the end (2014) of the historical period in the ‘historical + histsoc’ runs (‘2015soc-from-  
346 histsoc’). These runs are described in the red cells of **Table 24**.  
347

348 **Pre-industrial reference simulations (picontrol + 2015soc, picontrol + 2015soc-from-histsoc, picontrol +**  
349 **1850soc, picontrol + nat; default):** These simulations are included into the ISIMIP3, group II part of the  
350 protocol to allow for the estimation of the effect of climate change by comparing the future impact  
351 projections to simulations assuming the same background DHF but pre-industrial levels of CRF (see  
352 description of baseline simulations in section **1.1**).  
353

354 **Future impact projections assuming SSP-RCP-based climate-related forcings starting from ‘historical +**  
355 **histsoc’ simulations (ssp126 + 2015soc-from-histsoc, ssp370 + 2015soc-from-histsoc, ssp585 + 2015soc-**  
356 **from-histsoc; default):** These runs are a continuation of the group I ‘historical + histsoc’ simulations  
357 assuming fixed 2015 [DHFdirect human forcings](#) for the future. Note that this experiment is different from  
358 the experiment with fixed 2015 DHF for the future starting from the ‘historical + 2015soc’ group I  
359 experiment (see description below).  
360

361 These experiments have been introduced to describe the impacts of different scenarios of changes in the  
362 climate-related systems on today’s natural systems and societies, i.e. assuming present day population  
363 levels and distributions, land use patterns, water, and agricultural management measures etc.. In many  
364 cases, the projected changes in natural and human systems can be interpreted as the pure effect of the  
365 prescribed changes in the climate-related systems. However, they could also partly result from lagged  
366 effects of the historical changes in DHFs (‘histsoc’), CRF (‘historical’), or natural temporal trends induced

367 e.g. by re-growth of forests. To be able to separate natural trends from the effects of changing CRFs, these  
368 simulations can be compared to reference impact simulations with pre-industrial [CRFclimate-related](#)  
369 [forcings](#) forced with the same [DHFdirect-human-forcings](#) ('picontrol + 2015soc-from-histsoc', see  
370 description in group I section).

371  
372 **Future impact projections assuming SSP-RCP-based climate-related forcings starting from historical**  
373 **simulations with constant 2015 direct human forcings (ssp126 + 2015soc, ssp370 + 2015soc, ssp585 +**  
374 **2015soc; default):** These experiments continue the 'historical + 2015soc' experiments from ISIMIP3b,  
375 group I using [DHFdirect-human-forcings](#) held constant at 2015 levels for the historical period. Although  
376 the DHF in the future period is identical to the future simulations described above, the difference in  
377 historical forcing may affect the impact simulations in the future period. These simulations are also  
378 considered first priority as some of the impact models may not be able to handle varying [DHFdirect-human](#)  
379 [forcings](#) and therefore can only perform these experiments. Models participating in the '2015soc-from-  
380 histsoc' experiments described above are also asked to complete the '2015soc' runs to generate an as  
381 large as possible ensemble of consistent impact model simulations.

382  
383 **Future impact projections assuming SSP-RCP-based climate-related forcings starting from historical**  
384 **simulations assuming constant 1850 direct human forcings (ssp126 + 1850soc, ssp370 + 1850soc, ssp585**  
385 **+ 1850soc; default):** These experiments continue the default 'historical + 1850soc' experiments  
386 considered in ISIMIP3b, group I. They are included to estimate the impact of changes in the climate-  
387 related systems conditional on 1850 levels of [DHFdirect-human-forcings](#) that can be compared to the  
388 impact conditional on today's levels of [DHFdirect-human-forcings](#) ('2015soc').

389  
390 **Future impact projections assuming SSP-RCP-based climate-related forcings starting from historical**  
391 **simulations assuming no direct human forcings (ssp126 + nat, ssp370 + nat, ssp585 + nat; default):** These  
392 experiments continue the default 'historical + nat' experiments in ISIMIP3b, group I. They are included to  
393 estimate the effect of changes in the climate-related systems (here climate change itself and increasing  
394 CO<sub>2</sub> concentrations) assuming no [DHFdirect-human-forcings](#).

395  
396 **CO<sub>2</sub> sensitivity simulations (ssp126 + 2015soc-from-histsoc, ssp370 + 2015soc-from-histsoc, ssp585 +**  
397 **2015soc-from-histsoc, ssp585 + 2015soc, ssp585 + 1850soc, ssp585 + nat; 2015co2):** To separate the  
398 effects of increasing atmospheric CO<sub>2</sub> concentrations from the effects of other changes in the climate-  
399 related systems, the ISIMIP3b protocol includes sensitivity experiments where atmospheric CO<sub>2</sub>  
400 concentrations are held constant at 2015 levels. For SSP1-2.6 and SSP3-7.0, they are only introduced as  
401 deviations from the default '2015soc-from-histsoc' experiments while for SSP5-8.5 the effect can also be  
402 quantified conditional on all levels of direct human influences considered in the previous experiments.

403 **Future lightning sensitivity simulations (ssp126 + 2015soc-from-histsoc, ssp370 + 2015soc-from-histsoc,**  
404 **ssp585 + 2015soc-from-histsoc; varlightning):** To study the effects of future changes in lightning flash  
405 rates as opposed to using a stationary lightning climatology, the ISIMIP3b protocol includes sensitivity  
406 experiments where future lightning flash rates change along the RCPs. The future lightning data sensitivity

407 experiment is introduced as a deviation from the default ‘2015soc-from-histsoc’ experiment and only for  
 408 one climate model (UK-ESM). This sensitivity experiment has been introduced for the fire sector.

409 **Climate sensitivity simulations under high levels of CO<sub>2</sub> (ssp126 + 2015soc-from-histsoc, ssp585co2):** To  
 410 study the effects of high atmospheric CO<sub>2</sub> concentration without accompanying changes in climate, the  
 411 ISIMIP3b protocol includes a sensitivity experiment where the atmospheric CO<sub>2</sub> concentration are  
 412 prescribed according to RCP8.5, while the other [CRF climate-related forcings](#), in particular the atmospheric  
 413 forcings are from SSP1-2.6. The future climate sensitivity experiment is introduced as a deviation from the  
 414 default ‘ssp126 + 2015soc-from-histsoc’ experiment. This sensitivity experiment has been introduced for  
 415 the peat sector.

416 **‘De-biased’ sensitivity simulations within the marine ecosystems and fisheries sector (FishMIP) with de-**  
 417 **biased oceanic forcings and no or 2015soc direct human forcings for reference simulations based on**  
 418 **pre-industrial oceanic forcing (picontrol + nat, picontrol + 2015soc-from-histsoc; de-biased) and the**  
 419 **associated simulations accounting for different levels of climate change (ssp126 + nat, ssp370 + nat,**  
 420 **ssp858 + nat, ssp126 + 2015soc-from-histsoc, ssp370 + 2015soc-from-histsoc, ssp585 + 2015soc-from-**  
 421 **histsoc):** These simulations represent the future extensions of the ‘de-biased’ group I simulations  
 422 described above. They are designed to test the dynamical bias-adjustment suggested for the global  
 423 oceanic forcings under different levels of climate change (ssp126, ssp370, ssp585). The regional impact  
 424 projections within the sector are also based on de-biased oceanic forcings and are therefore also labeled  
 425 as ‘de-biased’ sensitivity experiments to ensure a consistent labeling across scales.

426  
 427 [Table 2: ISIMIP3b climate-model based experiments. The table provides a comprehensive list of all](#)  
 428 [ISIMIP3b, group I \(grey\) and group II \(red\) experiments defined by the assumed climate-related forcings](#)  
 429 [\(CRF\) and direct human forcings \(DHF\). Here the climate-related forcings are only described by the climate](#)  
 430 [\(oceanic and atmospheric\) and CO<sub>2</sub> forcings as we do not provide coastal water levels yet.](#)

Experiment	Short description	Period: Pre-industrial 1601-1849	Period: Historical 1850-2014	Period: Future 2015-2100
pre-industrial control	CRF: No changes in the climate-related systems, CO <sub>2</sub> and CH <sub>4</sub> fixed at 1850 levels	picontrol	picontrol	picontrol
2015soc-from-histsoc				
1st priority	DHF: Varying management before	1850soc	histsoc	2015soc-from-histsoc

	2015, then fixed at 2015 levels thereafter			
<b>pre-industrial control</b> 2015soc <b>1st priority</b>	<b>CRF:</b> No changes in the climate-related systems, CO <sub>2</sub> and CH <sub>4</sub> fixed at 1850 levels <b>DHF:</b> Fixed at 2015 levels for all periods	Does not have to be simulated as the following periods already provide 251 simulation years assuming stable baseline CRF and DHF. <i>ensi</i>	<b>picontrol</b>  <b>2015soc</b>	<b>picontrol</b>  <b>2015soc</b>
<b>pre-industrial control</b> 1850soc <b>2nd priority</b>	<b>CRF:</b> No changes in the climate-related systems, CO <sub>2</sub> and CH <sub>4</sub> fixed at 1850 levels <b>DHF:</b> Fixed at 1850 levels for all periods	Does not have to be simulated as the following periods already provide 251 simulation years assuming stable baseline CRF and DHF.	<b>picontrol</b>  <b>1850soc</b>	<b>picontrol</b>  <b>1850soc</b>
<b>pre-industrial control</b> nat <b>2nd priority</b>	<b>CRF:</b> No changes in the climate-related systems, CO <sub>2</sub> and CH <sub>4</sub> fixed at 1850 levels <b>DHF:</b> No direct human influences	Does not have to be simulated as the following periods already provide 251 simulation years assuming stable baseline CRF and DHF.	<b>picontrol</b>  <b>nat</b>	<b>picontrol</b>  <b>nat</b>
<b>RCP2.6</b> 2015soc-from-histsoc <b>1st priority</b>	<b>CRF:</b> Simulated historical changes in climate-related systems, CO <sub>2</sub> and CH <sub>4</sub> concentrations as observed in the historical period, then simulated SSP1-2.6 changes in the climate-related systems <b>DHF:</b> Varying management before 2015, then fixed at 2015 levels thereafter	Identical to picontrol + 1850soc run described above	<b>historical</b>  <b>histsoc</b>	<b>ssp126</b>  <b>2015soc-from-histsoc</b>

<b>RCP2.6</b> 2015soc <b>1st priority</b>	<b>CRF:</b> Simulated historical changes in climate-related systems, CO <sub>2</sub> and CH <sub>4</sub> concentrations as observed in the historical period, then simulated SSP1-2.6 changes in the climate-related systems	Identical to “picontrol + 2015soc” run	<b>historical</b>	<b>ssp126</b>
	<b>DHF:</b> Fixed at 2015 levels for all periods		<b>2015soc</b>	<b>2015soc</b>
<b>RCP2.6</b> 1850soc <b>2nd priority</b>	<b>CRF:</b> Simulated historical changes in climate-related systems, CO <sub>2</sub> and CH <sub>4</sub> concentrations as observed in the historical period, then simulated SSP1-2.6 changes in the climate-related systems	Identical to “picontrol + 1850soc” run	<b>historical</b>	<b>ssp126</b>
	<b>DHF:</b> Fixed at 1850 levels for all periods		<b>1850soc</b>	<b>1850soc</b>
<b>RCP2.6</b> nat <b>2nd priority</b>	<b>CRF:</b> Simulated historical changes in climate-related systems, CO <sub>2</sub> and CH <sub>4</sub> concentrations as observed in the historical period, then simulated SSP1-2.6 changes in the climate-related systems	Identical to “picontrol + nat” run	<b>historical</b>	<b>ssp126</b>
	<b>DHF:</b> No direct human influences		<b>nat</b>	<b>nat</b>

<b>CO<sub>2</sub> sensitivity RCP2.6</b>  2015soc-from-histsoc  <b>2nd priority</b>	<b>CRF:</b> Simulated historical changes in climate-related systems, CO <sub>2</sub> and CH <sub>4</sub> concentrations as observed in the historical period, then simulated SSP1-2.6 changes in the climate-related systems but fixed 2015 CO <sub>2</sub> concentrations	Identical to “picontrol + 1850soc” run	"histsoc" version of the historical period of the RCP2.6 experiment, as described above	<b>ssp126</b>  <b>Sensitivity experiment: 2015co2</b>
	<b>DHF:</b> Varying management before 2015, then fixed at 2015 levels thereafter			
<b>RCP7.0</b>  2015soc-from-histsoc  <b>1st priority</b>	<b>CRF:</b> Simulated historical changes in climate-related systems, CO <sub>2</sub> and CH <sub>4</sub> concentrations as observed in the historical period, then simulated SSP3-7.0 changes in the climate-related systems	Identical to “picontrol + 1850soc” run	"histsoc" version of the historical period of the RCP2.6 experiment	<b>ssp370</b>
	<b>DHF:</b> Varying management before 2015, then fixed at 2015 levels thereafter			
<b>RCP7.0</b>  2015soc  <b>1st priority</b>	<b>CRF:</b> Simulated historical changes in climate-related systems, CO <sub>2</sub> and CH <sub>4</sub> concentrations as observed in the historical period, then simulated SSP3-7.0 changes in the	Identical to “picontrol + 2015soc” run	Identical to "historical + 2015soc" run described above	<b>ssp370</b>

	climate-related systems			
	<b>DHF:</b> Fixed at 2015 levels for all periods			<b>2015soc</b>
<b>RCP7.0</b> 1850soc <b>2nd priority</b>	<b>CRF:</b> Simulated historical changes in climate-related systems, CO <sub>2</sub> and CH <sub>4</sub> concentrations as observed in the historical period, then simulated SSP3-7.0 changes in the climate-related systems	Identical to “picontrol + 1850soc” run	Identical to "historical + 1850soc" run described above	<b>ssp370</b>
	<b>DHF:</b> Fixed at 1850 levels for all periods			<b>1850soc</b>
<b>RCP7.0</b> nat <b>2nd priority</b>	<b>CRF:</b> Simulated historical changes in climate-related systems, CO <sub>2</sub> and CH <sub>4</sub> concentrations as observed in the historical period, then simulated SSP3-7.0 changes in the climate-related systems	Identical to “picontrol + nat” run	Identical to "historical + nat" run described above	<b>ssp370</b>
	<b>DHF:</b> No direct human influences			<b>nat</b>

<b>CO<sub>2</sub> sensitivity RCP7</b>  2015soc-from-histsoc  <b>2nd priority</b>	<b>CRF:</b> Simulated historical changes in climate-related systems, CO <sub>2</sub> and CH <sub>4</sub> concentrations as observed in the historical period, then simulated SSP3-7.0 changes in the climate-related systems but CO <sub>2</sub> concentrations fixed at 2015 levels	Identical to “picontrol + 1850soc” run	Identical to "historical + histsoc" run described above	<b>ssp370</b>  <b>Sensitivity experiment: 2015co2</b>
	<b>DHF:</b> Varying management before 2015, then fixed at 2015 levels thereafter			
<b>RCP8.5</b>  2015soc-from-histsoc  <b>1st priority</b>	<b>CRF:</b> Simulated historical changes in climate-related systems, CO <sub>2</sub> and CH <sub>4</sub> concentrations as observed in the historical period, then simulated SSP5-8.5 changes in the climate-related systems	Identical to “picontrol + 1850soc” run	Identical to "historical + histsoc" run described above	<b>ssp585</b>
	<b>DHF:</b> Varying management before 2015, then fixed at 2015 levels thereafter			
<b>RCP8.5</b>  2015soc  <b>1st priority</b>	<b>CRF:</b> Simulated historical changes in climate-related systems, CO <sub>2</sub> and CH <sub>4</sub> concentrations as observed in the historical period, then simulated SSP5-8.5	Identical to “picontrol + 2015soc” run	Identical to "historical + 2015soc" run described above	<b>ssp585</b>

	changes in the climate-related systems			
	<b>DHF:</b> Fixed at 2015 levels for all periods			<b>2015soc</b>
<b>RCP8.5</b> 1850soc <b>2nd priority</b>	<b>CRF:</b> Simulated historical changes in climate-related systems, CO <sub>2</sub> and CH <sub>4</sub> concentrations as observed in the historical period, then simulated SSP5-8.5 changes in the climate-related systems	Identical to “picontrol + 1850soc” run	Identical to "historical + 1850soc" run described above	<b>ssp585</b>
	<b>DHF:</b> Fixed at 1850 levels for all periods			<b>1850soc</b>
<b>RCP8.5</b> nat <b>2nd priority</b>	<b>CRF:</b> Simulated historical changes in climate-related systems, CO <sub>2</sub> and CH <sub>4</sub> concentrations as observed in the historical period, then simulated SSP5-8.5 changes in the climate-related systems	Identical to “picontrol + nat” run	Identical to "historical + nat" run	<b>ssp585</b>
	<b>DHF:</b> No direct human influences			<b>nat</b>
<b>CO<sub>2</sub> sensitivity</b> <b>RCP8.5</b>	<b>CRF:</b> Simulated historical changes in climate-related systems, CO <sub>2</sub> and CH <sub>4</sub> concentrations as	Identical to “picontrol + 1850soc” run	Identical to "historical + histsoc" run	<b>ssp585</b> <b>Sensitivity experiment:</b> <b>2015co2</b>

<p>2015soc-from-histsoc</p> <p><b>1st priority</b></p>	<p>observed in the historical period, then simulated SSP5-8.5 changes in the climate-related systems but CO<sub>2</sub> concentrations fixed at 2015 levels</p>			
	<p><b>DHF:</b> Varying management before 2015, then fixed at 2015 levels thereafter</p>			<p><b>2015soc-from-histsoc</b></p>
<p><b>CO<sub>2</sub> sensitivity RCP8.5</b></p> <p>2015soc</p> <p><b>1st priority</b></p>	<p><b>CRF:</b> Simulated historical changes in climate-related systems, CO<sub>2</sub> and CH<sub>4</sub> concentrations as observed in the historical period, then simulated SSP5-8.5 changes in the climate-related systems, but CO<sub>2</sub> concentrations fixed at 2015 levels</p>	<p>Identical to "picontrol + 2015soc" run</p>	<p>Identical to "historical + 2015soc" run</p>	<p><b>ssp585</b></p> <p><b>Sensitivity experiment: 2015co2</b></p>
	<p><b>DHF:</b> Fixed at 2015 levels for all periods</p>			<p><b>2015soc</b></p>
<p><b>CO<sub>2</sub> sensitivity RCP8.5</b></p> <p>1850soc</p> <p><b>2nd priority</b></p>	<p><b>CRF:</b> Simulated historical changes in climate-related systems, CO<sub>2</sub> and CH<sub>4</sub> concentrations as observed in the historical period, then simulated SSP5-8.5 changes in the climate-related systems, but CO<sub>2</sub> concentrations fixed at 2015 levels</p>	<p>Identical to "picontrol + 1850soc" run</p>	<p>Identical to "historical + 1850soc" run</p>	<p><b>ssp585</b></p> <p><b>Sensitivity experiment: 2015co2</b></p>

	<b>DHF:</b> Fixed at 1850 levels for all periods			<b>1850soc</b>
<b>CO<sub>2</sub> sensitivity RCP8.5</b>  nat  <b>1st priority</b>	<b>CRF:</b> Simulated historical changes in climate-related systems, CO <sub>2</sub> and CH <sub>4</sub> concentrations as observed in the historical period, then simulated SSP5-8.5 changes in the climate-related systems, but CO <sub>2</sub> concentrations fixed at 2015 levels	Identical to "picontrol + nat" run	Identical to "historical + nat" run	<b>ssp585</b>  <b>Sensitivity experiment: 2015co2</b>
	<b>DHF:</b> No direct human influences			nat
<b>Lightning sensitivity RCP2.6</b>  2015soc-from-histsoc  <b>2nd priority</b>	<b>CRF:</b> Simulated historical changes in climate-related systems, CO <sub>2</sub> and CH <sub>4</sub> concentrations as observed in the historical period, then simulated SSP1-2.6 changes in the climate-related systems including future lightning which in the default case is considered fixed at climatological levels	Identical to "picontrol + 1850soc" run	Identical to "historical + histsoc" run	<b>ssp126</b>  <b>Sensitivity experiment: varlightning</b>
	<b>DHF:</b> Varying management before 2015, then fixed at 2015 levels thereafter			<b>2015soc-from-histsoc</b>

<b>Lightning sensitivity RCP7.0</b>  2015soc-from-histsoc  <b>2nd priority</b>	<b>CRF:</b> Simulated historical changes in climate-related systems, CO <sub>2</sub> and CH <sub>4</sub> concentrations as observed in the historical period, then simulated SSP3-7.0 changes in the climate-related systems including future lightning which in the default case is considered fixed at climatological levels	Identical to "picontrol + 1850soc" run	Identical to "historical + histsoc" run	<b>ssp370</b>  <b>Sensitivity experiment: varlightning</b>
	<b>DHF:</b> Varying management before 2015, then fixed at 2015 levels thereafter			<b>2015soc-from-histsoc</b>
<b>Lightning sensitivity RCP8.5</b>  2015soc-from-histsoc  <b>2nd priority</b>	<b>CRF:</b> Simulated historical changes in climate-related systems, CO <sub>2</sub> and CH <sub>4</sub> concentrations as observed in the historical period, then simulated SSP5-8.5 changes in the climate-related systems including future lightning which in the default case is considered fixed at climatological levels	Identical to "picontrol + 1850soc" run	Identical to "historical + histsoc" run	<b>ssp585</b>  <b>Sensitivity experiment: varlightning</b>
	<b>DHF:</b> Varying management before 2015, then fixed at 2015 levels thereafter			<b>2015soc-from-histsoc</b>

<b>Climate sensitivity, RCP2.6 with RCP8.5 CO<sub>2</sub></b>  2015soc-from-histsoc  <b>2nd priority</b>	<b>CRF:</b> Simulated historical changes in climate-related systems, CO <sub>2</sub> and CH <sub>4</sub> concentrations as observed in the historical period, then CO <sub>2</sub> evolves according to SSP5-8.5 while all other CRFs change according to default SSP1-2.6 forcing data	Identical to “picontrol + 1850soc” run	Identical to "historical + histsoc" run	<b>ssp126</b>  <b>Sensitivity experiment: ssp585co2</b>
	<b>DHF:</b> Varying management before 2015, then fixed at 2015 levels thereafter			<b>2015soc-from-histsoc</b>
<b>Bias sensitivity, de-biased oceanic data for pre-industrial control</b>  nat  <b>2nd priority</b>	<b>CRF:</b> De-biased pre-industrial oceanic forcing, CO <sub>2</sub> fixed at 1850 levels	Not covered	<b>picontrol</b>	<b>picontrol</b>  <b>Sensitivity experiment: de-biased</b>
	<b>DHF:</b> no direct human influences			<b>nat</b>
<b>Bias sensitivity, de-biased oceanic data for SSP1-2.6</b>  nat  <b>2nd priority</b>	<b>CRF:</b> De-biased simulated historical oceanic forcing, then de-biased simulated SSP1-2.6 oceanic forcing	Not covered	<b>historical</b>	<b>ssp126</b>  <b>Sensitivity experiment: de-biased</b>
	<b>DHF:</b> no direct human influences			<b>nat</b>
	<b>CRF:</b> De-biased simulated historical oceanic forcing, then de-biased simulated	Not covered	<b>historical</b>	<b>ssp370</b>  <b>Sensitivity experiment: de-biased</b>

<b>Bias sensitivity, de-biased oceanic data for SSP3-7.0</b>	SSP3-7.0 oceanic forcing			
nat <b>2nd priority</b>	<b>DHF:</b> no direct human influences	Not covered	nat	nat
<b>Bias sensitivity, de-biased oceanic data for SSP5-8.5</b>	<b>CRF:</b> De-biased simulated historical oceanic forcing, then de-biased simulated SSP5-8.5 oceanic forcing	Not covered	historical	ssp585 <b>Sensitivity experiment: de-biased</b>
nat <b>2nd priority</b>	<b>DHF:</b> No direct human influences	Not covered	nat	nat
<b>Bias sensitivity, de-biased oceanic data for pre-industrial control</b>	<b>CRF:</b> De-biased pre-industrial oceanic forcing, CO <sub>2</sub> fixed at 1850 levels	Not covered	picontrol	picontrol <b>Sensitivity experiment: de-biased</b>
2015soc-from-histsoc <b>2nd priority</b>	<b>DHF:</b> Varying direct human influences before 2015, then fixed at 2015 levels thereafter	Not covered	histsoc	2015soc-from-histsoc
<b>Bias sensitivity, de-biased oceanic data for SSP1-2.6</b>	<b>CRF:</b> De-biased simulated historical oceanic forcing, then de-biased simulated SSP1-2.6 oceanic forcing	Not covered	historical	ssp126 <b>Sensitivity experiment: de-biased</b>
2015soc-from-histsoc <b>2nd priority</b>	<b>DHF:</b> Varying direct human influences before 2015, then fixed at 2015 levels thereafter	Not covered	histsoc	2015soc-from-histsoc

<b>Bias sensitivity, de-biased oceanic data for SSP3-7.0</b>  2015soc-from-histsoc  <b>2nd priority</b>	<b>CRF:</b> De-biased simulated historical oceanic forcing, then de-biased simulated SSP3-7.0 oceanic forcing	Not covered	historical	<b>ssp370</b>  <b>Sensitivity experiment: de-biased</b>
	<b>DHF:</b> Varying direct human influences before 2015, then fixed at 2015 levels thereafter	Not covered	histsoc	<b>2015soc-from-histsoc</b>
<b>Bias sensitivity, de-biased oceanic data for SSP5-8.5</b>  2015soc-from-histsoc  <b>2nd priority</b>	<b>CRF:</b> De-biased simulated historical oceanic forcing, then de-biased simulated SSP5-8.5 oceanic forcing	Not covered	historical	<b>ssp585</b>  <b>Sensitivity experiment: de-biased</b>
	<b>DHF:</b> Varying direct human influences before 2015, then fixed at 2015 levels thereafter	Not covered	histsoc	<b>2015soc-from-histsoc</b>

431

432

433

434

435

436

437

438

439

440

441

442

443

444

445

446

447

448

~~**Table 2: ISIMIP3b climate model based experiments.** The table provides a comprehensive list of all ISIMIP3b, group I (grey) and group II (red) experiments defined by the assumed climate-related forcings (CRF) and direct human forcings (DHF). Here the climate-related forcings are only described by the climate (oceanic and atmospheric) and CO<sub>2</sub> forcings as we do not provide coastal water levels yet.~~

## 2 Climate-related forcing data

### 2.1 Bias-adjusted and statistically downscaled atmospheric climate forcing

For ISIMIP3b we provide the daily atmospheric forcings for the same variables as in ISIMIP3a on the default 0.5° grid (see **Table 3**). These variables are from the output of CMIP6 climate model simulations, selected and processed as described below. We use the climate simulations from the piconrol (for pre-industrial conditions), historical (for historical conditions), ssp126, ssp370, and ssp585 (for future conditions under the scenarios SSP1-2.6, SSP3-7.0, and SSP5-8.5, respectively) CMIP6 experiments.

449  
450  
451  
452  
453

**Table 3:** Climate-related atmospheric forcing data provided within ISIMIP3b. The upper limits of [precipitation \(pr\)](#) and [snowfall \(prsn\)](#) correspond to 600 mm day-1 and 300 mm day-1, respectively, while the lower and upper limits of [Near-Surface Air Temperature \(tas\)](#), [Daily Maximum Near-Surface Air Temperature \(tasmax\)](#) and [Daily Minimum Near-Surface Air Temperature \(tasmin\)](#) correspond to -90°C and +70°C, respectively.

Variable	Variable specifier	Unit (maximum range, inner bounds if considered)	Resolution	Datasets
Near-Surface Relative Humidity	<b>hurs</b>	% ([1, 100], [0.01, 99.99])	0.5° grid, daily	Bias-adjusted and downscaled from GFDL-ESM4, IPSL-CM6A-LR, MPI-ESM1-2-HR, MRI-ESM2-0, and UKESM1-0-LL simulations generated for CMIP6.
Near-Surface Specific Humidity	<b>huss</b>	kg kg-1 ([0.0000001, 0.1])	0.5° grid, daily	Derived from bias-adjusted and downscaled hurs, ps, and tas from GFDL-ESM4, IPSL-CM6A-LR, MPI-ESM1-2-HR, MRI-ESM2-0, and UKESM1-0-LL simulations generated for CMIP6.
Precipitation (including snowfall)	<b>pr</b>	kg m-2 s-1 ([0, 600/86400], [0.1/86400, ∞])	0.5° grid, daily	Bias-adjusted and downscaled from GFDL-ESM4, IPSL-CM6A-LR, MPI-ESM1-2-HR, MRI-ESM2-0, and UKESM1-0-LL simulations generated for CMIP6.
Snowfall	<b>prsn</b>	kg m-2 s-1 ([0, 300/86400])  Maximum range and inner bounds of unitless snowfall ratio (prsnratio = prsn/pr):  ([0,1], [0.0001,0.9999])	0.5° grid, daily	Derived from bias-adjusted and downscaled pr and prsnratio from GFDL-ESM4, IPSL-CM6A-LR, MPI-ESM1-2-HR, MRI-ESM2-0, and UKESM1-0-LL simulations generated for CMIP6.
Surface Air Pressure	<b>ps</b>	Pa ([480, 110000])	0.5° grid, daily	Bias-adjusted and downscaled from GFDL-ESM4, IPSL-CM6A-LR, MPI-ESM1-2-HR, MRI-ESM2-0, and UKESM1-0-LL simulations generated for CMIP6.
Surface Downwelling Longwave Radiation	<b>rlds</b>	W m-2 ([40, 600])	0.5° grid, daily	Bias-adjusted and downscaled from GFDL-ESM4, IPSL-CM6A-LR, MPI-ESM1-2-HR, MRI-ESM2-0, and

				UKESM1-0-LL simulations generated for CMIP6.
Surface Downwelling Shortwave Radiation	<b>rsds</b>	W m <sup>-2</sup> ([0, 500])  Maximum range and inner bounds of normalized rsds used during bias adjustment: ([0,1], [0.0001, 0.9999])	0.5° grid, daily	Bias-adjusted and downscaled from GFDL-ESM4, IPSL-CM6A-LR, MPI-ESM1-2-HR, MRI-ESM2-0, and UKESM1-0-LL simulations generated for CMIP6.
Near-Surface Wind Speed	<b>sfcwind</b>	m s <sup>-1</sup> ([0.1, 50], [0.01,∞[)	0.5° grid, daily	Bias-adjusted and downscaled from GFDL-ESM4, IPSL-CM6A-LR, MPI-ESM1-2-HR, MRI-ESM2-0, and UKESM1-0-LL simulations generated for CMIP6.
Near-Surface Air Temperature	<b>tas</b>	K ([183.15, 343.15])	0.5° grid, daily	Bias-adjusted and downscaled from GFDL-ESM4, IPSL-CM6A-LR, MPI-ESM1-2-HR, MRI-ESM2-0, and UKESM1-0-LL simulations generated for CMIP6.
Daily Maximum Near-Surface Air Temperature	<b>tasmax</b>	K ([183.15, 343.15])  Maximum range and inner bounds considered for tasrange: ([0.01, ∞[, [0.01,∞[)  Maximum range and inner bounds considered for unitless tasskew: ([0,1], [0.0001,0.9999])	0.5° grid, daily	Derived from bias-adjusted and downscaled tasrange = tasmax - tasmin and tasskew = (tas - tasmin) / (tasmax - tasmin) from GFDL-ESM4, IPSL-CM6A-LR, MPI-ESM1-2-HR, MRI-ESM2-0, and UKESM1-0-LL simulations generated for CMIP6.
Daily Minimum Near-Surface Air Temperature	<b>tasmin</b>	K ([183.15, 343.15])  Maximum range and inner bounds considered for tasrange: ([0.01, ∞[, [0.01,∞[)  Maximum range and inner bounds considered for unitless	0.5° grid, daily	Derived from bias-adjusted and downscaled tasrange = tasmax - tasmin and tasskew = (tas - tasmin) / (tasmax - tasmin) from GFDL-ESM4, IPSL-CM6A-LR, MPI-ESM1-2-HR, MRI-ESM2-0, and UKESM1-0-LL simulations generated for CMIP6.

		tasskew: ([0,1], [0.0001,0.9999])		
--	--	--------------------------------------	--	--

454  
455 For the pre-industrial conditions, 500 years of piconrol output data are used and harmonised across  
456 [General Circulation Models \(GCMs\)](#) with respect to the time range they cover. This is possible because  
457 piconrol data only carry nominal year labels. We shift the GCM-specific piconrol time ranges listed in  
458 **Table 4** to 1601–2100. For the historical and future climate conditions, we provide input data for 1850–  
459 2014 and 2015–2100, respectively, in line with the time ranges covered by the corresponding CMIP6  
460 experiments. The common time axis is important as the use of the input data should be harmonised across  
461 all sectors. In particular, the year-by-year combination of the pre-industrial [CRFclimate-related forcing](#)  
462 with the historical [DHFdirect human forcing](#) should be done in the same way across all sectors and models.  
463

464 **Selection of climate models.** To limit the number of mandatory impact simulations and hence lower the  
465 barrier to participation in ISIMIP3b, we provide climate input data for only five selected CMIP6 climate  
466 models. The basic characteristics of the five GCMs are listed in **Table 4**. The models were selected based  
467 on data availability at the selection time (late 2019 to early 2020), performance in the historical period,  
468 structural independence, process representation and equilibrium climate sensitivity (ECS).  
469

470 To be included in ISIMIP3b, a GCM had to provide daily data for all variables listed in **Table 3** except for  
471 [near-surface specific humidity \(huss\)](#) (which was derived from [near-surface relative humidity \(hurs\)](#), [surface air](#)  
472 [pressure \(ps\)](#) and [near-surface air temperature \(tas\)](#), see below), ps if sea level pressure (psl) was available,  
473 so a proxy for ps could be computed based on psl and tas, and [near-surface wind speed \(sfcwind\)](#) if zonal  
474 and meridional near-surface wind components (uas, vas) were available, so a proxy for sfcwind could be  
475 computed based on uas and vas. Those daily data had to cover 500 piconrol years and all years of the  
476 historical, SSP1-2.6, SSP3-7.0, and SSP5-8.5. In addition, we favoured GCMs that provided the additional  
477 input data needed for the tropical cyclone modelling (**Table 5**) and the fisheries and marine ecosystems  
478 sector (FishMIP; **Table 10**).  
479

480 **Table 4:** Characteristics of CMIP6 climate models used in ISIMIP3b. Columns show (from left to right) the  
481 climate model acronym, the horizontal grid size (longitude x latitude) of the original atmospheric output  
482 data, the ensemble member used, the nominal time range covered by the piconrol data used, the  
483 [equilibriumeffective](#)equilibrium climate sensitivity (ECS) according to (Meehl et al., 2020), and the main  
484 model reference paper and the CMIP6 simulation data publications used. For definitions of climate model  
485 acronyms and modelling groups see (Durack, n.d.).

GCM	Grid size	Member	piconrol	ECS	References
GFDL-ESM4	288 x 180	r1i1p1f1	0001–0500	2.6°C	(Dunne et al., 2020; John et al., 2018; Krasting et al., 2018)
IPSL-CM6A-LR	144 x 143	r1i1p1f1	1870–2369	4.6°C	(Boucher et al., 2018, 2019, 2020)

MPI-ESM1-2-HR	384 x 192	r1i1p1f1	1850–2349	3.0°C	(Jungclaus et al., 2019; Mauritsen et al., 2019; Schupfner et al., 2019)
MRI-ESM2-0	320 x 160	r1i1p1f1	1850–2349	3.2°C	(Yukimoto, Kawai, et al., 2019; Yukimoto, Koshiro, et al., 2019a, 2019b)
UKESM1-0-LL	192 x 144	r1i1p1f2	1960–2459	5.3°C	(Good et al., 2019; Sellar et al., 2019; Tang et al., 2019)

486

487

488 According to a skill analysis (see **Figure 2**), the GCMs ACCESS-CM2, AWI-CM-1-1-MR, CESM2, CESM2-  
489 WACCM, CMCC-ESM2, EC-Earth3-AerChem, GFDL-CM4, GFDL-ESM4, HadGEM3-GC31-LL, HadGEM3-  
490 GC31-MM, MPI-ESM1-2-HR, MPI-ESM1-2-LR, MRI-ESM2-0, NorESM2-MM, SAM0-UNICON, TaiESM1, and  
491 UKESM1-0-LL perform relatively well in reproducing the main historically observed characteristics of the  
492 atmosphere. From that list, only GFDL-ESM4, MPI-ESM1-2-HR, MRI-ESM2-0, and UKESM1-0-LL provided  
493 all required daily data at the time of model selection. Another model that fulfilled all those data  
494 requirements and shows an average performance in the historical period is IPSL-CM6A-LR. These five  
495 GCMs were selected to be used in ISIMIP3b. With the exception of GFDL-ESM4, these models also provide  
496 the data needed for tropical cyclone modelling. GFDL-ESM4 is the model providing the most  
497 comprehensive oceanic bio-geochemical forcings for FishMIP while other models cover less and partly  
498 other oceanic variables (see **Table 816**). Three of the climate models (GFDL-ESM4, IPSL-CM6A-LR,  
499 UKESM1-0-LL) are successors of models already used in ISIMP2b and in the ISIMIP Fast Track.

500

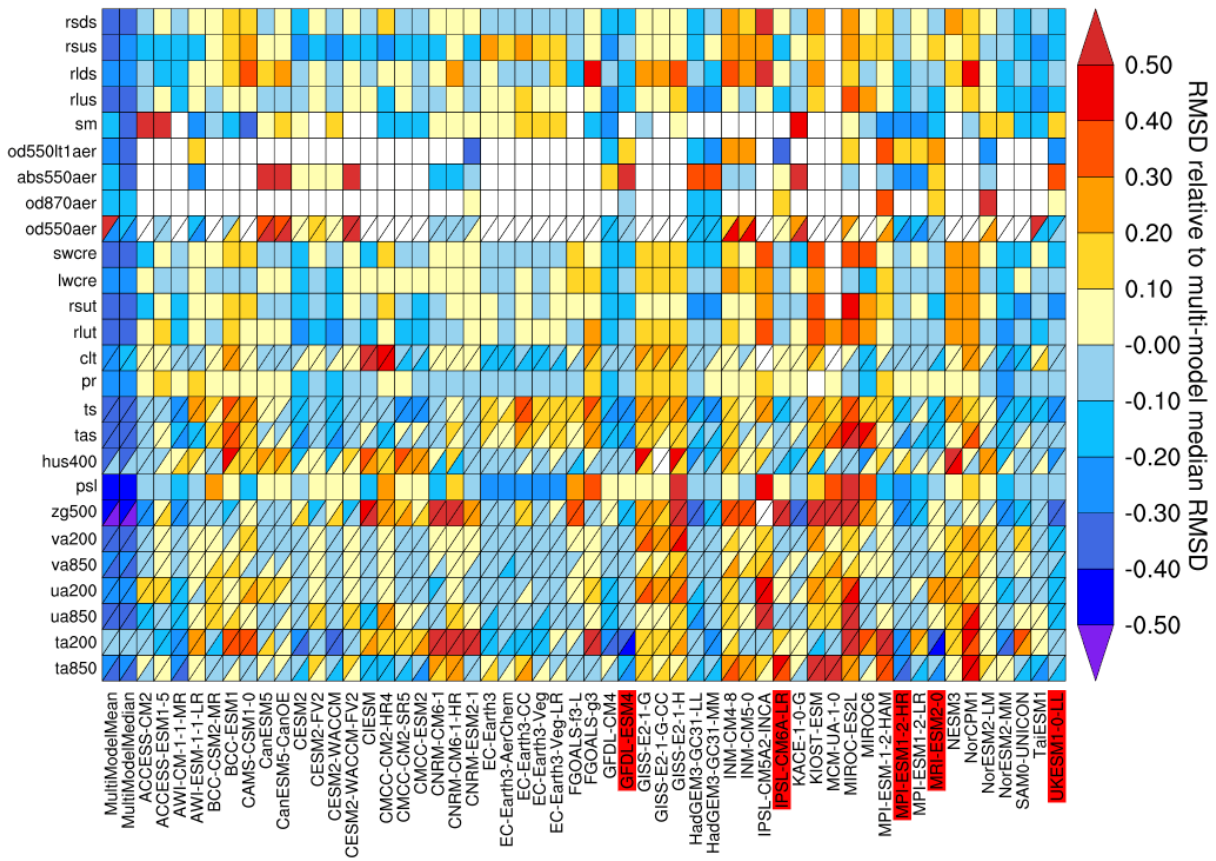


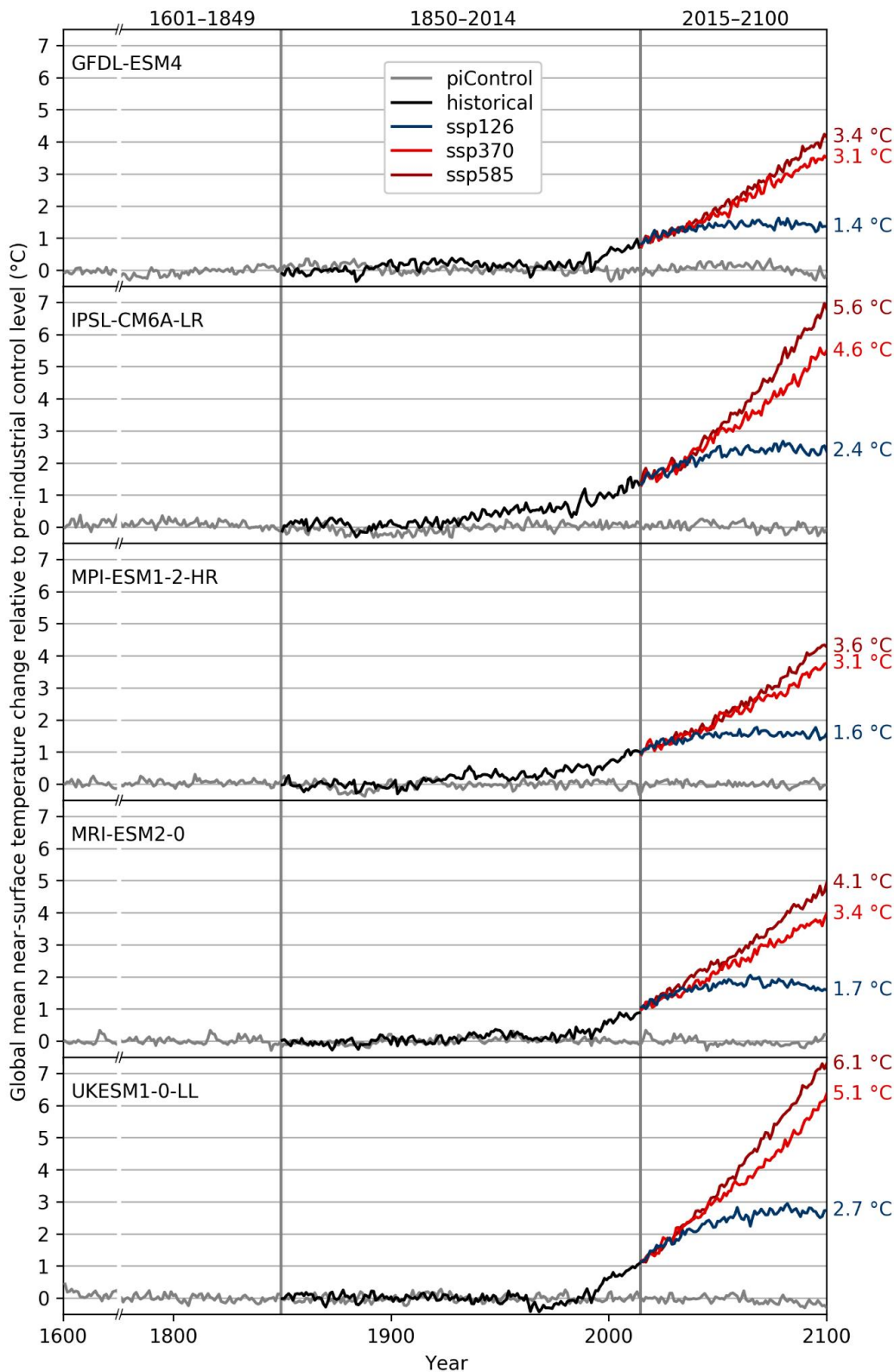
**Figure 2:** Relative space-time root-mean-square deviation (RMSD) calculated from the climatological seasonal cycle of the CMIP6 historical simulations (1980–1999) compared to observational datasets, for various CMIP6 GCMs (columns) and climate variables (rows), similar to Fig. 6 of (Bock et al., 2020). A relative performance is displayed, with blue shading being better and red shading worse than the median RMSD of all model results of the CMIP6 ensemble. A diagonal split of a grid square shows the relative error with respect to the reference data set (lower right triangle) and an alternative data set (upper left triangle), as listed in Table 5 of (Bock et al., 2020). White boxes are used when data are not available for a given model and variable. Models selected for ISIMIP3b are highlighted in red. Variables are (from top to bottom): Surface Downwelling Shortwave Radiation (rsds), Surface Upwelling Shortwave Radiation (rsus), Surface Downwelling Longwave Radiation (rlds), Surface Upwelling Longwave Radiation (rlus), Soil Moisture (sm), Ambient Fine Aerosol Optical Depth at 550 nm (od550lt1aer), Ambient Aerosol Absorption Optical Thickness at 550 nm (abs550aer), Ambient Aerosol Optical Depth at 870 nm (od870aer), Ambient Aerosol Optical Thickness at 550 nm (od550aer), Shortwave Cloud Radiative Effect (swcre), Longwave Cloud Radiative Effect (lwcre), Top-of-Atmosphere Outgoing Shortwave Radiation (rsut), Top-of-Atmosphere Outgoing Longwave Radiation (rlut), Total Cloud Cover Percentage (clt), Precipitation (pr), Surface Temperature (ts), Near-Surface Air Temperature (tas), Specific Humidity at 400 hPa (hus400), Sea Level Pressure (psl), Geopotential Height at 500 hPa (zg500), Northward Wind at 200 hPa (va200), Northward Wind at 850 hPa (va850), Eastward Wind at 200 hPa (ua200), Eastward Wind at 850 hPa (ua850), Air Temperature at 200 hPa (ta200), and Air Temperature at 850 hPa (ta850). Produced with ESMValTool v2.0 (Andela et al., 2020b, 2020a; Righi et al., 2020).

The five GCMs are structurally independent in terms of their ocean and atmosphere model components. Furthermore, all of them have a coupled climate and carbon cycle and in some cases, fully interactive

524 chemistry and aerosol components. We favoured models that applied prognostic couplings between  
525 processes and model domains wherever possible to maximise the coverage of simulated feedbacks.

526  
527 The five GCMs provide a good representation of both the mean and the range of the full CMIP6 multi-  
528 model ensemble ECS. According to (Meehl et al., 2020), the CMIP6 multi-model mean ECS is 3.7°C, which  
529 is precisely met by the mean ECS of the five ISIMIP3b GCMs. The transient climate response (TCR) of 2.0°C  
530 is also precisely met. This provides an improvement over ISIMIP2b, in the sense of the selected GCM  
531 subset reflecting the statistics of the larger CMIP ensemble. In ~~ISIMIP2b~~ that case the mean ECS for the full  
532 CMIP5 was 3.2°C compared with a mean ECS of 3.72°C for the four ISMIP2b GCMs (see Table S1 and S2 in  
533 (Jägermeyr et al., 2021)). The ISIMIP3b ensemble includes three models with below-average ECS (GFDL-  
534 ESM4, MPI-ESM1-2-HR, MRI-ESM2-0) and two models with above-average ECS (IPSL-CM6A-LR, UKESM1-  
535 0-LL) (see **Table 412**). In line with their ECS values, we find GFDL-ESM4 and UKESM1-0-LL to project the  
536 weakest and strongest global warming, respectively, under any future scenario considered (see **Figure 3**).  
537 Under SSP5-8.5, the global mean near-surface temperature in 2100 is about 3°C larger in UKESM1-0-LL  
538 than in GFDL-ESM4. Under SSP1-2.6, the projections are about 1.5°C apart. The ensemble mean warming  
539 of the ISIMIP3b CMIP6 models is significantly higher than the warming of the ISIMIP2b CMIP5 models,  
540 across global land area by an average of 0.3°C, but over the main breadbasket cropland regions by more  
541 than 0.5°C between 1983–2013 and 2069–2099, under both SSP1-2.6 and SSP5-8.5 (Table S1 in (Jägermeyr  
542 et al., 2021)). This is in line with the higher median ECS in CMIP6 compared to CMIP5; indeed, some CMIP6  
543 models have an ECS above the assessed likely (2.5°C to 4°C) and very likely (2°C to 5°C) ranges in the IPCC's  
544 sixth assessment report (AR6) (Forster et al., 2021). **The reasons for these higher estimates of ECS are**  
545 **complex, with cloud feedback processes playing an important role** (Zelinka et al., 2020). **While the**  
546 **plausibility of the very high ECS estimates has been questioned, recent studies indicate CMIP6 models**  
547 **with high ECS tend to simulate cloud properties better than low ECS models** (Bock & Lauer, 2024); **also,**  
548 **unaccounted natural variability may have biased the IPCC's assessed ranges somewhat low** (Liang et al.,  
549 2024; Watanabe et al., 2024)(Liang et al., 2024; Watanabe et al., 2024).;

550  
551 **The ISIMIP3b ensemble reflects the spread in ECS of the overall CMIP6 ensemble, with two models above**  
552 **the AR6 likely range and one of these (UKESM1-0-LL) above the very likely range. The strong warming**  
553 **response of these models should be kept in mind when conducting ISIMIP3b-based impacts studies.**  
554 **However, depending on the region and variable of interest, the high ECS does not necessarily have any**  
555 **bearing on the magnitude or realism of projected regional impacts, and any further selection of models**  
556 **should not be based solely on ECS but on the models' suitability for the impacts variables in question**  
557 **(Swaminathan et al., 2024)(Swaminathan et al., 2024). In many applications, results can be harmonized**  
558 **by describing the simulated impacts in terms of global mean temperature changes instead of time for the**  
559 **different emission scenarios.**



561  
562  
563  
564  
565  
566

**Figure 3:** Time series of annual global mean near-surface temperature change relative to pre-industrial levels (1601–1849 average) as simulated with GFDL-ESM4, IPSL-CM6A-LR, MPI-ESM1-2-HR, MRI-ESM2-0 and UKESM1-0-LL (from top to bottom). Colour coding indicates the underlying CMIP6 experiments (grey: pre-industrial control, black: historical, blue: SSP1-2.6, light red: SSP3-7.0, dark red: SSP5-8.5) with corresponding time periods given at the top. Numbers to the right of the plot represent end-of-century warming levels under the different future

scenarios, expressed as the global multi-year mean near-surface temperature change from 1601–1849 to 2070–2100.

**Bias adjustment and statistical downscaling.** To make the GCM-based climate forcing usable for the impact modellers we apply a bias adjustment ensuring that the GCM simulations match the observed distribution of climate data over the historical reference period (1979–2014). In addition to the bias adjustment a statistical downscaling to our standard 0.5° grid is included in the pre-processing of the surface and near-surface atmospheric variables (see **Table 311**). The method used for the bias adjustment and statistical downscaling (BASD) in ISIMIP3b is version 2.5 of ISIMIP3BASD (Lange, 2019b, 2021a).

ISIMP3BASD has several advantages compared to the method used for bias adjustment and statistical downscaling in ISIMIP2b (Frieler et al., 2017; Lange, 2017, 2018). First, it clearly separates the adjustment of biases in climate model output at 1° or 2° resolution, whatever is closest to the original output data, from the statistical downscaling to the target resolution of 0.5°. Compared to ISIMIP2b, where climate model output was first spatially interpolated to the target resolution and then bias-adjusted, the new approach avoids the associated underestimation of ~~improves~~ the spatial variability at the target resolution (Lange, 2019b). Second, the new quantile mapping method preserves trends in each quantile of the distribution of the daily data and adjusts biases in distribution quantiles of the daily data more accurately than the ISIMIP2b bias adjustment methods (Lange, 2019b).

For trend preservation, we first produce pseudo-future observations by shifting the historically observed daily data by the simulated future climate change. Here, the signal of climate change is the difference or the ratio between the inverse empirical cumulative distribution function of the historical period and the respective distribution functions of each 36-year period of the future. Using the difference ensures additive trend preservation and using the ratio ensures multiplicative trend preservation under bias adjustment. We apply additive trend preservation for near-surface air temperature (tas), sea level pressure (psl, see **Table 36**), and surface downwelling longwave radiation (rlds). We apply primarily multiplicative trend preservation for precipitation including snowfall (pr), near-surface wind speed (sfcWind), and the range (tasrange = tasmax - tasmin) between the daily maximum and minimum near-surface air temperatures (tasmax and tasmin, respectively) that can transition smoothly to additive trend preservation for data with large negative biases in the historical period (Lange, 2019b). In a second step, the future simulations are mapped onto the pseudo-future observations by quantile mapping. Both steps, the generation of the pseudo future observations and the quantile mapping of the future simulations onto the pseudo observations, are applied for each day of the year separately. The distributions include data from the 31 days around the considered day and all years of the reference or future period, respectively. This means a sample size of 31x36 values for each day of the year. Through this approach the bias adjustment implicitly also adjusts the multi-year mean annual cycle and a mix of year-to-year and day-to-day variability (Haerter et al., 2011).

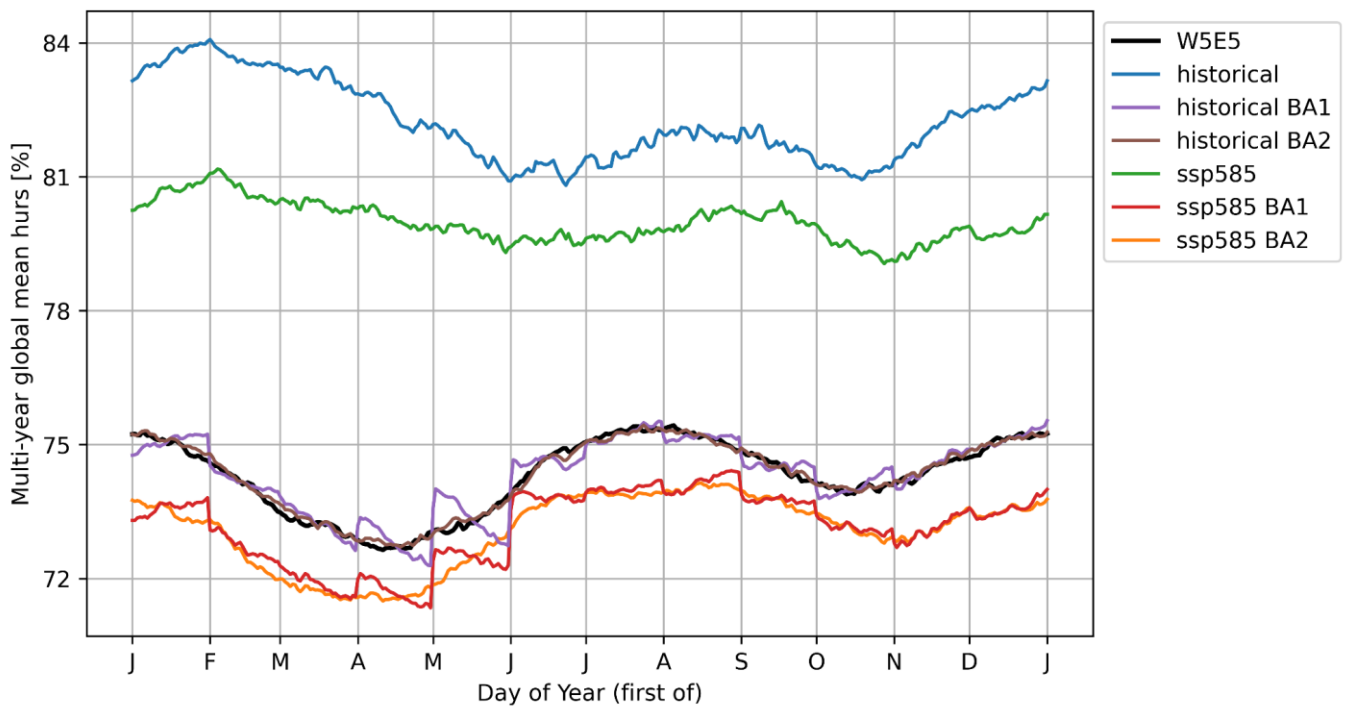
In addition, the method adjusts the frequency of daily data falling outside of the inner bounds specified in **Table 311** (e.g. the dry day frequency, i.e. the number of days with precipitation below 0.1 mm day<sup>-1</sup>).

608  
609  
610  
611  
612  
613  
614  
615  
616  
617  
618  
619  
620  
621  
622  
623  
624  
625  
626  
627  
628  
629  
630  
631  
632

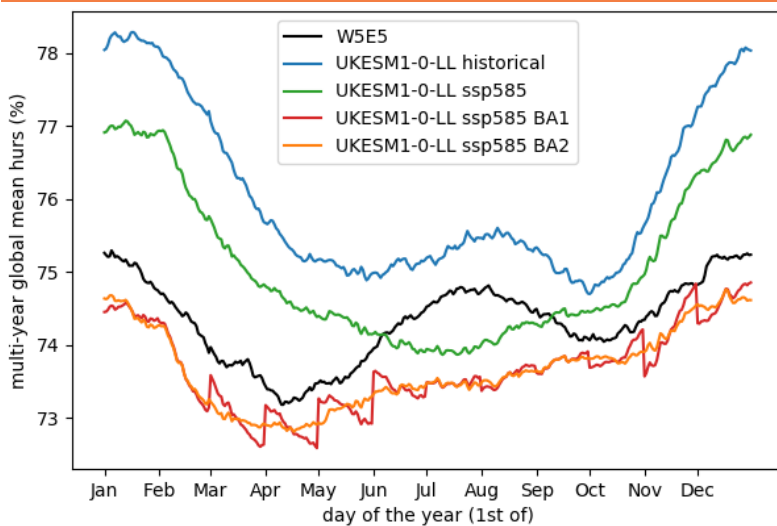
Four variables were adjusted and downscaled indirectly: near-surface specific humidity (huss) was derived from adjusted and downscaled near-surface relative humidity (hurs), surface air pressure (ps), and near-surface air temperature (tas) using the equations of (Buck, 1981) as described in (Weedon et al., 2010), snowfall (prsn) was derived from adjusted and downscaled precipitation including snow (pr) and the snowfall ratio (prsnratio = prsn / pr), and daily maximum and daily minimum near-surface air temperatures (tasmax and tasmin, respectively) were derived from adjusted and downscaled tas, and the tasrange = tasmax - tasmin and skewness of the daily temperature cycle tasskew = (tas - tasmin) / (tasmax - tasmin).

The basic characteristics of ISIMIP3BASD (version 1.0) are described in (Lange, 2019b). However, the method finally used to generate the forcing data now provided within ISIMIP3b (ISIMIP3BASD version 2.5) deviates from the original version in some aspects. In the following we describe the most important updates of the procedure relative to the one described in (Lange, 2019b). For a complete list of differences between the two versions of the BASD method and the full history of which feature was added in which update, see the CHANGELOG included in the archive of code version 2.5 (Lange, 2021a).

In (Lange, 2019b) the bias-adjustment was applied on a monthly basis, i.e. the pseudo-future observations and the quantile mapping described above was applied to all daily January data, February data and so forth. This approach can introduce discontinuities at the transition from one month to another (see **Figure 4**). That is why for ISIMIP3b the adjustment is done in the running window mode with steps of one day and a window width of 31 days as described above. This approach resolves the discontinuity issue (see **Figure 4**), as suggested by (Thiemeßl et al., 2012); (Thrasher et al., 2012); (Gennaretti et al., 2015); and (Grenier, 2018).



633



634

635 Figure 4: Global multi-year daily mean near-surface relative humidity for UKESM1-0-LL historical (1979-  
 636 2014) and SSP5-8.5 (2065-2100), with uncorrected historical simulated data in blue, uncorrected  
 637 future simulated data in green, historical bias-adjusted data in purple and brown, future bias-adjusted data in red and  
 638 orange, and observational reference data in black. The bias is effectively reduced throughout all days of the year  
 639 (brown line closely matching the black line) when a smooth annual cycle is produced if ISIMIP3BASD v2.5 is applied  
 640 in running-window mode in steps of one day (brown and orange, BA2). In contrast, a month-by-month application,  
 641 which was the only option in ISIMIP3BASD v1.0, generates discontinuities at each turn of the month (purple and  
 642 red, BA1).

643

644 Since ps, rlds and tas can show significant trends within the 36-year training and application periods  
 645 ISIMIP3BASD v1.0 includes a detrending of these variables within these intervals before the pseudo future  
 646 observations and the transfer functions are estimated and applied. Afterwards the trend is added back  
 647 again. This is done to prevent the confusion of trends with interannual variability during quantile mapping

(Lange, 2019b; Maraun, 2013). In contrast to v1.0, in v2.5, applied to generate the ISIMIP3b forcings data, the detrending is only applied if the trend is significantly different from zero at the 5% level.

We also changed the method used to generate future pseudo-observations of bounded variables (equations (8) and (9) of (Lange, 2019b)), in order to stabilise results in some edge cases. If, e.g., the historically observed relative dry-day frequency was 0.0 while the simulated frequency was 0.8 for the historical period and 0.9 for some future period, then, according to equation (9) of (Lange, 2019b), the future pseudo-observed frequency would be equal to  $1 - (1 - 0.0)(1 - 0.9)/(1 - 0.8) = 0.5$ . As this is considered unrealistic we apply a revised version of equation (9) of (Lange, 2019b) that reads

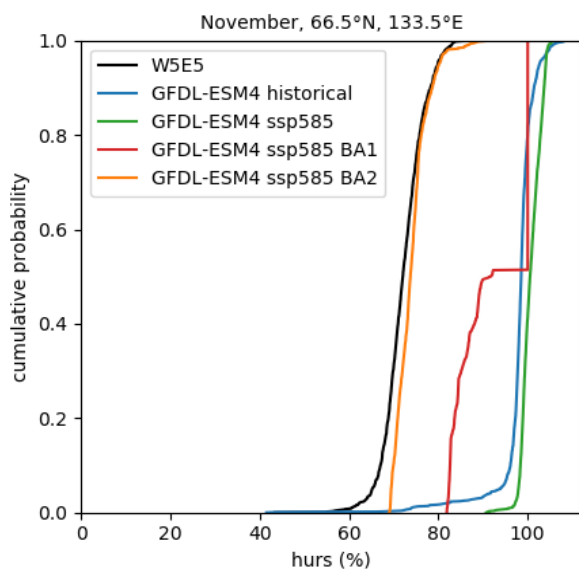
$$P^{obs}_{fut} = \begin{cases} P^{sim}_{fut} & \text{if } P^{sim}_{hist} = P^{obs}_{hist}, \\ 0 + (P^{obs}_{hist} - 0)(P^{sim}_{fut} - 0)/(P^{sim}_{hist} - 0) & \text{if } P^{sim}_{fut} \leq P^{sim}_{hist} > P^{obs}_{hist}, \\ 1 - (1 - P^{obs}_{hist})(1 - P^{sim}_{fut})/(1 - P^{sim}_{hist}) & \text{if } P^{sim}_{fut} \geq P^{sim}_{hist} < P^{obs}_{hist}, \\ P^{obs}_{hist} + P^{sim}_{fut} - P^{sim}_{hist} & \text{otherwise.} \end{cases} \quad (1)$$

In this revised relation, the otherwise case applies if  $P^{sim}_{fut} < P^{sim}_{hist} < P^{obs}_{hist}$  or  $P^{sim}_{fut} > P^{sim}_{hist} > P^{obs}_{hist}$ . Hence it applies to the aforementioned edge case, where it produces a less extreme future pseudo-observed relative frequency of  $0.0 + 0.9 - 0.8 = 0.1$ . Equation (8) of (Lange, 2019b) was revised analogously to equation (9).

Furthermore, we refined the method used to generate future pseudo-observations (step 5 of the bias adjustment algorithm of (Lange, 2019b)) for all variables with at least one bound: In v1.0, the future pseudo observations were generated by transferring simulated trends in all distribution quantiles to the observational reference data. That included trends in, e.g., precipitation quantiles below the wet-day threshold. However, in some cases, the trend transfer turned many dry days into wet days, with a profound impact on the shape of the distribution of future pseudo-observed wet-day precipitation. As a result, simulated trends in wet-day precipitation intensity were not well preserved. In v2.5, trend transfers are restricted to values within threshold. This particularly improves the preservation of trends in wet-day precipitation intensities.

We also modified the bias adjustment method for Near-Surface Relative Humidity (hurs) because ISIMIP3BASD v1.0 turned out to produce unrealistic distributions of hurs under climate change if there are too many cases of supersaturation ( $hurs \geq 100\%$ ) in the simulated data. This is the case for several of the CMIP6 GCMs selected for ISIMIP3b, particularly in high-latitude winter: While no supersaturations are found in the observational reference data, the GCM simulates many supersaturations in the historical reference period and even more so in a future period, under SSP5-8.5 (see **Figure 5**). ISIMIP3BASD v1.0 preserves this projected trend and hence produces future bias-adjusted hurs data with many supersaturations. In v2.5, this trend is no longer preserved. Instead, the supersaturation probability is fixed at the observed level, which is zero or very close to zero in all seasons and grid cells for W5E5. Future

688 pseudo observations of hurs are generated by applying the revised (see above) equation (8) of (Lange,  
 689 2019b) to all hurs values after capping them at 100%. The new approach was motivated by findings from  
 690 (Ruosteenoja et al., 2017, 2018). They analysed hurs data from CMIP5 and showed that (i)  
 691 supersaturations in those data are mostly spurious, resulting from, e.g., inconsistencies in the  
 692 interpolation of temperature and specific humidity to the near-surface level, and (ii) climatological mean  
 693 value trends of hurs become more consistent with trends in relative humidity from the lowest model level  
 694 if hurs is capped at 100% before trends are calculated.



696  
 697  
 698 **Figure 5:** Empirical cumulative distribution functions of near-surface relative humidity in high-latitude winter  
 699 (November, 66.5°N, 133.5°E) for GFDL-ESM4 historical (1979-2014) and SSP5-8.5 (2065-2100), with historical  
 700 simulated data in blue, future simulated data in green, future bias-adjusted data in red and orange, and  
 701 observational reference data in black. The simulated climate change signal is well preserved with ISIMIP3BASD v2.5  
 702 using a fixed supersaturation (hurs  $\geq 100\%$ ) probability and equation (1) applied to all hurs values after capping  
 703 them at 100% to generate future pseudo observations (orange, BA2). In contrast, the simulated climate change  
 704 signal is not well preserved if the supersaturation probability is allowed to change and equations (8) and (9) of  
 705 (Lange, 2019b) are used to generate future pseudo observations of hurs (red, BA1).

706  
 707 In addition, while ISIMIP3BASD v1.0 applies parametric quantile mapping to all climate variables, we used  
 708 a nonparametric approach for the bias adjustment of near-surface relative humidity (hurs), the snowfall  
 709 ratio (prsnratio), surface downwelling shortwave radiation (rsds), and the skewness of the daily  
 710 temperature (tasskew) since the parametric quantile mapping method previously used for those variables  
 711 suffered from occasionally unstable beta distribution fits.

712  
 713 Moreover, the parametric quantile mapping described in (Lange, 2019b) does not only adjust biases in  
 714 quantiles of the simulated daily data but also adjusts biases in the likelihood of individual events, as in  
 715 (Switanek et al., 2017). To avoid overfitting artifacts we did not adjust event likelihoods for ISIMIP3b.

717 Finally, the diurnal temperature range (*tasrange*) was ultimately bias-adjusted using a Weibull  
 718 distribution, not a Rice distribution as described in (Lange, 2019b) because the Weibull distribution fits  
 719 the data better in most cases, in particular in the upper tail.

720  
 721 For further details of the application of ISIMIP3BASD v2.5 for ISIMIP3b, including the exact Python  
 722 commands and application periods used per CMIP6 experiment, see the ISIMIP3b bias adjustment fact  
 723 sheet (Lange, 2021b).

724  
 725 In addition, we use a new observational target dataset. Instead of using the EWEMBI dataset (E2OBS,  
 726 WFDEI and ERAI data merged and bias-corrected for ISIMIP; (Lange, 2019a) in ISIMIP3b we adjust the  
 727 climate forcing data to version 2.0 of the W5E5 dataset (WFDE5 over land merged with ERA5 over the  
 728 ocean; (Lange et al., 2021). The data cover the entire globe at 0.5° horizontal and daily temporal resolution  
 729 from 1979 to 2019. W5E5 v2.0 is derived by applying version 2.0 of the WATCH Forcing Data methodology  
 730 (WFDE5; (Cucchi et al., 2020) to ERA5 reanalysis data (Hersbach et al., 2020) and precipitation data from  
 731 version 2.3 of the Global Precipitation Climatology Project (GPCP; (Adler et al., 2003)).

732  
 733 The statistical downscaling method did not change between v1.0 and v2.5 of ISIMIP3BASD, i.e. for  
 734 ISIMIP3b we use the approach described (Lange, 2019b). This method adds the spatiotemporal variability  
 735 that is missing at the low spatial resolution at which the bias adjustment is done (1° or 2°, depending on  
 736 the GCM), compared to the target resolution of the downscaling (0.5°). The method is a modified version  
 737 of the MBCn algorithm from (Cannon, 2018), which in turn is a stochastic, multivariate, non-parametric  
 738 quantile mapping method. We use it to transfer the statistical relationship between low-resolution and  
 739 high-resolution W5E5 data to the GCM output that was previously bias-adjusted using low-resolution  
 740 W5E5 data. In comparison to the approach used in ISIMIP2b (a spatial interpolation to the target  
 741 resolution followed by a bias adjustment at that resolution), the approach used in ISIMIP3b is less prone  
 742 to inflate temporal variability and deflate spatial variability, i.e. the ISIMIP3b approach produces more  
 743 realistic spatiotemporal variability patterns at the target resolution (Lange, 2019b).

## 745 2.2 Tropical cyclones

746  
 747 **Table 5:** Information about tropical cyclone tracks and windfields provided as climate-related forcing data  
 748 within ISIMIP3b.

Variable	Variable specifier	Unit	Resolution	Datasets
Time associated with a given location of the storm centre	<b>time</b>	hours since 1950-01-01 00:00	along-track, 2-hourly (MIT model) 6-hourly (CHAZ model)	MIT (Emanuel et al., 2008) and -CHAZ (Lee et al., 2018)
Latitudinal coordinate of storm centre	<b>lat</b>	degrees north	along-track, 2-hourly (MIT model) 6-hourly (CHAZ model)	MIT (Emanuel et al., 2008) and -CHAZ (Lee et al., 2018)

Longitudinal coordinate of storm centre	<b>lon</b>	degrees east	along-track, 2-hourly (MIT model) 6-hourly (CHAZ model)	MIT (Emanuel et al., 2008) and -CHAZ (Lee et al., 2018)
Central pressure	<b>pres</b>	hPa	along-track, 2-hourly	MIT (Emanuel et al., 2008)
Maximum 1-minute sustained wind speed	<b>windspatialmax</b>	<del>ms<sup>-1</sup>knots</del>	along-track, 2-hourly (MIT model) 6-hourly (CHAZ model)	MIT (Emanuel et al., 2008) and -CHAZ (Lee et al., 2018)
Radius of maximum wind speeds	<b>rmw</b>	km	along-track, 2-hourly	MIT (Emanuel et al., 2008)
Wind speed on the 850 hPa pressure level	<b>ua850</b> <b>va850</b>	<del>ms<sup>-1</sup>knots (MIT model), ms<sup>-1</sup> (CHAZ model)</del>	along-track, 2-hourly (MIT model) 6-hourly (CHAZ model)	MIT (Emanuel et al., 2008) and -CHAZ (Lee et al., 2018)
Temperature on the 600 hPa pressure level	<b>ta600</b>	K	along-track, 2-hourly (MIT model) 6-hourly (CHAZ model)	MIT (Emanuel et al., 2008) and -CHAZ (Lee et al., 2018)
Frequency of TC occurrence	<b>freqyear</b>	count per year	annual	MIT (Emanuel et al., 2008)
Gridded lifetime maximum 1-minute sustained wind speed	<b>windlifetimemax</b>	ms <sup>-1</sup>	Per storm on a 300 arc-seconds (~10 km) grid	Wind fields calculated with Holland and Emanuel-Rotunno wind profiles (Holland, 1980, 2008) for <del>MIT both sets of synthetic tracks (CHAZ and MIT)</del>
Maximum 24-hourly rainfall total during the whole storm duration	<b>maxrain</b>	mm	per storm on a 300 arc-seconds (~10 km) grid	Maximum 24-hourly rainfall (Zhu et al., 2013) calculated for Holland and Emanuel-Rotunno wind profiles for <del>MIT both sets of synthetic tracks (CHAZ and MIT)</del>

749

750 We provide large ensembles of potential realisations of TC tracks and intensities that are consistent with  
751 the large-scale atmospheric and oceanic conditions simulated by ~~four of the five~~ the 5 ISIMIP3b GCMs (see  
752 **Table 64**) and for a selection of scenarios considered in ISIMIP3b (see **Table 1**). ~~We provide gridded wind~~  
753 ~~(maximum 1-minute sustained wind speeds during the whole duration of the TC) and rainfall (maximum~~  
754 ~~24 hourly amounts of rain during the whole duration of the TC) fields at a spatial resolution of 300 arc-~~  
755 ~~seconds (approximately 10 km) by the same approaches also applied to the historically observed tracks~~  
756 ~~(Frieler et al., 2024a), section 3.2).~~

The tracks are generated by two different statistical-dynamical approaches, the MIT approach and the CHAZ approach detailed below. ~~that, forced by data from the ISIMIP3b GCMs listed in data (see Table 64), these allow generating large ensembles of potential realisations of numerous a large number of synthetic storms.~~ For the MIT, approach, we provide gridded wind (maximum 1-minute sustained wind speeds during the whole duration of the TC) and rainfall (maximum 24-hourly amounts of rain during the whole duration of the TC) fields at a spatial resolution of 300 arc-seconds (approximately 10 km) using the same approaches also applied to the historically observed tracks ((Frieler et al., 2024), section 3.2).

Both methods to generate the TC tracks consist of a genesis, a track, and an intensity module:

~~The MIT approach.~~ Within MIT (Emanuel et al., 2008), the time-evolving state of the atmosphere and ocean surface given by the GCMs is randomly (uniformly distributed in time and space) seeded by weak proto-cyclones (genesis module). The seed disturbances are assumed to move with the GCM-provided large-scale flow in which they are embedded, plus a westward and poleward component owing to planetary curvature and rotation (track module). Their intensity is calculated using the Coupled Hurricane Intensity Prediction System (CHIPS; (Emanuel et al., 2004), a simple axisymmetric hurricane model coupled to a reduced upper ocean model to account for the effects of upper ocean mixing of cold water to the surface (intensity module). Applied to the synthetically generated tracks, this model simulates which of the seeded proto-cyclones develop into TCs, reaching maximum 1-minute sustained wind speeds of at least 35 knots, or dissipate due to unfavourable environments. The probabilistic seeding of proto-cyclones is repeated until the desired number of storms per year is reached (in our case, 1500). For each year, the share of proto-cyclones that dissipated in the process is used to derive an estimate of annual TC occurrences (**freqyear**). Extensive comparisons to historical events (Emanuel et al., 2008) have revealed that the statistical properties of the simulated events are consistent with historical TC genesis.

~~1500 tracks were generated globally and F~~for each year of the ISIMIP3b period 1850—2100 (except for GFDL-ESM4, where tracks were only generated for 1850-2014 and 2061-2100, and MRI-ESM2-0 for 1950-2100, see **Table 1**), 1500 tracks were generated, globally. Depending on the application, a simple subsampling (Meiler et al., 2022) or a more advanced bias-correction and emulation procedure (Geiger et al., 2021) might be necessary to extract properly-sized sets of potential realisations from the MIT ensembles.

The “ISIMIP3b tropical cyclone tracks MIT” dataset shall only be used for noncommercial purposes, including teaching and research at universities, colleges and other educational institutions, research at non-profit research institutions, and personal non-profit purposes. It is accessible through the ISIMIP data portal after agreeing to the corresponding license.

For using the tracks for commercial purposes, including but not restricted to consulting activities, software or data products, and a commercial entity participating in research projects, please contact Kerry Emanuel (MIT, email: emanuel@mit.edu) for an appropriate license.

~~The MIT track data shall be used for non-commercial research or academic purposes only. Data can be made available by the ISIMIP team upon written consent by Kerry Emanuel (MIT, email: emanuel@mit.edu).~~

795 ~~The~~ **CHAZ approach.** CHAZ (Lee et al., 2018) seed disturbances are also initialised randomly, but, in  
796 contrast to the MIT model, the global seeding rate and the local probabilities are derived from two  
797 versions of a TC genesis index (TCGI, (Tippett et al., 2011) (genesis module) and intended to represent the  
798 environmental conditions instead of being adjusted to produce a prescribed number of TCs. It is noted  
799 that CHAZ’s projection of global and basin-wide TC annual frequency is sensitive to the choice of the  
800 particular variable used to represent moisture in its genesis module. Simulations using column relative  
801 humidity (CRH) as the moisture variable tend to project an overall increase in global TC frequency, while  
802 those using saturation deficit (SD) show a decrease (Camargo et al., 2014), (Lee et al., 2020). Both  
803 parameters describe how far the atmosphere is from saturation, and they have very similar spatial  
804 patterns in the present climate, so historical data cannot be used to determine which variable is the best  
805 choice to represent the climate. These two configurations reflect the uncertainty of TC frequency  
806 projections (Sobel et al., 2021). Here we provide CHAZ downscaling using both choices of moisture  
807 variable to account for this uncertainty.

808 Similar to MIT, CHAZ then moves the synthetic storms by advection of the environmental steering flow  
809 plus a beta drift (track module). The evolution of synthetic storm intensity is calculated using the  
810 surrounding atmospheric conditions through an empirical multiple linear regression model plus a  
811 stochastic component (intensity module, (Lee et al., 2015, 2016)). The stochastic component accounts for  
812 internal storm dynamics that do not depend explicitly on the environment. While, in MIT, TC occurrence  
813 frequency is provided as an additional variable, in CHAZ, this information is implicitly contained in the  
814 number of TCs that were seeded by the genesis module and that reached TC strength according to the  
815 intensity module.

816 For ISIMIP3b, 20 different CHAZ realisations of the genesis and subsequent tracks are generated with 40  
817 ensemble members each from the intensity module for the historical period and for all RCP-SSP  
818 combinations considered within ISIMIP3b. For each of the 20 realisations, we compute wind and rain fields  
819 for the first ensemble member from the intensity ensemble. The design of 20 realisations allows CHAZ to  
820 generate similar numbers (~1800) of synthetic storms per year per GCM as the MIT models over the  
821 historical period. The exact number of storms per year in CHAZ varies by GCM, by scenario, by the choice  
822 of humidity variables in CHAZ’s genesis component (Lee et al., 2020). On average, CHAZ generates 1817,  
823 1802, 1820, 1810, 1842 storms per year for GFDL-ESM4, IPSL-CM6A-LR, MPI-ESM1-2-HR, MRI-ESM2-0,  
824 and UKESM1-0-LL, respectively. The CHAZ model has been shown to capture the statistical properties of  
825 the observed storms when forced by a global reanalysis data (Lee et al., 2018). Its CMIP6 downscaling  
826 results are reported in (Fosu et al., 2024). (Sobel et al., 2019) used both models to study cyclone risk at  
827 Mumbai, India and showed that MIT and CHAZ generate comparable return periods (frequency of  
828 exceedance) of maximum wind speeds at landfall. However, a frequency bias-correction might still be  
829 necessary, depending on the application (Meiler et al., 2022).

830 The “ISIMIP3b tropical cyclone tracks (CHAZ)” dataset shall only be used for non-commercial purposes,  
831 including teaching and research at universities, colleges and other educational institutions, research at  
832 non-profit research institutions, and personal non-profit purposes. It is accessible through the ISIMIP data  
833 portal after agreeing to the corresponding license.

834 For using the tracks for commercial purposes, including but not restricted to consulting activities, software  
 835 or data products, and a commercial entity participating in research projects, please contact Chia-Ying Lee  
 836 (Columbia University, email: [cl3225@columbia.edu](mailto:cl3225@columbia.edu)) for an appropriate license.

837 ~~⊖~~  
 838 ~~The track data generated by the CHAZ approach shall be used for non-commercial research or academic~~  
 839 ~~purposes only. Data can be made available by the ISIMIP team upon written consent by Chia-Ying Lee~~  
 840 ~~(Columbia University, email: [cl3225@columbia.edu](mailto:cl3225@columbia.edu)).~~

841  
 842 **Table 6:** Climate input data interpolated to 2° horizontal resolution and provided without bias adjustment  
 843 for tropical cyclone modelling with MIT and CHAZ.

Variable	Variable specifier	Unit	Resolution	Datasets
Sea Water Potential Temperature	<b>thetao</b>	°C	2° grid, model specific levels (m from surface to 200m depth), monthly	<a href="#">GFDL-ESM4</a> , IPSL-CM6A-LR, MPI-ESM1-2-HR, MRI-ESM2-0, and UKESM1-0-LL simulations generated for CMIP6.
Sea Surface Temperature	<b>tos</b>	°C	2° grid over the ocean, monthly	<a href="#">GFDL-ESM4</a> , IPSL-CM6A-LR, MPI-ESM1-2-HR, MRI-ESM2-0, and UKESM1-0-LL simulations generated for CMIP6.
Surface Temperature	<b>ts</b>	K	2° grid covering land and ocean areas, monthly	<a href="#">GFDL-ESM4</a> , IPSL-CM6A-LR, MPI-ESM1-2-HR, MRI-ESM2-0, and UKESM1-0-LL simulations generated for CMIP6.  ts may differ from tos in regions of sea ice where tos refers to temperatures under the ice while ts refers to temperatures at the surface.
Air Temperature	<b>ta</b>	K	2° grid; 15 pressure levels (from 1000 to 30 hPa), monthly	<a href="#">GFDL-ESM4</a> , IPSL-CM6A-LR, MPI-ESM1-2-HR, MRI-ESM2-0, and UKESM1-0-LL simulations generated for CMIP6.
Specific Humidity	<b>hus</b>	kg kg-1	2° grid; 15 pressure levels (from 1000 to 30 hPa), monthly	<a href="#">GFDL-ESM4</a> , IPSL-CM6A-LR, MPI-ESM1-2-HR, MRI-ESM2-0, and UKESM1-0-LL simulations generated for CMIP6.
Relative Humidity at 600 hPa	<b>hur</b>	%	2° grid, monthly	<a href="#">GFDL-ESM4</a> , IPSL-CM6A-LR, MPI-ESM1-2-HR, MRI-ESM2-0, and UKESM1-0-LL simulations generated for CMIP6.

Precipitable water (water vapour content vertically integrated through the atmospheric column)	<b>prw</b>	kg m <sup>-2</sup>	2° grid, monthly	<a href="#">GFDL-ESM4</a> , IPSL-CM6A-LR, MPI-ESM1-2-HR, MRI-ESM2-0, and UKESM1-0-LL simulations generated for CMIP6.
Sea Level Pressure	<b>psl</b>	Pa	2° grid, monthly	<a href="#">GFDL-ESM4</a> , IPSL-CM6A-LR, MPI-ESM1-2-HR, MRI-ESM2-0, and UKESM1-0-LL simulations generated for CMIP6.
Eastward Wind	<b>ua</b>	m s <sup>-1</sup>	2° grid; 200, 250, 850 hPa; monthly	<a href="#">GFDL-ESM4</a> , IPSL-CM6A-LR, MPI-ESM1-2-HR, MRI-ESM2-0, and UKESM1-0-LL simulations generated for CMIP6.
Northward Wind	<b>va</b>	m s <sup>-1</sup>	2° grid; 200, 250, 850 hPa; monthly	<a href="#">GFDL-ESM4</a> , IPSL-CM6A-LR, MPI-ESM1-2-HR, MRI-ESM2-0, and UKESM1-0-LL simulations generated for CMIP6.
Eastward Wind	<b>ua</b>	m s <sup>-1</sup>	2° grid; 250, 850 hPa; daily	<a href="#">GFDL-ESM4</a> , IPSL-CM6A-LR, MPI-ESM1-2-HR, MRI-ESM2-0, and UKESM1-0-LL simulations generated for CMIP6.
Northward Wind	<b>va</b>	m s <sup>-1</sup>	2° grid; 250, 850 hPa; daily	<a href="#">GFDL-ESM4</a> , IPSL-CM6A-LR, MPI-ESM1-2-HR, MRI-ESM2-0, and UKESM1-0-LL simulations generated for CMIP6.

844

## 845 2.3 Coastal water levels

846

847 **Table 7:** Coastal water level specifications

Variable	Variable specifier	Unit	Resolution	Datasets
Coastal water levels	<b>cwl</b>	m	custom coastal grid  Hourly or daily maxima	planned

848

849

We do not yet provide coastal water levels as forcing data for ISIMIP3b. However, we plan to generate time series of coastal water levels from 1900 to 2100 at hourly resolution or for daily maxima. The data set and method will be described in a separate manuscript. Similar to the hourly water level dataset of ISIMIP3a (see section 3.3 of (Frieler et al., 2024) and (Treu et al., 2023)), we will combine longer-term annual sea level change with estimates of short-term coastal water level variation. Concerning the long-term sea level change component, we ~~go beyond will further develop~~ the ISIMIP2b approach (Frieler et al., 2017) and use tide gauge, satellite, vertical land motion and global climate model data to constrain a model with observations and IPCC AR6 projections in a Bayesian setting building on (Perrette & Mengel, 2025). ~~The (Perrette & Mengel, 2025) model Modelled global contributions from ice sheets and fingerprints are translated to regional sea level rise via fingerprints. A new aspect is that we include an estimation of vertical land motion to provide relative coastal water levels instead of geocentric coastal water levels. The~~ model allows for smooth projections of relative sea level from observational time series collected at tide gauge stations with an explicit representation of the different components of sea level rise (Perrette & Mengel, submitted 2024). To become usable for ISIMIP3 ~~the approach we will a) extend the approach will be extended~~ to all coastlines and b) use GCM output directly for the global thermosteric and local sterodynamic components (Gregory et al., 2019) of sea level rise, which are modeled by the GCMs. Extension to all coastlines is possible for the ice sheet, glacier and sterodynamic components as they rely on spatial fingerprints or GCM output. Processes driving vertical land motion that are not related to large scale climate processes are however more difficult to model. They are estimated from data as residual vertical land motion in (Perrette & Mengel, 2025). As we do not have data at all coastlines we will extrapolate in time and space the historical rates from tide gauge sites or apply zero rates for this component. Using the explicit component structure of the model, we replace the global thermosteric and the local sterodynamic parts by the output from ISIMIP GCMs. To that end, we reference the gridded sterodynamic simulation data with observations of that component so that they smoothly emerge from the historical period. We do not adjust variability or trends of the GCM data. The method will provide relative sea level projections (including vertical land motion), which can be directly used in coastal impact studies. We plan to estimate the short-term coastal water level variation by a machine-learning approach that is trained to reproduce simulations of the Global TideSurge and SurgeTide Model (GTSM) ~~model~~ driven by ERA5 reanalysis data (Muis et al., 2020) or simulations from HighResMIP (Muis et al., 2023). We are currently testing the dependency of the short-term water level variation on available atmospheric information at GCM resolution. If the predictive power is high enough we will use the findings to provide computationally efficient water level projections specific for the ISIMIP GCMs.

## 2.4 Ocean data

In the default experiments, the ocean variables provided by the GCMs are not subject to bias-adjustment, unlike the atmospheric forcing data (section 2.4.1). This is due to the absence of a comprehensive global observational oceanic dataset to serve as a reference for the adjustment.

However, in order to mitigate potential biases in global impact model simulations stemming from biases in raw oceanic forcing data, we provide a de-biased version to be used in a sensitivity experiment (see **Table 2**). They will be derived from an ocean-biogeochemistry model forced by bias-adjusted monthly

891 atmospheric surface flux data from four of the five ISIMIP3b GCMs. The approach preserves the monthly  
 892 variability of the underlying GCM while the daily variability is added from an independent simulation (see  
 893 section **2.4.2**).

894 For the regional impact model simulations, observational data for individual variables have either been  
 895 applied directly (if the required forcing was observed) to rectify biases in regional oceanic forcings by the  
 896 delta method or have first been translated into the required forcing variable by model simulations (see  
 897 section **2.4.3**). In the delta approach absolute simulated deviations from reference levels are added to the  
 898 observed reference levels. The regional bias-adjustment is independent from the generation of the global  
 899 de-biased forcing data.

900 In order to gauge the effects of these adjustments on the corresponding impact simulations, the protocol  
 901 includes sensitivity experiments (**'de-biased'**) grounded on these adjusted [CRFclimate-related forcings](#)  
 902 (see **Table 2**). The comparison of associated impact simulation to the default ones is expected to provide  
 903 valuable insights into the effects of potential biases in the [CRFclimate-related forcings](#). The 'de-biased'  
 904 experiments are considered a starting point to develop methods to bias-adjust the oceanic forcings in  
 905 further ISIMIP simulation rounds and make these simulations the default ones. Following the ISIMIP  
 906 'consistency framing' the bias-adjustment should also preserve the daily variability of the original GCM  
 907 simulations to allow for a cross-sectoral integration on daily time scale. .

908 **2.4.1 Raw data without bias adjustment (default experiment)**

909 In ISIMIP3b, a set of physical and biogeochemical ocean variables nearly identical to that in ISIMIP3a is  
 910 provided (see section **3.4**, **Table 8** of (Frieler et al., 2023) and **Table 8** below). These variables are obtained  
 911 from the CMIP6 GCMs, which also supply the atmospheric forcing for ISIMIP3b, except for MRI-ESM2-0,  
 912 which lacks bio-geochemical variables. In other models, only certain individual variables are missing (see  
 913 **Table 8**). Obtaining both atmospheric and oceanic variables from the same set of GCMs ensures  
 914 consistency between the fisheries and marine ecosystems sector and other ISIMIP sectors. The available  
 915 variables in ISIMIP3b are interpolated from the native grids of the ocean models to a regular 1° grid. This  
 916 resolution is comparatively lower than that of the ISIMIP3a ocean input data due to the generally reduced  
 917 native resolution of CMIP6 GCM simulations compared to the ocean model used to generate the oceanic  
 918 forcings based on observational atmospheric forcings for ISIMIP3a.

919  
 920 **Table 8:** Oceanic climate-related forcing data provided within ISIMIP3b. Variables with suffixes -bot, -surf,  
 921 and -vint were obtained from the seafloor, the top layer of the ocean, and vertical integration,  
 922 respectively.

Variable	Variable specifier	Unit	Resolution	Datasets
Mass concentration of total phytoplankton expressed as chlorophyll	chl	kg m-3	1° grid, vertically resolved, monthly	GFDL-ESM4, IPSL-CM6A-LR, MPI-ESM1-2-HR, UKESM1-0-LL

Sea floor depth	<b>deptho</b>	m	1° grid, constant	GFDL-ESM4, IPSL-CM6A-LR, MPI-ESM1-2-HR, UKESM1-0-LL
Downward flux of particulate organic carbon	<b>expc-bot</b>	mol m <sup>-2</sup> s <sup>-1</sup>	1° grid, monthly	GFDL-ESM4, IPSL-CM6A-LR, MPI-ESM1-2-HR, UKESM1-0-LL
Particulate organic carbon content	<b>intpoc</b>	kg m <sup>-2</sup>	1° grid, monthly	GFDL-ESM4, MPI-ESM1-2-HR, UKESM1-0-LL
Net primary organic carbon production by all types of phytoplankton	<b>intpp</b>	mol m <sup>-2</sup> s <sup>-1</sup>	1° grid, monthly	GFDL-ESM4, IPSL-CM6A-LR, MPI-ESM1-2-HR, UKESM1-0-LL
Net primary organic carbon production by diatoms	<b>intppdiat</b>	mol m <sup>-2</sup> s <sup>-1</sup>	1° grid, monthly	GFDL-ESM4, IPSL-CM6A-LR, UKESM1-0-LL
Net Primary Organic Carbon Production by Other Phytoplankton	<b>intppmisc</b>	mol m <sup>-2</sup> s <sup>-1</sup>	1° grid, monthly	GFDL-ESM4, IPSL-CM6A-LR, UKESM1-0-LL
Net Primary Mole Productivity of Carbon by Picophytoplankton	<b>intpppico</b>	mol m <sup>-2</sup> s <sup>-1</sup>	1° grid, monthly	GFDL-ESM4
Net Primary Organic Carbon Production of Carbon by Diazotrophs	<b>intppdiaz</b>	mol m <sup>-2</sup> s <sup>-1</sup>	1° grid, monthly	GFDL-ESM4, MPI-ESM1-2-HR
Mixed layer depth defined by delta rho = 0.125	<b>mloitstmax</b>	m	1° grid, monthly	IPSL-CM6A-LR, MPI-ESM1-2-HR, UKESM1-0-LL
Dissolved oxygen concentration	<b>o2, o2-bot, o2-surf</b>	mol m <sup>-3</sup>	1° grid, vertically resolved, ocean bottom and surface fields, monthly	GFDL-ESM4, IPSL-CM6A-LR, MPI-ESM1-2-HR, UKESM1-0-LL

pH	<b>ph, ph-bot, ph-surf</b>	1	1° grid, vertically resolved, ocean bottom and surface fields, monthly	GFDL-ESM4, IPSL-CM6A-LR, MPI-ESM1-2-HR, UKESM1-0-LL
Total phytoplankton carbon concentration	<b>phyc, phyc-vint</b>	mol m-3	1° grid, vertically resolved and vertically integrated, monthly	GFDL-ESM4, IPSL-CM6A-LR, MPI-ESM1-2-HR, UKESM1-0-LL
Concentration of diatoms expressed as carbon in sea water	<b>phydiat, phydiat-vint</b>	mol m-3	1° grid, vertically resolved and vertically integrated, monthly	GFDL-ESM4, IPSL-CM6A-LR, UKESM1-0-LL
Concentration of diazotrophs expressed as carbon in Sea Water	<b>phydiaz, phydiaz-vint</b>	mol m-3	1° grid, vertically resolved and vertically integrated, monthly	GFDL-ESM4, MPI-ESM1-2-HR
Mole Content of Miscellaneous Phytoplankton Expressed as Carbon in Sea Water	<b>phymisc, phymisc-vint</b>	mol m-2	1° grid, vertically resolved and vertically integrated, monthly	GFDL-ESM4, IPSL-CM6A-LR, MPI-ESM1-2-HR, UKESM1-0-LL
Mole Concentration of Picophytoplankton Expressed as Carbon in Sea Water	<b>phypico, phypico-vint</b>	mol m-3	1° grid, vertically resolved and vertically integrated, monthly	GFDL-ESM4
Net Downward Shortwave Radiation at Sea Water Surface	<b>rsndts</b>	W m-2	1° grid, monthly	GFDL-ESM4, IPSL-CM6A-LR, MPI-ESM1-2-HR
Sea Ice Area Fraction	<b>siconc</b>	%	1° grid, monthly	GFDL-ESM4, IPSL-CM6A-LR, MPI-ESM1-2-HR, UKESM1-0-LL

Sea water salinity	<b>so, so-bot, so-surf</b>	0.001	1° grid, vertically resolved, ocean bottom and surface fields, monthly	GFDL-ESM4, IPSL-CM6A-LR, MPI-ESM1-2-HR, UKESM1-0-LL
Sea water potential temperature	<b>thetao</b>	°C	1° grid, vertically resolved, monthly	GFDL-ESM4, IPSL-CM6A-LR, MPI-ESM1-2-HR, UKESM1-0-LL
Ocean model cell thickness	<b>thkcello</b>	m	1° grid, vertically resolved, monthly	GFDL-ESM4, IPSL-CM6A-LR, MPI-ESM1-2-HR, UKESM1-0-LL
Sea water potential temperature at sea floor (bottom)	<b>tob</b>	°C	1° grid, monthly	GFDL-ESM4, IPSL-CM6A-LR, MPI-ESM1-2-HR, UKESM1-0-LL
Sea surface temperature	<b>tos</b>	°C	1° grid, monthly	GFDL-ESM4, IPSL-CM6A-LR, MPI-ESM1-2-HR, UKESM1-0-LL
Sea water zonal velocity	<b>uo</b>	m s-1	1° grid, vertically resolved, monthly	IPSL-CM6A-LR, MPI-ESM1-2-HR, UKESM1-0-LL
Sea water meridional velocity	<b>vo</b>	m s-1	1° grid, vertically resolved, monthly	IPSL-CM6A-LR, MPI-ESM1-2-HR, UKESM1-0-LL
Concentration of mesozooplankton expressed as carbon in sea water	<b>zmeso, zmeso-vint</b>	mol m-3	1° grid, vertically resolved and vertically integrated, monthly	GFDL-ESM4, IPSL-CM6A-LR, UKESM1-0-LL
Concentration of microzooplankton expressed as carbon in sea water	<b>zmicro, zmicro-vint</b>	mol m-3	1° grid, vertically resolved and vertically integrated, monthly	GFDL-ESM4, IPSL-CM6A-LR, UKESM1-0-LL

Total Zooplankton Carbon Concentration	<b>zooc, zooc-vint</b>	mol m-3	1° grid, vertically resolved and vertically integrated, monthly	GFDL-ESM4, IPSL-CM6A-LR, MPI-ESM1-2-HR, UKESM1-0-LL
--	------------------------	---------	---	---

923

924

#### 2.4.2 Bias-adjusted global ocean forcings ('de-biased' sensitivity experiment)

925

926

927

928

929

930

931

932

933

934

935

936

937

938

939

940

941

942

943

944

945

946

947

948

GCMs have been shown to have limitations in accurately representing various aspects of the present climate system (Eyring et al., 2023), (Séférian et al., 2020), that are also expected to affect regional physical and biogeochemical oceanic projections (Li et al., 2016), (Tagliabue et al., 2021). In particular, biases in sea-surface temperature (SST, variable 'tos') and nutricline as well as thermocline depth influence oceanic primary productivity, which in turn has major influence on various marine ecosystem processes. Thus, reducing the substantial biases in GCMs' ocean variables through bias-adjustment is desirable. Typically, for bias-adjustment of atmospheric variables, statistical approaches are used where a transfer function is trained to map the simulated historical distribution of the relevant variables to the observed distribution and then applied to future simulations. Yet for oceanic variables, the scarcity of comprehensive sub-surface observational data globally does not allow for a similar, direct adjustment of the relevant variables. However, standalone ocean-biogeochemistry simulations, when driven by observation-based atmospheric reanalysis data, have been demonstrated to considerably alleviate SST-related biases and typically provide satisfactory simulations of the physical ocean and marine biogeochemistry for the historical period (e.g. (Tsuji et al., 2020), (Barrier et al., 2023)). Thus, an alternative process-oriented bias-adjustment approach has been developed that relies on a comprehensive ocean-biogeochemistry model that is forced by bias-adjusted atmospheric forcings. The adjustment of the ISIMIP3b oceanic forcings builds on such a dynamical de-biasing approach (Lengaigne et al., 2025), which relies on conducting forced oceanic simulations using the NEMO-PISCES physical-biogeochemical ocean model (Madec, 2015), which is the oceanic component of the IPSL-CM6A-LR climate model. The ocean model needs to be forced with high-frequency (3-hourly) surface momentum, heat and freshwater fluxes. Since from the CMIP6 pre-industrial, historical, and future scenario simulations used in ISIMIP3b these variables are only available at monthly resolution, additional steps are necessary to generate climatological high-frequency fluxes first. In the following, we first describe these preparatory steps, and then the de-biasing strategy, in more detail.

949

950

951

952

953

954

955

956

957

958

**High-frequency surface flux forcing.** Initially, a climatological simulation spanning the historical period from 1958 to 2022 is performed by forcing the ocean model NEMO-PISCES with a single repeating annual cycle representative of the 1990s' climate conditions sourced from the "Repeat Year Forcing" (RYF) from JRA55 reanalysis (Stewart et al., 2020). This simulation is driven using the CORE bulk formulae (Large W. G., 2004), incorporating all surface atmospheric variables at 3-hourly resolution from JRA55 RYF as inputs and storing 3-hourly momentum, heat and freshwater fluxes from this simulation. These 3-hourly JRA55 RYF fluxes are added to the monthly seasonal flux anomalies available from the ISIMIP3b climate models for the pre-industrial (picontrol), historical (historical) and future SSP1-2.6 (ssp126), SSP3-7.0 (ssp370), and SSP5-8.5 (ssp585) scenarios. In this way, 3-hourly surface flux forcings are created for all

959 ISIMIP3b scenarios. Notably, this procedure results in sub-monthly variability mirroring that of the JRA55  
960 RYF, rather than the variability simulated by the coupled climate model. This means that any projected  
961 changes in sub-monthly variability due to climate change are not integrated in the final de-biased product.  
962 However, to date, marine ecosystem modellers have not analysed sub-monthly variability anyways (and  
963 most marine ecosystem models are not suited to account for sub-monthly variability of forcings), making  
964 this approach suitable.

965 Alternatively, de-biased ocean simulations including GCM-based sub-monthly variability could be  
966 constructed by an alternative approach. In this scenario, 3-hourly surface atmospheric variables would be  
967 extracted directly from each GCM simulation, rather than from JRA55 RYF forced oceanic simulations.  
968 Forcing NEMO-PISCES with these variables using bulk formulae would once again produce the necessary  
969 3-hourly surface fluxes, this time with variability consistent with the coupled GCM across all timescales.  
970 This approach however requires running a separate ocean simulation for each GCM and scenario to derive  
971 the surface fluxes, necessitating a much larger number of ocean model runs than the approach using  
972 JRA55 RYF. In addition, the 3-hourly input from the GCMs is not available without gaps.

973

974 **De-biasing strategy.** The 3-hourly surface fluxes, constructed as described above, then serve as forcings  
975 for another set of ocean model simulations. Notably, these simulations are not driven with bulk formulae  
976 but directly with surface fluxes to enable an online implementation of the surface heat flux feedbacks  
977 triggered by climate change into the forced ocean biogeochemistry model for historical and future  
978 simulations (Lengaigne et al., 2025). For bias-adjustment, the part of the anomalous surface fluxes that  
979 directly depends on climate change-induced SST warming is separated from the part that does not. Only  
980 the latter part is used as a direct flux input to the ocean model, while the former is implemented within  
981 NEMO-PISCES as an online relaxation to the warming signal from the debiased historical and future  
982 simulations using a spatially and seasonally variable feedback damping coefficient. This SST feedback  
983 coefficient, derived from observed surface variables, represents the Newtonian cooling negative feedback  
984 related to latent heat fluxes through the Clausius-Clapeyron relationship and the negative feedback  
985 related to upward long-wave radiation through Stefan's law (Zhang & Li, 2014) and the positive downward  
986 longwave radiation feedback related to increasing temperature (Shakespeare & Roderick, 2022).  
987 Application of this approach to the ocean model effectively reproduces the global SST changes simulated  
988 by CMIP6 models, as demonstrated in (Lengaigne et al., 2025).

989 In this way, physical and biogeochemical ocean simulations are generated for piconrol and historical  
990 climate forcings as well as for each of the future climate change scenarios, ensuring that the background  
991 climatological state is constrained by the reanalysis, while still accounting for both interannual and long-  
992 term climate variability simulated by the underlying GCM. Consequently, the resulting ocean-  
993 biogeochemistry simulations considerably mitigate the strong present-day climatological biases identified  
994 in the coupled models. Depending on data availability for the relevant monthly fluxes, this de-biasing  
995 procedure can be applied to any climate model.

996 Additionally, to generate observation-based oceanic forcings for ISIMIP3a, a reference simulation is also  
997 forced with the full JRA55 forcing (Tsujino et al., 2018) that includes observed inter-annual and decadal  
998 variability. This oceanic forcing is expected to be a valuable additional [CRFclimate-related forcing](#)  
999 for impact model evaluation within ISIMIP3a akin to the GFDL-MOM6-COBALT2 reanalysis-driven historical

1000 dataset used in ISIMIP3a (Frieler et al., 2024a). The set of variables included in the de-biased dataset is a  
 1001 subset to the one in the raw GCM dataset (**Table 8**), detailed in **Table 9**.

1002  
 1003 **Table 9:** Bias-adjusted ocean data to be used by global impact models in the ‘de-biased’ sensitivity  
 1004 experiment in the fisheries and marine ecosystems sector

Variable	Variable specifier  (variables in brackets are not directly available as model output but will have to be derived in post-processing)	Unit	Resolution	Forcing datasets
Mass concentration of total phytoplankton expressed as chlorophyll	<b>chl</b>	kg m <sup>-3</sup>	1° grid, vertically resolved, monthly	JRA55+IPSL-CM6A-LR
Sea floor depth	<b>deptho</b>	m	1° grid, constant	JRA55+IPSL-CM6A-LR
Downward flux of particulate organic carbon	<b>expc-bot</b>	mol m <sup>-2</sup> s <sup>-1</sup>	1° grid, monthly	JRA55+IPSL-CM6A-LR
Net primary organic carbon production by all types of phytoplankton	<b>intpp</b>	mol m <sup>-2</sup> s <sup>-1</sup>	1° grid, monthly	JRA55+IPSL-CM6A-LR
Net primary organic carbon production by diatoms	<b>intppdiat</b>	mol m <sup>-2</sup> s <sup>-1</sup>	1° grid, monthly	JRA55+IPSL-CM6A-LR
Net Primary Organic Carbon Production by Other Phytoplankton	<b>intppmisc</b>	mol m <sup>-2</sup> s <sup>-1</sup>	1° grid, monthly	JRA55+IPSL-CM6A-LR
Mixed layer depth defined by delta rho = 0.125	<b>mlostmax</b>	m	1° grid, monthly	JRA55+IPSL-CM6A-LR
Dissolved oxygen concentration	<b>o2, (o2-bot), o2-surf</b>	mol m <sup>-3</sup>	1° grid, vertically resolved, ocean bottom and surface fields, monthly	JRA55+IPSL-CM6A-LR

pH	<b>ph, (ph-bot), ph-surf</b>	1	1° grid, vertically resolved, ocean bottom and surface fields, monthly	JRA55+IPSL-CM6A-LR
Total phytoplankton carbon concentration	<b>phyc, (phyc-vint)</b>	mol m <sup>-3</sup>	1° grid, vertically resolved and vertically integrated, monthly	JRA55+IPSL-CM6A-LR
Concentration of diatoms expressed as carbon in sea water	<b>phydiat, (phydiat-vint)</b>	mol m <sup>-3</sup>	1° grid, vertically resolved and vertically integrated, monthly	JRA55+IPSL-CM6A-LR
Mole Content of Miscellaneous Phytoplankton Expressed as Carbon in Sea Water	<b>phymisc, (phymisc-vint)</b>	mol m <sup>-2</sup>	1° grid, vertically resolved and vertically integrated, monthly	JRA55+IPSL-CM6A-LR
Net Downward Shortwave Radiation at Sea Water Surface	<b>rsndts</b>	W m <sup>-2</sup>	1° grid, monthly	JRA55+IPSL-CM6A-LR
Sea water salinity	<b>so, (so-bot), so-surf</b>	0.001	1° grid, vertically resolved, ocean bottom and surface fields, monthly	JRA55+IPSL-CM6A-LR
Sea water potential temperature	<b>thetao</b>	°C	1° grid, vertically resolved, monthly	JRA55+IPSL-CM6A-LR
Ocean model cell thickness	<b>thkcello</b>	m	1° grid, vertically resolved, monthly	JRA55+IPSL-CM6A-LR
Sea water potential temperature at sea floor (bottom)	<b>(tob)</b>	°C	1° grid, monthly	JRA55+IPSL-CM6A-LR
Sea surface temperature	<b>tos</b>	°C	1° grid, monthly	JRA55+IPSL-CM6A-LR
Sea water zonal velocity	<b>uo</b>	m s <sup>-1</sup>	1° grid, vertically resolved, monthly	JRA55+IPSL-CM6A-LR
Sea water meridional velocity	<b>vo</b>	m s <sup>-1</sup>	1° grid, vertically resolved, monthly	JRA55+IPSL-CM6A-LR

Concentration of mesozooplankton expressed as carbon in sea water	<b>zmeso, (zmeso-vint)</b>	mol m-3	1° grid, vertically resolved and vertically integrated, monthly	JRA55+IPSL-CM6A-LR
Concentration of microzooplankton expressed as carbon in sea water	<b>zmicro, (zmicro-vint)</b>	mol m-3	1° grid, vertically resolved and vertically integrated, monthly	JRA55+IPSL-CM6A-LR
Total Zooplankton Carbon Concentration	<b>zooc, (zooc-vint)</b>	mol m-3	1° grid, vertically resolved and vertically integrated, monthly	JRA55+IPSL-CM6A-LR

1005

1006

### 2.4.3 Bias-adjusted regional ocean forcings ('de-biased' sensitivity experiment)

1007

1008

1009

1010

1011

1012

1013

1014

1015

1016

1017

1018

1019

1020

Regional marine ecosystem models are most often calibrated to reproduce observed environmental variables when driven by observed sea surface and bottom temperature, primary production (phytoplankton production), and zooplankton biomass. However, that would still lead to biases in the historical simulations if the impact model was forced by biased simulated input data instead of observational data. To reduce this effect the GCM-based input data has been adjusted such that the historical GCM simulations match observational data for certain regions (Eddy et al., 2025). The adjustment is based on the delta approach where simulated and observational forcing data  $X_{sim}$  and  $X_{obs}$  are averaged across a given historical reference period to determine the bias  $\Delta = \text{mean}(X_{sim}) - \text{mean}(X_{obs})$  that is then subtracted from the simulated forcing data. This method preserves the trend in the forcing data and its internal variability. Some ocean forcing variables are not an exact match with variables used in regional marine ecosystem models. For example, sea water potential temperature ( $\theta_{\text{sea}}$ ), concentration of diatoms ( $\text{phydiat-vint}$ ), or concentration of mesozooplankton ( $\text{zmeso-vint}$ ) may first be converted to other indicators that are then used as input for the regional marine ecosystem models. In these cases the derived indicator is corrected using the delta method (see **Table 10**).

1021

**Table 10:** Bias-adjusted ocean data to be used by regional impact models in the 'de-biased' sensitivity experiment in the fisheries and marine ecosystems sector

1022

Variable	Variable specifier	Unit	Resolution	Forcing datasets
Southern Benguela Current				

Net primary organic carbon production by all types of phytoplankton	<b>intpp</b>	mol m <sup>-2</sup> s <sup>-1</sup>	1° grid, monthly	Corrected based on observed primary production for the southern Benguela current based on the delta method where the adjustment target is data from 1978 for the EwE model and 1990 for the Atlantis model
Sea water potential temperature	<b>thetao</b>	°C	1° grid, vertically resolved, monthly	Raw GCM temperature data converted to temperatures at 0-50, 50-100, 100-300 and 300-500 m according to the configuration for the southern Benguela Atlantis model, and 0-50 and 300-500 m for the EwE model.
Cook Strait				
Net primary organic carbon production by all types of phytoplankton	<b>intpp</b>	mol m <sup>-2</sup> s <sup>-1</sup>	1° grid, monthly	Corrected based on observed primary production for Cook Strait using the delta method where observational target data is from 1950
East Bass Strait				
Net primary organic carbon production by all types of phytoplankton	<b>intpp</b>	mol m <sup>-2</sup> s <sup>-1</sup>	1° grid, monthly	Corrected based on observed primary production for East Bass Strait using the delta method where observational target data is from 1994
East Bering Sea				
Concentration of diatoms expressed as carbon in sea water	<b>phydiat-vint</b>	mol m <sup>-3</sup>	1/4° grid, vertically resolved and vertically integrated, monthly	Converted to phytoplankton size classes used in East Bering Sea mizer model then corrected using the delta method for the period 1982–1993
Concentration of diazotrophs expressed as carbon in sea water	<b>phydiaz-vint</b>	mol m <sup>-3</sup>	1/4° grid, vertically resolved and vertically integrated, monthly	Converted to phytoplankton size classes used in East Bering Sea mizer model then corrected using the delta method for the period 1982–1993

Concentration of picoplankton expressed as carbon in sea water	<b>phypico-vint</b>	mol m-3	1/4° grid, vertically resolved and vertically integrated, monthly	Converted to phytoplankton size classes used in East Bering Sea mizer model then corrected using the delta method for the period 1982–1993
Concentration of mesozooplankton expressed as carbon in sea water	<b>zmeso-vint</b>	mol m-3	1/4° grid, vertically resolved and vertically integrated, monthly	Converted to zooplankton size classes used in East Bering Sea mizer model then corrected using the delta method for the period 1982–1993
Concentration of microzooplankton expressed as carbon in sea water	<b>zmicro-vint</b>	mol m-3	1/4° grid, vertically resolved and vertically integrated, monthly	Converted to zooplankton size classes used in East Bering Sea mizer model then corrected using the delta method for the period 1982–1993
Sea surface temperature	<b>tos</b>	°C	1/4° grid, monthly	Corrected based on configuration for the East Bering Sea mizer model using the delta method for the period 1982–1993
Hawai'i				
Concentration of diatoms expressed as carbon in sea water	<b>phydiat-vint</b>	mol m-3	1/4° grid, vertically resolved and vertically integrated, monthly	Converted to phytoplankton size classes used in Hawaii mizer model (Woodworth-Jefcoats, 2022) then corrected using the delta method
Concentration of diazotrophs expressed as carbon in sea water	<b>phydiaz-vint</b>	mol m-3	1/4° grid, vertically resolved and vertically integrated, monthly	Converted to phytoplankton size classes used in Hawaii mizer model then corrected using the delta method
Concentration of picoplankton expressed as carbon in sea water	<b>phypico-vint</b>	mol m-3	1/4° grid, vertically resolved and vertically integrated, monthly	Converted to phytoplankton size classes used in Hawaii mizer model then corrected using the delta method

Concentration of mesozooplankton expressed as carbon in sea water	<b>zmeso-vint</b>	mol m-3	1/4° grid, vertically resolved and vertically integrated, monthly	Converted to zooplankton size classes used in Hawaii mizer model then corrected using the delta method
Concentration of microzooplankton expressed as carbon in sea water	<b>zmicro-vint</b>	mol m-3	1/4° grid, vertically resolved and vertically integrated, monthly	Converted to zooplankton size classes used in Hawaii mizer model then corrected using the delta method
Sea water potential temperature	<b>thetao</b>	°C	1/4° grid, vertically resolved, monthly	Converted to temperature used in Hawaii Mizer model then corrected based on observed sea water potential temperature for Hawaii using the delta method from 1961–1980 with observed temperature data from the World Ocean Atlas

1023

1024

1025

## 2.5 Future Lightning Data

1026

1027

1028

1029

For the ‘varlighting’ sensitivity experiment we provide temporally varying lightning density (strokes km<sup>-2</sup> day<sup>-1</sup>) for the period 2015-2100 on monthly resolution (monthly mean of daily lightning stroke density) and the standard 0.5° global grid. This dataset may be used in a range of applications, for example, to understand the influence of lightning on wildfire ignition or atmospheric composition.

1030

1031

1032

1033

1034

The lightning density is derived from future climate simulations by UKESM1-0-LL and an empirical relationship between Convective Available Potential Energy (CAPE) and lightning strokes based on the WWLLN Global Lightning Climatology and time-series (WGLC) (Kaplan & Lau, 2021, 2022). Daily mean CAPE is calculated from non bias-adjusted air temperature, air pressure, and specific humidity on pressure levels from the surface to the top of the troposphere.

1035

1036

1037

1038

1039

The relationship between daily CAPE and daily lightning is estimated by linear regression of log-transformed CAPE derived from the GCM-calculated CAPE during the period of overlapping model output and observed daily lightning from WGLC (2015-2020) for each gridcell and month of the year. Where <10 observations of daily lightning were available over the calibration period, we used global mean regression parameters.

1040

1041

1042

The empirical relationships are applied to the daily CAPE data from the UKESM1-0-LL simulations for all three climate scenarios SSP1-2.6, SSP3-7.0, and SSP5-8.5. The associated lightning densities were monthly averaged. To maintain the spatial structure of lightning observed at present, lightning anomalies

1043 compared to the simulated 2015-2020 climatological reference were added to the observed present-day  
 1044 lightning climatology from WGLC for 2015-2020. The ‘varlightning’ sensitivity experiment is assumed to  
 1045 start from the default historical group I simulation, assuming the Flash Rate Monthly Climatology (Cecil,  
 1046 2006), not changing with climate change.

1047  
 1048  
 1049

**Table 11:** Future lightning forcing data provided within ISIMIP3b.

Variable	Variable specifier	Unit	Resolution	Datasets
Monthly flash rate	<b>lightning</b>	km-2 d-1	0.5° grid, monthly	Derived from UKESM1-0-LL (SSP1-2.6, SSP3-7.0, and SSP5-8.5) using an empirical relationship between Convective Available Potential Energy (CAPE) and lightning densities (Kaplan et al., 2023).

1050  
 1051  
 1052

### 3 Conclusions

1053  
 1054  
 1055  
 1056  
 1057  
 1058  
 1059  
 1060  
 1061  
 1062  
 1063  
 1064  
 1065  
 1066  
 1067

This paper gives an overview over the ISIMIP3b, group I and II experiments and the provided climate-related forcing data sets. The simulations assuming fixed 2015 direct human forcings and a low (ssp126) and two high emission scenarios (ssp370 and ssp585) are designed to describe the impacts of different levels of climate change on present day natural and human systems. The set-up allows e.g. for testing to what degree the (bio-)physical impacts scale with global mean temperature change and could therefore be translated to other global warming pathways than the ones considered here. While a functional relationship between the considered impact indicator and global mean temperature change (or other climate variables) could be trained on ssp585 simulations because of the high warming levels reached, its performance could then be tested on ssp370 and ssp126. However, in such a setting it has to be taken into account that ssp370 is different from the other scenarios with regard to particularly high aerosol emissions and high decreases in forest areas going beyond the assumptions in the other models. So it has been shown that the increase of global mean precipitation with global warming is much weaker in SSP3-7.0 than in the other scenarios (Shiogama et al., 2023).

1068  
 1069  
 1070  
 1071  
 1072  
 1073  
 1074

This paper is intended to work as a catalogue where the climate impact modellers can find all relevant information about the climate-related forcings needed as reference for the impact model simulations generated within the CMIP6-based ISIMIP3b, group I (historical period) and group II (future projections). As a continuous process we would like to improve or complement these data sets wherever possible. So this paper can also be read as a call to either contribute by additional input data that allows other sectors to join the current simulation round or by methods that could be used to generate additional data sets

1075 for the next simulation round that will likely build on CMIP7 simulations. The following climate-related  
1076 forcings have been identified as still missing and particularly critical to be added to a fourth simulation  
1077 round of ISIMIP: i) temporally resolved lightning data accounting for changes in climate, ii) bias-adjusted  
1078 oceanic forcing data, iii) projected coastal water levels in high temporal resolution accounting for  
1079 extremes and representing the effects of long term sea level rise in line with the underlying global climate  
1080 simulations, and v) ozone concentration fields in line with the GCM simulations. While a bias-adjustment  
1081 of the oceanic forcings is already suggested in section 2.4.2, the approach does not preserve the daily  
1082 variability of the raw oceanic forcings as it requires atmospheric surface flux only available in monthly  
1083 resolution from the ISIMIP3b GCMs. To ensure the consistency on daily time scale, we have submitted an  
1084 associated request for CMIP7 whose simulations will be used within the next round of ISIMIP. The  
1085 generation of high resolution coastal water levels is ongoing research described in section 2.2.3. In  
1086 particular the generation of the short term variability that will have to be added to the long term trends  
1087 in water levels still has to be developed and prove to fulfill the demands. In addition, it would be great to  
1088 also provide estimates of the extreme coastal water levels associated with the tropical cyclone tracks and  
1089 wind fields we provide within ISIMIP3b (see section 2.2). There is a general demand for higher resolution  
1090 ~~CRFclimate-related forcings~~ including both, the oceanic and the atmospheric components ideally  
1091 accounting for heat island effects. As the ISIMIP ~~CRFclimate-related forcings~~ have to be globally consistent  
1092 in the sense that they have to represent the daily variability of the underlying coarse resolution GCMs, we  
1093 cannot use data from dynamical downscaling approaches using boundary conditions from different GCM  
1094 runs as for example available through CORDEX. However, it seems to be appealing to harmonize the  
1095 selection of the ISIMIP GCMs with a priority setting regarding the GCM-based boundary conditions within  
1096 CORDEX.

1097  
1098 The climate-related forcings described here are also provided as input for the new ISIMIP3b, group III  
1099 simulations where the associated Direct Human Forcings (DHF) are not held constant at 2015 levels but  
1100 are projected into the future in line with i) the population growth and economic development associated  
1101 with the considered Shared Socioeconomic Pathways (SSPs) and mitigation measures required to reach  
1102 the prescribed levels of climate forcings associated with the climate projections ('no adaptation'  
1103 experiments) and ii) additionally accounting for the impacts of climate change ('adaptation' experiments).  
1104 The collection of the associated DHF will be described in a separate paper.

1105  
1106 **Code and data availability.** -All generated ISIMIP3 climate-related forcing data described in this paper is  
1107 publicly available at the ISIMIP data repository The repository is hosted by the Potsdam Institute for  
1108 Climate Impact Research (PIK) e.V. which is part of the TIB DOI Consortium ensuring persistent, FAIR-  
1109 compliant data publication, by committing to adhering to the DataCite Consortium Agreement. This  
1110 includes commitments to data persistence (§4 a.) as well as maintaining and updating metadata (§4 c.),  
1111 which forbids “withdrawing content without posting a notification”. In compliance with these rules a  
1112 system to document and trace back data issues has been implemented in the repository to comply with  
1113 this requirement. Additionally, should PIK be unable to continue hosting the ISIMIP repository, it will take  
1114 responsibility for coordinating a timely transfer of the full repository and its DOI infrastructure to an  
1115 appropriate, trusted archive or institutional partner to ensure uninterrupted access and citation

1116 continuity. DOIs are used to refer to datasets in a persistent way. Whenever a dataset is replaced a copy  
1117 is kept on tape, and a new DOI is issued, while the old DOI is kept online with information on how to  
1118 retrieve the archived data. Whenever we need to replace datasets, we will create a new version of the  
1119 DOI, marked by a version number at the end. This ensures that every DOI references exactly the datasets,  
1120 which were public at the time of registration. Detailed information can be found in the ISIMIP terms of  
1121 use at <https://www.isimip.org/gettingstarted/terms-of-use/> (ISIMIP terms of use, 2023).

1122 ~~The MIT data on tropical cyclone tracks with wind and precipitation fields data shall be used for non-~~  
1123 ~~commercial research or academic purposes only. Data can be made available by the ISIMIP team upon~~  
1124 ~~written consent by Kerry Emanuel (MIT, email: [emanuel@mit.edu](mailto:emanuel@mit.edu)).~~

1125 ~~All other input data described are available for participating modelers with a respective account from the~~  
1126 ~~DKRZ server. Data will be made publicly available, and most data are already publicly available at the~~  
1127 ~~ISIMIP data repository at <https://data.isimip.org/> (ISIMIP data repository, 2025) and availability is~~  
1128 ~~documented in the ISIMIP Input data table [https://www.isimip.org/gettingstarted/input-data-bias-](https://www.isimip.org/gettingstarted/input-data-bias-adjustment/)~~  
1129 ~~adjustment/ (ISIMIP input data table, 2025) where the way to access the data is described as well. Model~~  
1130 ~~output is already partly available <https://data.isimip.org/> (ISIMIP data repository, 2025). The ISIMIP~~  
1131 ~~repository fulfills the archive standards as stated in the “GMD code and data policy”. The repository is~~  
1132 ~~hosted and maintained by the Potsdam Institute for Climate Impact Research (PIK). Data can only be~~  
1133 ~~published or removed from the repository by the ISIMIP data team, which is monitored by the ISIMIP~~  
1134 ~~steering committee according to the organizational structure of ISIMIP. DOIs are used to refer to datasets~~  
1135 ~~in a persistent way. Whenever a dataset is replaced for any reason a copy is kept on tape, and a new DOI~~  
1136 ~~is issued, while the old DOI is kept online with information on how to retrieve the archived data. Detailed~~  
1137 ~~information can be found in the ISIMIP terms of use at <https://www.isimip.org/gettingstarted/terms-of-use/>~~  
1138 ~~(ISIMIP terms of use, 2023).~~

#### 1140 **Author contributions**

1141 KF lead the project and developed the concept with contributions from JS, MM, CO, CPOR, SH, JLB, CSH,  
1142 CMP, TDE, KOC, CN, RH, DPT, OM, SJC, JJ, SR, GL, SC, EB, AGS, NS, JC, SH, CB, AG, FL, SNG, HMS, FH, TH,  
1143 RM, DP, WT, DMB, RL, AIA, MF, MB, RR, and IDG. JV, MB, JK, IDVDV, LN, IJS supported the quality control  
1144 and curation of the climate-related forcing data and the protocol development together with the sectoral  
1145 ISIMIP coordinators listed as co-authors. SL developed the method and generated the downscaled and  
1146 bias-adjusted atmospheric climate forcing data. MM and ST provided the description of the approach to  
1147 generate the coastal water level data. ML provided the description of the method to bias-adjust the global  
1148 oceanic forcings. TV, DQC, CYL, SJC, and KE provided TC data. JOK and AK provided the future lightning  
1149 data. KF prepared the manuscript with contributions from all co-authors.

#### 1151 **Competing interests**

1152 At least one of the (co-)authors is a member of the editorial board of GMD

#### 1153 **Acknowledgements**

1154 This article is based upon work from COST Action CA19139 PROCLIAS (PROcess-based models for CLimate  
1155 Impact Attribution across Sectors), supported by COST (European Cooperation in Science and Technology;  
1156 <https://www.cost.eu>). SL received funding from the German Research Foundation (DFG, project number  
1157 427397136). MB acknowledges funding from the BELSPO STEREO IV project SR/00/414. SC, AGS, MB and  
1158

1160 NS acknowledge funding through NERC NE/V01854X/1 (MOTHERSHIP). This research has received funding  
1161 from the German Federal Ministry of Education and Research (BMBF) under the research projects QUIDIC  
1162 (grant agreement no. 01LP1907A) and ISI-Access (16QK05), from the Horizon 2020 Framework  
1163 Programme of the European Union under the projects RECEIPT (grant agreement no. 820712) and from  
1164 the Horizon Europe research and innovation programme under grant agreement No 101135481  
1165 (COMPASS). C.-Y. L is supported by Palisades Geophysical Institute (PGI) Young Scientist Award. KOC  
1166 acknowledges support from the National Research Foundation of South Africa (grant 136481) and the  
1167 resources from the Cluster for High Performance Computing-CSIR. FL is supported by the National Key  
1168 Research and Development Program of China (2022YFE0106500). DPT acknowledges funding from the  
1169 Jarislowsky Foundation and NSERC. IDG acknowledges funding of the European Research Council (ERC  
1170 Starting Grant, GROW-101041110).

1171  
1172  
1173  
1174

1175 **References**

1176

- 1177 Adler, R. F., Huffman, G. J., Chang, A., Ferraro, R., Xie, P.-P., Janowiak, J., Rudolf, B., Schneider, U., Curtis,  
1178 S., Bolvin, D., Gruber, A., Susskind, J., Arkin, P., & Nelkin, E. (2003). The Version-2 Global  
1179 Precipitation Climatology Project (GPCP) Monthly Precipitation Analysis (1979–Present). *Journal of*  
1180 *Hydrometeorology*, 4(6), 1147–1167. [https://doi.org/10.1175/1525-  
1181 7541\(2003\)004<1147:TVGPCP>2.0.CO;2](https://doi.org/10.1175/1525-7541(2003)004<1147:TVGPCP>2.0.CO;2)
- 1182 Andela, B., Broetz, B., de Mora, L., Drost, N., Eyring, V., Koldunov, N., Lauer, A., Mueller, B., Predoi, V.,  
1183 Righi, M., Schlund, M., Vegas-Regidor, J., Zimmermann, K., Adeniyi, K., Arnone, E., Bellprat, O., Berg,  
1184 P., Bock, L., Caron, L.-P., ... Weigel, K. (2020b). *ESMValTool*.  
1185 <https://doi.org/10.5281/zenodo.3970975>
- 1186 Andela, B., Broetz, B., Drost, N., Eyring, V., Koldunov, N., Lauer, A., Predoi, V., Righi, M., Schlund, M.,  
1187 Zimmermann, K., Bock, L., Diblen, F., Dreyer, L., Earnshaw, P., Hassler, B., & Little, B. (2020a).  
1188 *ESMValCore*. <https://doi.org/10.5281/zenodo.3952695>
- 1189 Barrier, N., Lengaigne, M., Rault, J., Person, R., Ethé, C., Aumont, O., & Maury, O. (2023). Mechanisms  
1190 underlying the epipelagic ecosystem response to ENSO in the equatorial Pacific ocean. *Progress in*  
1191 *Oceanography*, 213, 103002. <https://doi.org/10.1016/j.pocean.2023.103002>
- 1192 Bock, L., & Lauer, A. (2024). Cloud properties and their projected changes in CMIP models with low to  
1193 high climate sensitivity. *Atmospheric Chemistry and Physics*, 24(3), 1587–1605.  
1194 <https://doi.org/10.5194/acp-24-1587-2024>
- 1195 Bock, L., Lauer, A., Schlund, M., Barreiro, M., Bellouin, N., Jones, C., Meehl, G. A., Predoi, V., Roberts, M.  
1196 J., & Eyring, V. (2020). Quantifying progress across different CMIP phases with the ESMValTool.  
1197 *Journal of Geophysical Research*, 125(21). <https://doi.org/10.1029/2019jd032321>
- 1198 Boucher, O., Denvil, S., Levvasseur, G., Cozic, A., Caubel, A., Foujols, M.-A., Meurdesoif, Y., Cadule, P.,

1199 Devilliers, M., Dupont, E., & Lurton, T. (2019). *IPSL IPSL-CM6A-LR model output prepared for CMIP6*  
1200 *ScenarioMIP* [Dataset]. Earth System Grid Federation. <https://doi.org/10.22033/ESGF/CMIP6.1532>

1201 Boucher, O., Denvil, S., Levavasseur, G., Cozic, A., Caubel, A., Foujols, M.-A., Meurdesoif, Y., Cadule, P.,  
1202 Devilliers, M., Ghattas, J., Lebas, N., Lurton, T., Mellul, L., Musat, I., Mignot, J., & Cheruy, F. (2018).  
1203 *IPSL IPSL-CM6A-LR model output prepared for CMIP6 CMIP* [Dataset]. Earth System Grid Federation.  
1204 <https://doi.org/10.22033/ESGF/CMIP6.1534>

1205 Boucher, O., Servonnat, J., Albright, A. L., Aumont, O., Balkanski, Y., Bastrikov, V., Bekki, S., Bonnet, R.,  
1206 Bony, S., Bopp, L., Braconnot, P., Brockmann, P., Cadule, P., Caubel, A., Cheruy, F., Codron, F., Cozic,  
1207 A., Cugnet, D., D'Andrea, F., ... Vuichard, N. (2020). Presentation and evaluation of the IPSL-CM6A-  
1208 LR climate model. *Journal of Advances in Modeling Earth Systems*, *12*(7).  
1209 <https://doi.org/10.1029/2019ms002010>

1210 Büchner, M., & Reyer, C. (2022). *ISIMIP3b atmospheric composition input data* [Dataset]. ISIMIP  
1211 Repository. <https://doi.org/10.48364/ISIMIP.482153.1>

1212 Buck, A. L. (1981). New Equations for Computing Vapor Pressure and Enhancement Factor. *Journal of*  
1213 *Applied Meteorology and Climatology*, *20*(12), 1527–1532. <https://doi.org/10.1175/1520->  
1214 [0450\(1981\)020<1527:NEFCVP>2.0.CO;2](https://doi.org/10.1175/1520-0450(1981)020<1527:NEFCVP>2.0.CO;2)

1215 Camargo, S. J., Tippett, M. K., Sobel, A. H., Vecchi, G. A., & Zhao, M. (2014). Testing the Performance of  
1216 Tropical Cyclone Genesis Indices in Future Climates Using the HiRAM Model. *Journal of Climate*,  
1217 *27*(24), 9171–9196. <https://doi.org/10.1175/JCLI-D-13-00505.1>

1218 Cannon, A. J. (2018). Multivariate quantile mapping bias correction: an N-dimensional probability  
1219 density function transform for climate model simulations of multiple variables. *Climate Dynamics*,  
1220 *50*(1), 31–49. <https://doi.org/10.1007/s00382-017-3580-6>

1221 Cecil, D. (2006). *LIS/OTD 0.5 Degree High Resolution Monthly Climatology (HRMC)* [Dataset]. NASA  
1222 Global Hydrometeorology Resource Center DAAC. <https://doi.org/10.5067/LIS/LIS-OTD/DATA303>

1223 Cucchi, M., Weedon, G. P., Amici, A., Bellouin, N., Lange, S., Müller Schmied, H., Hersbach, H., &  
1224 Buontempo, C. (2020). WFDE5: bias-adjusted ERA5 reanalysis data for impact studies. *Earth System*  
1225 *Science Data*, 12(3), 2097–2120. <https://doi.org/10.5194/essd-12-2097-2020>

1226 Dunne, J. P., Horowitz, L. W., Adcroft, A. J., Ginoux, P., Held, I. M., John, J. G., Krasting, J. P., Malyshev, S.,  
1227 Naik, V., Paulot, F., Shevliakova, E., Stock, C. A., Zadeh, N., Balaji, V., Blanton, C., Dunne, K. A.,  
1228 Dupuis, C., Durachta, J., Dussin, R., ... Zhao, M. (2020). The GFDL earth system model version 4.1  
1229 (GFDL-ESM 4.1): Overall coupled model description and simulation characteristics. *Journal of*  
1230 *Advances in Modeling Earth Systems*, 12(11). <https://doi.org/10.1029/2019ms002015>

1231 Durack, P. J. (n.d.). *CMIP6 source\_id values*. Retrieved January 16, 2023, from [https://wcrp-](https://wcrp-cmip.github.io/CMIP6_CVs/docs/CMIP6_source_id.html)  
1232 [cmip.github.io/CMIP6\\_CVs/docs/CMIP6\\_source\\_id.html](https://wcrp-cmip.github.io/CMIP6_CVs/docs/CMIP6_source_id.html)

1233 Eddy, T. D., Heneghan, R. F., Bryndum-Buchholz, A., Fulton, E. A., Harrison, C. S., Tittensor, D. P., Lotze,  
1234 H. K., Ortega-Cisneros, K., Novaglio, C., Bianchi, D., Büchner, M., Bulman, C., Cheung, W. W. L.,  
1235 Christensen, V., Coll, M., Everett, J. D., Fierro-Arcos, D., Galbraith, E. D., Gascuel, D., ... Blanchard, J.  
1236 L. (2025). Global and regional marine ecosystem models reveal key uncertainties in climate change  
1237 projections. *Earth's Future*, 13(3). <https://doi.org/10.1029/2024ef005537>

1238 Emanuel, K., DesAutels, C., Holloway, C., & Korty, R. (2004). Environmental Control of Tropical Cyclone  
1239 Intensity. *Journal of the Atmospheric Sciences*, 61(7), 843–858. [https://doi.org/10.1175/1520-](https://doi.org/10.1175/1520-0469(2004)061<0843:ECOTCI>2.0.CO;2)  
1240 [0469\(2004\)061<0843:ECOTCI>2.0.CO;2](https://doi.org/10.1175/1520-0469(2004)061<0843:ECOTCI>2.0.CO;2)

1241 Emanuel, K., Quesada-Chacón, D., Novak, L., & Otto, C. (2025). *ISIMIP3b tropical cyclone tracks (MIT)*  
1242 [Dataset]. ISIMIP Repository. <https://doi.org/10.48364/ISIMIP.682793>

1243 Emanuel, K., Sundararajan, R., & Williams, J. (2008). Hurricanes and Global Warming: Results from  
1244 Downscaling IPCC AR4 Simulations. *Bulletin of the American Meteorological Society*, 89(3), 347–  
1245 368. <https://doi.org/10.1175/BAMS-89-3-347>

1246 Eyring, V., Bony, S., Meehl, G. A., Senior, C. A., Stevens, B., Stouffer, R. J., & Taylor, K. E. (2016). Overview

1247 of the Coupled Model Intercomparison Project Phase 6 (CMIP6) experimental design and  
1248 organization. *Geoscientific Model Development*, 9(5), 1937–1958. [https://doi.org/10.5194/gmd-9-](https://doi.org/10.5194/gmd-9-1937-2016)  
1249 1937-2016

1250 Eyring, V., Gillett, N. P., Achuta Rao, K. M., Barimalala, R., Barreiro Parrillo, M., Bellouin, N., V. Masson-  
1251 Delmotte, P. Zhai, A. Pirani, S. L. Connors, C. Péan, S. Berger, & Intergovernmental Panel on Climate  
1252 Change (IPCC). (2023). Human Influence on the Climate System. In *Climate Change 2021 – The*  
1253 *Physical Science Basis: Working Group I Contribution to the Sixth Assessment Report of the*  
1254 *Intergovernmental Panel on Climate Change* (pp. 423–552). Cambridge University Press.  
1255 <https://doi.org/10.1017/9781009157896.005>

1256 Forster, P., Storelvmo, T., Armour, K., Collins, W., Dufresne, J.-L., Frame, D., Lunt, D. J., Mauritsen, T.,  
1257 Palmer, Watanabe, M., Wild, M., & Zhang, H. (2021). The earth’s energy budget, climate feedbacks  
1258 and climate sensitivity. In *Climate Change 2021 – The Physical Science Basis* (pp. 923–1054).  
1259 Cambridge University Press. <https://doi.org/10.1017/9781009157896.009>

1260 Fosu, B., Sobel, A., Camargo, S., Tippet, M., Hemmati, M., Bowen, S., & Bloemendaal, N. (2024).  
1261 Assessing future tropical cyclone risk using downscaled 1 CMIP6 projections. *Journal of Catastrophe*  
1262 *Risk and Resilience*, 2(1). <https://doi.org/10.63024/dpva-2pa1>

1263 Frieler, K., Lange, S., Piontek, F., Reyer, C. P. O., Schewe, J., Warszawski, L., Zhao, F., Chini, L., Denvil, S.,  
1264 Emanuel, K., Geiger, T., Halladay, K., Hurtt, G., Mengel, M., Murakami, D., Ostberg, S., Popp, A.,  
1265 Riva, R., Stevanovic, M., ... Yamagata, Y. (2017). Assessing the impacts of 1.5 °C global warming –  
1266 simulation protocol of the Inter-Sectoral Impact Model Intercomparison Project (ISIMIP2b).  
1267 *Geoscientific Model Development*, 10(12), 4321–4345. <https://doi.org/10.5194/gmd-10-4321-2017>

1268 Frieler, K., Volkholz, J., Lange, S., Schewe, J., Mengel, M., del Rocío Rivas López, M., Otto, C., Reyer, C. P.  
1269 O., Karger, D. N., & del Valle Gitta Lasslop Sarah Chadburn Eleanor Burke Angela Gallego-Sala Noah  
1270 Smith Jinfeng Chang Stijn Hantson Chantelle Burton Anne Gädeke Fang Li Simon N. Gosling Hannes

1271 Müller Schmied Fred Hattermann Jida Wang Fangfang Yao Thomas Hickler Rafael Marcé Don  
1272 Pierson Wim Thiery Daniel Mercado-Bettín Robert Ladwig Ana Isabel Ayala-Zamora Matthew  
1273 Forrest and Michel Bechtold, J. T. M. S. T. C. M. J. L. B. C. S. H. C. M. P. T. D. E. K. O.-C. C. N. Y. R. R.  
1274 A. W. C. S. X. L. R. H. D. T. O. M. M. B. T. V. T. W. F. S. I. J. S. J. K. I. V. J. J. C. M. S. R. J. K. I. D. V.  
1275 (2024, January 4). *Scenario setup and forcing data for impact model evaluation and impact*  
1276 *attribution within the third round of the Inter-Sectoral Model Intercomparison Project (ISIMIP3a).*  
1277 Geoscientific Model Development. [https://www.google.com/url?q=https://doi.org/10.5194/gmd-](https://www.google.com/url?q=https://doi.org/10.5194/gmd-17-1-2024&sa=D&source=docs&ust=1704377607845951&usg=AOvVaw3hFVXAV75ZSOClc8itQfEs)  
1278 [17-1-2024&sa=D&source=docs&ust=1704377607845951&usg=AOvVaw3hFVXAV75ZSOClc8itQfEs](https://www.google.com/url?q=https://doi.org/10.5194/gmd-17-1-2024&sa=D&source=docs&ust=1704377607845951&usg=AOvVaw3hFVXAV75ZSOClc8itQfEs)  
1279 Frieler, K., Volkholz, J., Lange, S., Schewe, J., Mengel, M., Otto, C., Reyer, C. P. O., Karger, D. N., Malle, J.  
1280 T., Treu, S., Menz, C., Blanchard, J. L., Harrison, C. S., Petrik, C. M., Eddy, T. D., Ortega-Cisneros, K.,  
1281 Novaglio, C., Rousseau, Y., Watson, R. A., ... Bechtold, M. (2024a). Scenario setup and forcing data  
1282 for impact model evaluation and impact attribution within the third round of the Inter-Sectoral  
1283 Impact Model Intercomparison Project (ISIMIP3a). *Geoscientific Model Development*, 17(1), 1–51.  
1284 <https://doi.org/10.5194/gmd-17-1-2024>  
1285 Frieler, K., Volkholz, J., Lange, S., Schewe, J., Mengel, M., Rivas López, M. del R., Otto, C., Reyer, C. P. O.,  
1286 Karger, D. N., Malle, J. T., Treu, S., Menz, C., Blanchard, J. L., Harrison, C. S., Petrik, C. M., Eddy, T.  
1287 D., Ortega-Cisneros, K., Novaglio, C., Rousseau, Y., ... Bechtold, M. (2023). Scenario set-up and  
1288 forcing data for impact model evaluation and impact attribution within the third round of the Inter-  
1289 Sectoral Model Intercomparison Project (ISIMIP3a). In *EGUsphere*.  
1290 <https://doi.org/10.5194/egusphere-2023-281>  
1291 Geiger, T., Gütschow, J., Bresch, D. N., Emanuel, K., & Frieler, K. (2021). Double benefit of limiting global  
1292 warming for tropical cyclone exposure. *Nature Climate Change*, 11(10), 861–866.  
1293 <https://doi.org/10.1038/s41558-021-01157-9>  
1294 Gennaretti, F., Sangelantoni, L., & Grenier, P. (2015). Toward daily climate scenarios for Canadian Arctic

1295 coastal zones with more realistic temperature-precipitation interdependence. *JGR: Atmospheres*,  
1296 *120*(23), 11,862–11,877. <https://doi.org/10.1002/2015JD023890>

1297 Gillett, N. P., Shiogama, H., Funke, B., Hegerl, G., Knutti, R., Matthes, K., Santer, B. D., Stone, D., &  
1298 Tebaldi, C. (2016). The detection and Attribution Model Intercomparison Project (DAMIP v1.0)  
1299 contribution to CMIP6. *Geoscientific Model Development*, *9*(10), 3685–3697.  
1300 <https://doi.org/10.5194/gmd-9-3685-2016>

1301 Good, P., Sellar, A., Tang, Y., Rumbold, S., Ellis, R., Kelley, D., Kuhlbrodt, T., & Walton, J. (2019). *MOHC*  
1302 *UKESM1.0-LL model output prepared for CMIP6 ScenarioMIP* [Dataset]. Earth System Grid  
1303 Federation. <https://doi.org/10.22033/ESGF/CMIP6.1567>

1304 Gregory, J. M., Griffies, S. M., Hughes, C. W., Lowe, J. A., Church, J. A., Fukimori, I., Gomez, N., Kopp, R.  
1305 E., Landerer, F., Cozannet, G. L., Ponte, R. M., Stammer, D., Tamsiea, M. E., & van de Wal, R. S. W.  
1306 (2019). Concepts and terminology for sea level: Mean, variability and change, both local and global.  
1307 *Surveys in Geophysics*, *40*(6), 1251–1289. <https://doi.org/10.1007/s10712-019-09525-z>

1308 Grenier, P. (2018). Two Types of Physical Inconsistency to Avoid with Univariate Quantile Mapping: A  
1309 Case Study over North America Concerning Relative Humidity and Its Parent Variables. *Journal of*  
1310 *Applied Meteorology and Climatology*, *57*(2), 347–364. <https://doi.org/10.1175/JAMC-D-17-0177.1>

1311 Haerter, J. O., Hagemann, S., Moseley, C., & Piani, C. (2011). Climate model bias correction and the role  
1312 of timescales. *Hydrology and Earth System Sciences*, *15*(3), 1065–1079.  
1313 <https://doi.org/10.5194/hess-15-1065-2011>

1314 Hausfather, Z., & Peters, G. P. (2020, January 29). *Emissions – the “business as usual” story is misleading*.  
1315 Nature Publishing Group UK. <https://doi.org/10.1038/d41586-020-00177-3>

1316 Hersbach, H., Bell, B., Berrisford, P., Hirahara, S., Horányi, A., Muñoz-Sabater, J., Nicolas, J., Peubey, C.,  
1317 Radu, R., Schepers, D., Simmons, A., Soci, C., Abdalla, S., Abellan, X., Balsamo, G., Bechtold, P.,  
1318 Biavati, G., Bidlot, J., Bonavita, M., ... Jean-Noël Thépaut. (2020). The ERA5 global reanalysis.

1319 *Quarterly Journal of the Royal Meteorological Society*, 146(730), 1999–2049.

1320 <https://doi.org/10.1002/qj.3803>

1321 Holland. (1980). An Analytic Model of the Wind and Pressure Profiles in Hurricanes, *Mon. Weather*

1322 *Rev*, 108, 1212–1218.

1323 Holland. (2008). A revised hurricane pressure–wind model. *Monthly Weather Review*, 136(9), 3432–

1324 3445. <https://doi.org/10.1175/2008mwr2395.1>

1325 *ISIMIP3b simulation protocol*. (2023). <https://protocol.isimip.org/>

1326 Jägermeyr, J., Müller, C., Ruane, A. C., Elliott, J., Balkovic, J., Castillo, O., Faye, B., Foster, I., Folberth, C.,

1327 Franke, J. A., Fuchs, K., Guarin, J. R., Heinke, J., Hoogenboom, G., Iizumi, T., Jain, A. K., Kelly, D.,

1328 Khabarov, N., Lange, S., ... Rosenzweig, C. (2021). Climate impacts on global agriculture emerge

1329 earlier in new generation of climate and crop models. *Nature Food*, 2(11), 873–885.

1330 <https://doi.org/10.1038/s43016-021-00400-y>

1331 John, J. G., Blanton, C., McHugh, C., Radhakrishnan, A., Rand, K., Vahlenkamp, H., Wilson, C., Zadeh, N.

1332 T., Dunne, J. P., Dussin, R., Horowitz, L. W., Krasting, J. P., Lin, P., Malyshev, S., Naik, V., Ploshay, J.,

1333 Shevliakova, E., Silvers, L., Stock, C., ... Zeng, Y. (2018). *NOAA-GFDL GFDL-ESM4 model output*

1334 *prepared for CMIP6 ScenarioMIP* [Dataset]. Earth System Grid Federation.

1335 <https://doi.org/10.22033/ESGF/CMIP6.1414>

1336 Jungclaus, J., Bittner, M., Wieners, K.-H., Wachsmann, F., Schupfner, M., Legutke, S., Giorgetta, M.,

1337 Reick, C., Gayler, V., Haak, H., de Vrese, P., Raddatz, T., Esch, M., Mauritsen, T., von Storch, J.-S.,

1338 Behrens, J., Brovkin, V., Claussen, M., Crueger, T., ... Roeckner, E. (2019). *MPI-M MPIESM1.2-HR*

1339 *model output prepared for CMIP6 CMIP* [Dataset]. Earth System Grid Federation.

1340 <https://doi.org/10.22033/ESGF/CMIP6.741>

1341 Kaplan, J. O., Koch, A., & Lau, K. H.-K. (2023). *Estimated future global lightning strokes (2010-2100)*.

1342 <https://doi.org/10.5281/zenodo.7511843>

1343 Kaplan, J. O., & Lau, K. H.-K. (2021). The WGLC global gridded lightning climatology and time series.  
1344 *Earth System Science Data*, 13(7), 3219–3237. <https://doi.org/10.5194/essd-13-3219-2021>

1345 Kaplan, J. O., & Lau, K. H.-K. (2022). World Wide Lightning Location Network (WWLLN) Global Lightning  
1346 Climatology (WGLC) and time series, 2022 update. *Earth System Science Data*, 14(12), 5665–5670.  
1347 <https://doi.org/10.5194/essd-14-5665-2022>

1348 Krasting, J. P., John, J. G., Blanton, C., McHugh, C., Nikonov, S., Radhakrishnan, A., Rand, K., Zadeh, N. T.,  
1349 Balaji, V., Durachta, J., Dupuis, C., Menzel, R., Robinson, T., Underwood, S., Vahlenkamp, H., Dunne,  
1350 K. A., Gauthier, P. P. G., Ginoux, P., Griffies, S. M., ... Zhao, M. (2018). *NOAA-GFDL GFDL-ESM4*  
1351 *model output prepared for CMIP6 CMIP* [Dataset]. Earth System Grid Federation.  
1352 <https://doi.org/10.22033/ESGF/CMIP6.1407>

1353 Lange, S. (2017). *ISIMIP2b Bias-Correction Code*. <https://doi.org/10.5281/zenodo.1069050>

1354 Lange, S. (2018). Bias correction of surface downwelling longwave and shortwave radiation for the  
1355 EWEMBI dataset. *Earth System Dynamics*, 9(2), 627–645. <https://doi.org/10.5194/esd-9-627-2018>

1356 Lange, S. (2019a). *Earth2Observe, WFDEI and ERA-interim data merged and bias-corrected for ISIMIP*  
1357 *(EWEMBI)* [Dataset]. <https://doi.org/10.5880/pik.2019.004>

1358 Lange, S. (2019b). Trend-preserving bias adjustment and statistical downscaling with ISIMIP3BASD  
1359 (v1.0). *Geoscientific Model Development*, 12(7), 3055–3070. [https://doi.org/10.5194/gmd-12-3055-](https://doi.org/10.5194/gmd-12-3055-2019)  
1360 2019

1361 Lange, S. (2021a). *ISIMIP3BASD*. <https://doi.org/10.5281/zenodo.4686991>

1362 Lange, S. (2021b). *ISIMIP3b bias adjustment fact sheet*.  
1363 [https://www.isimip.org/documents/413/ISIMIP3b\\_bias\\_adjustment\\_fact\\_sheet\\_Gnsz7CO.pdf](https://www.isimip.org/documents/413/ISIMIP3b_bias_adjustment_fact_sheet_Gnsz7CO.pdf)

1364 Lange, S., & Büchner, M. (2021). *ISIMIP3b bias-adjusted atmospheric climate input data* [Dataset]. ISIMIP  
1365 Repository. <https://doi.org/10.48364/ISIMIP.842396.1>

1366 Lange, S., Menz, C., Gleixner, S., Cucchi, M., Weedon, G. P., Amici, A., Bellouin, N., Schmied, H. M.,

1367 Hersbach, H., Buontempo, C., & Cagnazzo, C. (2021). *WFDE5 over land merged with ERA5 over the*  
1368 *ocean (W5E5 v2.0)* [Dataset]. ISIMIP Repository. <https://doi.org/10.48364/ISIMIP.342217>

1369 Lange, S., Quesada-Chacón, D., & Büchner, M. (2023). *Secondary ISIMIP3b bias-adjusted atmospheric*  
1370 *climate input data* [Dataset]. ISIMIP Repository. <https://doi.org/10.48364/ISIMIP.581124.3>

1371 Lan, X., Tans, P., & Thoning, K. W. (2023). *Trends in globally-averaged CO2 determined from NOAA*  
1372 *Global Monitoring Laboratory measurements. Version 2023-01 NOAA/GML* [Dataset].  
1373 <https://gml.noaa.gov/ccgg/trends/>

1374 Large W. G., A. S. G. Y. (2004). *Diurnal to decadal global forcing for ocean and sea ice models: the data*  
1375 *sets and flux climatologies* (No. NCAR/TN460+STR). CGD Division of the National Centre for  
1376 Atmospheric Research (NCAR). [https://www.researchgate.net/profile/Stephen-](https://www.researchgate.net/profile/Stephen-Yeager/publication/281588002_Diurnal_to_Decadal_Global_Forcing_for_Ocean_and_Sea-Ice_Models_The_Data_Sets_and_Flux_Climatologies/links/55eede7108ae199d47bfaf41/Diurnal-to-Decadal-Global-Forcing-for-Ocean-and-Sea-Ice-Models-The-Data-Sets-and-Flux-Climatologies.pdf)  
1377 [Yeager/publication/281588002\\_Diurnal\\_to\\_Decadal\\_Global\\_Forcing\\_for\\_Ocean\\_and\\_Sea-](https://www.researchgate.net/profile/Stephen-Yeager/publication/281588002_Diurnal_to_Decadal_Global_Forcing_for_Ocean_and_Sea-Ice_Models_The_Data_Sets_and_Flux_Climatologies/links/55eede7108ae199d47bfaf41/Diurnal-to-Decadal-Global-Forcing-for-Ocean-and-Sea-Ice-Models-The-Data-Sets-and-Flux-Climatologies.pdf)  
1378 [Ice\\_Models\\_The\\_Data\\_Sets\\_and\\_Flux\\_Climatologies/links/55eede7108ae199d47bfaf41/Diurnal-](https://www.researchgate.net/profile/Stephen-Yeager/publication/281588002_Diurnal_to_Decadal_Global_Forcing_for_Ocean_and_Sea-Ice_Models_The_Data_Sets_and_Flux_Climatologies/links/55eede7108ae199d47bfaf41/Diurnal-to-Decadal-Global-Forcing-for-Ocean-and-Sea-Ice-Models-The-Data-Sets-and-Flux-Climatologies.pdf)  
1379 [to-Decadal-Global-Forcing-for-Ocean-and-Sea-Ice-Models-The-Data-Sets-and-Flux-](https://www.researchgate.net/profile/Stephen-Yeager/publication/281588002_Diurnal_to_Decadal_Global_Forcing_for_Ocean_and_Sea-Ice_Models_The_Data_Sets_and_Flux_Climatologies/links/55eede7108ae199d47bfaf41/Diurnal-to-Decadal-Global-Forcing-for-Ocean-and-Sea-Ice-Models-The-Data-Sets-and-Flux-Climatologies.pdf)  
1380 [Climatologies.pdf](https://www.researchgate.net/profile/Stephen-Yeager/publication/281588002_Diurnal_to_Decadal_Global_Forcing_for_Ocean_and_Sea-Ice_Models_The_Data_Sets_and_Flux_Climatologies/links/55eede7108ae199d47bfaf41/Diurnal-to-Decadal-Global-Forcing-for-Ocean-and-Sea-Ice-Models-The-Data-Sets-and-Flux-Climatologies.pdf)

1381 Lee, C.-Y., Camargo, S. J., Sobel, A. H., & Tippett, M. K. (2020). Statistical–Dynamical Downscaling  
1382 Projections of Tropical Cyclone Activity in a Warming Climate: Two Diverging Genesis Scenarios.  
1383 *Journal of Climate*, 33(11), 4815–4834. <https://doi.org/10.1175/JCLI-D-19-0452.1>

1384 Lee, C.-Y., Camargo, S. J., Sobel, A., Tippett, M. K., Quesada-Chacón, D., Büchner, M., Novak, L., & Otto,  
1385 C. (2025). *ISIMIP3b tropical cyclone tracks (CHAZ)* [Dataset]. ISIMIP Repository.  
1386 <https://doi.org/10.48364/ISIMIP.808980>

1387 Lee, C.-Y., Tippett, M. K., Camargo, S. J., & Sobel, A. H. (2015). Probabilistic Multiple Linear Regression  
1388 Modeling for Tropical Cyclone Intensity. *Monthly Weather Review*, 143(3), 933–954.  
1389 <https://doi.org/10.1175/MWR-D-14-00171.1>

1390 Lee, C.-Y., Tippett, M. K., Sobel, A. H., & Camargo, S. J. (2016). Rapid intensification and the bimodal

1391 distribution of tropical cyclone intensity. *Nature Communications*, 7, 10625.

1392 <https://doi.org/10.1038/ncomms10625>

1393 Lee, C.-Y., Tippett, M. K., Sobel, A. H., & Camargo, S. J. (2018). An environmentally forced tropical  
1394 cyclone hazard model. *Journal of Advances in Modeling Earth Systems*, 10(1), 223–241.

1395 <https://doi.org/10.1002/2017ms001186>

1396 Lengaigne, M., Pang, S., Silvy, Y., Danielli, V., Gopika, S., Sadhvi, K., Dutheil, C., Rousset, C., Ethé, C.,  
1397 Person, R., Madec, G., Barrier, N., Maury, O., Dalaut, L., Menkes, C., Nicol, S., Gorgues, T., Melet, A.,  
1398 & Guihou, K. (2025). Vialard: An ocean modelling framework for mitigating oceanic projections  
1399 from global climate models present-day biases. In *Earth future*.

1400 Liang, Y., Gillett, N. P., & Monahan, A. H. (2024). Accounting for Pacific climate variability increases  
1401 projected global warming. *Nature Climate Change*, 14(6), 608–614.

1402 <https://doi.org/10.1038/s41558-024-02017-y>

1403 Li, G., Xie, S.-P., Du, Y., & Luo, Y. (2016). Effects of excessive equatorial cold tongue bias on the  
1404 projections of tropical Pacific climate change. Part I: the warming pattern in CMIP5 multi-model  
1405 ensemble. *Climate Dynamics*, 47(12), 3817–3831. <https://doi.org/10.1007/s00382-016-3043-5>

1406 Madec, G. (2015). NEMO ocean engine, Version 3.6 stable Note du Pole de modelisation de l'Institut  
1407 Pierre-Simon Laplace, vol. 27. *IPSL, Paris: France*.

1408 Maraun, D. (2013). Bias Correction, Quantile Mapping, and Downscaling: Revisiting the Inflation Issue.  
1409 *Journal of Climate*, 26(6), 2137–2143. <https://doi.org/10.1175/JCLI-D-12-00821.1>

1410 Mauritsen, T., Bader, J., Becker, T., Behrens, J., Bittner, M., Brokopf, R., Brovkin, V., Claussen, M.,  
1411 Crueger, T., Esch, M., Fast, I., Fiedler, S., Fläschner, D., Gayler, V., Giorgetta, M., Goll, D. S., Haak, H.,  
1412 Hagemann, S., Hedemann, C., ... Roeckner, E. (2019). Developments in the MPI-M Earth System  
1413 Model version 1.2 (MPI-ESM1.2) and Its Response to Increasing CO<sub>2</sub>. *Journal of Advances in  
1414 Modeling Earth Systems*, 11(4), 998–1038. <https://doi.org/10.1029/2018MS001400>

1415 Meehl, G. A., Senior, C. A., Eyring, V., Flato, G., Lamarque, J.-F., Stouffer, R. J., Taylor, K. E., & Schlund, M.  
1416 (2020). Context for interpreting equilibrium climate sensitivity and transient climate response from  
1417 the CMIP6 Earth system models. *Science Advances*, 6(26), eaba1981.  
1418 <https://doi.org/10.1126/sciadv.aba1981>

1419 Meiler, S., Vogt, T., Bloemendaal, N., Ciullo, A., Lee, C.-Y., Camargo, S. J., Emanuel, K., & Bresch, D. N.  
1420 (2022). Intercomparison of regional loss estimates from global synthetic tropical cyclone models.  
1421 *Nature Communications*, 13(1), 6156. <https://doi.org/10.1038/s41467-022-33918-1>

1422 Meinshausen, M., Nicholls, Z. R. J., Lewis, J., Gidden, M. J., Vogel, E., Freund, M., Beyerle, U., Gessner, C.,  
1423 Nauels, A., Bauer, N., Canadell, J. G., Daniel, J. S., John, A., Krummel, P. B., Luderer, G.,  
1424 Meinshausen, N., Montzka, S. A., Rayner, P. J., Reimann, S., ... Wang, R. H. J. (2020). The shared  
1425 socio-economic pathway (SSP) greenhouse gas concentrations and their extensions to 2500.  
1426 *Geoscientific Model Development*, 13(8), 3571–3605. <https://doi.org/10.5194/gmd-13-3571-2020>

1427 Meinshausen, M., Smith, S. J., Calvin, K., Daniel, J. S., Kainuma, M. L. T., Lamarque, J.-F., Matsumoto, K.,  
1428 Montzka, S. A., Raper, S. C. B., Riahi, K., Thomson, A., Velders, G. J. M., & van Vuuren, D. P. P.  
1429 (2011). The RCP greenhouse gas concentrations and their extensions from 1765 to 2300. *Climatic  
1430 Change*, 109(1), 213. <https://doi.org/10.1007/s10584-011-0156-z>

1431 Meinshausen, M., Vogel, E., Nauels, A., Lorbacher, K., Meinshausen, N., Etheridge, D. M., Fraser, P. J.,  
1432 Montzka, S. A., Rayner, P. J., Trudinger, C. M., Krummel, P. B., Beyerle, U., Canadell, J. G., Daniel, J.  
1433 S., Enting, I. G., Law, R. M., Lunder, C. R., O'Doherty, S., Prinn, R. G., ... Weiss, R. (2017). Historical  
1434 greenhouse gas concentrations for climate modelling (CMIP6). *Geoscientific Model Development*,  
1435 10(5), 2057–2116. <https://doi.org/10.5194/gmd-10-2057-2017>

1436 Muis, S., Aerts, J. C. J. H., Á. Antolínez, J. A., Dullaart, J. C., Duong, T. M., Erikson, L., Haarsma, R. J.,  
1437 Apecechea, M. I., Mengel, M., Le Bars, D., O'Neill, A., Ranasinghe, R., Roberts, M. J., Verlaan, M.,  
1438 Ward, P. J., & Yan, K. (2023). Global projections of storm surges using high-resolution CMIP6

1439 climate models. *Earth's Future*, 11(9). <https://doi.org/10.1029/2023ef003479>

1440 Muis, S., Apecechea, M. I., Dullaart, J., de Lima Rego, J., Madsen, K. S., Su, J., Yan, K., & Verlaan, M.  
1441 (2020). A High-Resolution Global Dataset of Extreme Sea Levels, Tides, and Storm Surges, Including  
1442 Future Projections. *Frontiers in Marine Science*, 7. <https://doi.org/10.3389/fmars.2020.00263>

1443 O'Neill, B. C., Tebaldi, C., van Vuuren, D. P., Eyring, V., Friedlingstein, P., Hurtt, G., Knutti, R., Kriegler, E.,  
1444 Lamarque, J.-F., Lowe, J., Meehl, G. A., Moss, R., Riahi, K., & Sanderson, B. M. (2016). The Scenario  
1445 Model Intercomparison Project (ScenarioMIP) for CMIP6. *Geoscientific Model Development*, 9(9),  
1446 3461–3482. <https://doi.org/10.5194/gmd-9-3461-2016>

1447 Perrette, M., & Mengel, M. (submitted 2024). *Relative sea level projections constrained by historical*  
1448 *trends at tide gauge sites*.

1449 Perrette, M., & Mengel, M. (2025). *Relative sea level projections at tide-gauge locations* [Dataset].  
1450 Zenodo. <https://doi.org/10.1126/sciadv.ado4506>

1451 Quesada-Chacón, D., Novak, L., Hamester, L., & Otto, C. (2025). *ISIMIP3b tropical cyclone wind and rain*  
1452 *fields (MIT)* [Dataset]. ISIMIP Repository. <https://doi.org/10.48364/ISIMIP.779038>

1453 Righi, M., Andela, B., Eyring, V., Lauer, A., Predoi, V., Schlund, M., Vegas-Regidor, J., Bock, L., Brötz, B., de  
1454 Mora, L., Diblen, F., Dreyer, L., Drost, N., Earnshaw, P., Hassler, B., Koldunov, N., Little, B., Loosveldt  
1455 Tomas, S., & Zimmermann, K. (2020). Earth System Model Evaluation Tool (ESMValTool) v2.0 –  
1456 technical overview. *Geoscientific Model Development*, 13(3), 1179–1199.  
1457 <https://doi.org/10.5194/gmd-13-1179-2020>

1458 Ruosteenoja, K., Jylhä, K., Räisänen, J., & Mäkelä, A. (2017). Surface air relative humidities spuriously  
1459 exceeding 100% in CMIP5 model output and their impact on future projections. *JGR Atmospheres*,  
1460 122(18), 9557–9568. <https://doi.org/10.1002/2017JD026909>

1461 Ruosteenoja, K., Jylhä, K., Räisänen, J., & Mäkelä, A. (2018). Reply to comment by genthon et al. On  
1462 “surface air relative humidities spuriously exceeding 100% in CMIP5 model output and their impact

1463 on future projections." *Journal of Geophysical Research*, 123(16), 8728–8734.

1464 <https://doi.org/10.1029/2018jd028680>

1465 Schupfner, M., Wieners, K.-H., Wachsmann, F., Steger, C., Bittner, M., Jungclaus, J., Früh, B., Pankatz, K.,

1466 Giorgetta, M., Reick, C., Legutke, S., Esch, M., Gayler, V., Haak, H., de Vrese, P., Raddatz, T.,

1467 Mauritsen, T., von Storch, J.-S., Behrens, J., ... Roeckner, E. (2019). *DKRZ MPI-ESM1.2-HR model*

1468 *output prepared for CMIP6 ScenarioMIP* [Dataset]. Earth System Grid Federation.

1469 <https://doi.org/10.22033/ESGF/CMIP6.2450>

1470 Séférian, R., Berthet, S., Yool, A., Palmiéri, J., Bopp, L., Tagliabue, A., Kwiatkowski, L., Aumont, O.,

1471 Christian, J., Dunne, J., Gehlen, M., Ilyina, T., John, J. G., Li, H., Long, M. C., Luo, J. Y., Nakano, H.,

1472 Romanou, A., Schwinger, J., ... Yamamoto, A. (2020). Tracking Improvement in Simulated Marine

1473 Biogeochemistry Between CMIP5 and CMIP6. *Current Climate Change Reports*, 6(3), 95–119.

1474 <https://doi.org/10.1007/s40641-020-00160-0>

1475 Sellar, A. A., Jones, C. G., Mulcahy, J. P., Tang, Y., Yool, A., Wiltshire, A., O'Connor, F. M., Stringer, M.,

1476 Hill, R., Palmieri, J., Woodward, S., Mora, L., Kuhlbrodt, T., Rumbold, S. T., Kelley, D. I., Ellis, R.,

1477 Johnson, C. E., Walton, J., Abraham, N. L., ... Zerroukat, M. (2019). UKESM1: Description and

1478 evaluation of the U.k. earth system model. *Journal of Advances in Modeling Earth Systems*, 11(12),

1479 4513–4558. <https://doi.org/10.1029/2019ms001739>

1480 Shakespeare, C. J., & Roderick, M. L. (2022). Diagnosing instantaneous forcing and feedbacks of

1481 downwelling longwave radiation at the surface: A simple methodology and its application to CMIP5

1482 models. *Journal of Climate*, 35(12), 3785–3801. <https://doi.org/10.1175/jcli-d-21-0865.1>

1483 Shiogama, H., Fujimori, S., Hasegawa, T., Hayashi, M., Hirabayashi, Y., Ogura, T., Iizumi, T., Takahashi, K.,

1484 & Takemura, T. (2023). Important distinctiveness of SSP3–7.0 for use in impact assessments. *Nature*

1485 *Climate Change*, 13(12), 1276–1278. <https://doi.org/10.1038/s41558-023-01883-2>

1486 Sobel, A. H., Lee, C.-Y., Bowen, S. G., Camargo, S. J., Cane, M. A., Clement, A., Fosu, B., Hart, M., Reed, K.

1487 A., Seager, R., & Tippet, M. K. (2021). Near-term tropical cyclone risk and coupled Earth system  
1488 model biases. *Proceedings of the National Academy of Sciences of the United States of America*,  
1489 *120*(33), e2209631120. <https://doi.org/10.1073/pnas.2209631120>

1490 Sobel, A. H., Lee, C.-Y., Camargo, S. J., Mandli, K. T., Emanuel, K. A., Mukhopadhyay, P., & Mahakur, M.  
1491 (2019). Tropical Cyclone Hazard to Mumbai in the Recent Historical Climate. *Monthly Weather*  
1492 *Review*, *147*(7), 2355–2366. <https://doi.org/10.1175/MWR-D-18-0419.1>

1493 Stewart, K. D., Kim, W. M., Urakawa, S., Hogg, A. M., Yeager, S., Tsujino, H., Nakano, H., Kiss, A. E., &  
1494 Danabasoglu, G. (2020). JRA55-do-based repeat year forcing datasets for driving ocean–sea-ice  
1495 models. *Ocean Modelling*, *147*, 101557. <https://doi.org/10.1016/j.ocemod.2019.101557>

1496 Swaminathan, R., Schewe, J., Walton, J., Zimmermann, K., Jones, C., Betts, R. A., Burton, C., Jones, C. D.,  
1497 Mengel, M., Reyer, C. P. O., Turner, A. G., & Weigel, K. (2024). Regional impacts poorly constrained  
1498 by climate sensitivity. *Earth's Future*, *12*(12). <https://doi.org/10.1029/2024ef004901>

1499 Switanek, M. B., Troch, P. A., Castro, C. L., Leuprecht, A., Chang, H.-I., Mukherjee, R., & Demaria, E. M. C.  
1500 (2017). Scaled distribution mapping: a bias correction method that preserves raw climate model  
1501 projected changes. *Hydrology and Earth System Sciences*, *21*(6), 2649–2666.  
1502 <https://doi.org/10.5194/hess-21-2649-2017>

1503 Tagliabue, A., Kwiatkowski, L., Bopp, L., Butenschön, M., Cheung, W., Lengaigne, M., & Vialard, J. (2021).  
1504 Persistent Uncertainties in Ocean Net Primary Production Climate Change Projections at Regional  
1505 Scales Raise Challenges for Assessing Impacts on Ecosystem Services. *Frontiers in Climate*, *3*.  
1506 <https://doi.org/10.3389/fclim.2021.738224>

1507 Tang, Y., Rumbold, S., Ellis, R., Kelley, D., Mulcahy, J., Sellar, A., Walton, J., & Jones, C. (2019). *MOHC*  
1508 *UKESM1.0-LL model output prepared for CMIP6 CMIP* [Dataset]. Earth System Grid Federation.  
1509 <https://doi.org/10.22033/ESGF/CMIP6.1569>

1510 Themeßl, M. J., Gobiet, A., & Heinrich, G. (2012). Empirical-statistical downscaling and error correction

1511 of regional climate models and its impact on the climate change signal. *Climatic Change*, 112(2),  
1512 449–468. <https://doi.org/10.1007/s10584-011-0224-4>

1513 Thrasher, B., Maurer, E. P., McKellar, C., & Duffy, P. B. (2012). Technical Note: Bias correcting climate  
1514 model simulated daily temperature extremes with quantile mapping. *Hydrology and Earth System  
1515 Sciences*, 16(9), 3309–3314. <https://doi.org/10.5194/hess-16-3309-2012>

1516 Tippet, M. K., Camargo, S. J., & Sobel, A. H. (2011). A Poisson Regression Index for Tropical Cyclone  
1517 Genesis and the Role of Large-Scale Vorticity in Genesis. *Journal of Climate*, 24(9), 2335–2357.  
1518 <https://doi.org/10.1175/2010JCLI3811.1>

1519 Treu, S., Muis, S., Dangendorf, S., Wahl, T., Oelsmann, J., Heinicke, S., Frieler, K., & Mengel, M. (2023).  
1520 Reconstruction of hourly coastal water levels and counterfactuals without sea level rise for impact  
1521 attribution. In *Earth System Science Data Discussions*. <https://doi.org/10.5194/essd-2023-112>

1522 Tsujino, H., Urakawa, L. S., Griffies, S. M., Danabasoglu, G., Adcroft, A. J., Amaral, A. E., Arsouze, T.,  
1523 Bentsen, M., Bernardello, R., Böning, C. W., Bozec, A., Chassignet, E. P., Danilov, S., Dussin, R.,  
1524 Exarchou, E., Fogli, P. G., Fox-Kemper, B., Guo, C., Ilicak, M., ... Yu, Z. (2020). Evaluation of global  
1525 ocean–sea-ice model simulations based on the experimental protocols of the Ocean Model  
1526 Intercomparison Project phase 2 (OMIP-2). *Geoscientific Model Development*, 13(8), 3643–3708.  
1527 <https://doi.org/10.5194/gmd-13-3643-2020>

1528 Tsujino, H., Urakawa, S., Nakano, H., Small, R. J., Kim, W. M., Yeager, S. G., Danabasoglu, G., Suzuki, T.,  
1529 Bamber, J. L., Bentsen, M., Böning, C. W., Bozec, A., Chassignet, E. P., Curchitser, E., Boeira Dias, F.,  
1530 Durack, P. J., Griffies, S. M., Harada, Y., Ilicak, M., ... Yamazaki, D. (2018). JRA-55 based surface  
1531 dataset for driving ocean–sea-ice models (JRA55-do). *Ocean Modelling*, 130, 79–139.  
1532 <https://doi.org/10.1016/j.ocemod.2018.07.002>

1533 Watanabe, M., Kang, S. M., Collins, M., Hwang, Y.-T., McGregor, S., & Stuecker, M. F. (2024). Possible  
1534 shift in controls of the tropical Pacific surface warming pattern. *Nature*, 630(8016), 315–324.

1535 <https://doi.org/10.1038/s41586-024-07452-7>

1536 Weedon, G. P., Gomes, S., Viterbo, P., Österle, H., Adam, J. C., Bellouin, N., Boucher, O., & Best, M.  
1537 (2010). *The watch forcing data 1958-2001: a meteorological forcing data set for land surface- and*  
1538 *hydrological-models*. 41. [https://publications.pik-potsdam.de/pubman/item/item\\_16400](https://publications.pik-potsdam.de/pubman/item/item_16400)

1539 Woodworth-Jefcoats, P. (2022). *therMizer-FishMIP-2022-HI: Code and data for FishMIP 2022 ISIMIP 3a -*  
1540 *Hawaii longline fishing ground regional model*. Github. [https://github.com/pwoodworth-](https://github.com/pwoodworth-jefcoats/therMizer-FishMIP-2022-HI)  
1541 [jefcoats/therMizer-FishMIP-2022-HI](https://github.com/pwoodworth-jefcoats/therMizer-FishMIP-2022-HI)

1542 Yukimoto, S., Kawai, H., Koshiro, T., Oshima, N., Yoshida, K., Urakawa, S., Tsujino, H., Deushi, M., Tanaka,  
1543 T., Hosaka, M., Yabu, S., Yoshimura, H., Shindo, E., Mizuta, R., Obata, A., Adachi, Y., & Ishii, M.  
1544 (2019). The Meteorological Research Institute Earth System Model Version 2.0, MRI-ESM2.0:  
1545 Description and Basic Evaluation of the Physical Component. *Journal of the Meteorological Society*  
1546 *of Japan. Ser. II, 97(5)*, 931–965. <https://doi.org/10.2151/jmsj.2019-051>

1547 Yukimoto, S., Koshiro, T., Kawai, H., Oshima, N., Yoshida, K., Urakawa, S., Tsujino, H., Deushi, M., Tanaka,  
1548 T., Hosaka, M., Yoshimura, H., Shindo, E., Mizuta, R., Ishii, M., Obata, A., & Adachi, Y. (2019a). *MRI*  
1549 *MRI-ESM2.0 model output prepared for CMIP6 CMIP* [Dataset]. Earth System Grid Federation.  
1550 <https://doi.org/10.22033/ESGF/CMIP6.621>

1551 Yukimoto, S., Koshiro, T., Kawai, H., Oshima, N., Yoshida, K., Urakawa, S., Tsujino, H., Deushi, M., Tanaka,  
1552 T., Hosaka, M., Yoshimura, H., Shindo, E., Mizuta, R., Ishii, M., Obata, A., & Adachi, Y. (2019b). *MRI*  
1553 *MRI-ESM2.0 model output prepared for CMIP6 ScenarioMIP* [Dataset]. Earth System Grid  
1554 Federation. <https://doi.org/10.22033/ESGF/CMIP6.638>

1555 Zelinka, M. D., Myers, T. A., McCoy, D. T., Po-Chedley, S., Caldwell, P. M., Ceppi, P., Klein, S. A., & Taylor,  
1556 K. E. (2020). Causes of higher climate sensitivity in CMIP6 models. *Geophysical Research Letters*,  
1557 *47(1)*. <https://doi.org/10.1029/2019gl085782>

1558 Zhang, L., & Li, T. (2014). A simple analytical model for understanding the formation of sea surface

1559 temperature patterns under global warming. *Journal of Climate*, 27(22), 8413–8421.  
1560 <https://doi.org/10.1175/jcli-d-14-00346.1>

1561 Zhu, L., Quiring, S. M., & Emanuel, K. A. (2013). Estimating tropical cyclone precipitation risk in Texas.  
1562 *Geophysical Research Letters*, 40(23), 6225–6230. <https://doi.org/10.1002/2013gl058284>

1563 Adler, R. F., Huffman, G. J., Chang, A., Ferraro, R., Xie, P.-P., Janowiak, J., Rudolf, B., Schneider, U., Curtis,  
1564 S., Bolvin, D., Gruber, A., Susskind, J., Arkin, P., & Nelkin, E. (2003). The Version-2 Global  
1565 Precipitation Climatology Project (GPCP) Monthly Precipitation Analysis (1979–Present). *Journal of*  
1566 *Hydrometeorology*, 4(6), 1147–1167. [https://doi.org/10.1175/1525-](https://doi.org/10.1175/1525-7541(2003)004<1147:TVGPCP>2.0.CO;2)  
1567 [7541\(2003\)004<1147:TVGPCP>2.0.CO;2](https://doi.org/10.1175/1525-7541(2003)004<1147:TVGPCP>2.0.CO;2)

1568 Andela, B., Broetz, B., de Mora, L., Drost, N., Eyring, V., Koldunov, N., Lauer, A., Mueller, B., Predoi, V.,  
1569 Righi, M., Schlund, M., Vegas-Regidor, J., Zimmermann, K., Adeniyi, K., Arnone, E., Bellprat, O., Berg,  
1570 P., Bock, L., Caron, L.-P., ... Weigel, K. (2020). ESMValTool. <https://doi.org/10.5281/zenodo.3970975>

1571 Andela, B., Broetz, B., de Mora, L., Drost, N., Eyring, V., Koldunov, N., Lauer, A., Predoi, V., Righi, M.,  
1572 Schlund, M., Vegas-Regidor, J., Zimmermann, K., Bock, L., Diblen, F., Dreyer, L., Earnshaw, P.,  
1573 Hassler, B., Little, B., & Loosveldt-Tomas, S. (2020). ESMValCore.  
1574 <https://doi.org/10.5281/zenodo.3952695>

1575 Barrier, N., Lengaigne, M., Rault, J., Person, R., Ethé, C., Aumont, O., & Maury, O. (2023). Mechanisms  
1576 underlying the epipelagic ecosystem response to ENSO in the equatorial Pacific ocean. *Progress in*  
1577 *Oceanography*, 213, 103002. <https://doi.org/10.1016/j.pocean.2023.103002>

1578 Bock, L., Lauer, A., Schlund, M., Barreiro, M., Bellouin, N., Jones, C., Meehl, G. A., Predoi, V., Roberts, M.  
1579 J., & Eyring, V. (2020). Quantifying progress across different CMIP phases with the ESMValTool.  
1580 *Journal of Geophysical Research*, 125(21). <https://doi.org/10.1029/2019jd032321>

1581 Boucher, O., Denvil, S., Levvasseur, G., Cozic, A., Caubel, A., Foujols, M.-A., Meurdesoif, Y., Cadule, P.,

1582 Devilliers, M., Dupont, E., & Lurton, T. (2019). IPSL IPSL-CM6A-LR model output prepared for CMIP6  
1583 ScenarioMIP [Dataset]. Earth System Grid Federation. <https://doi.org/10.22033/ESGF/CMIP6.1532>

1584 Boucher, O., Denvil, S., Levavasseur, G., Cozic, A., Caubel, A., Foujols, M.-A., Meurdesoif, Y., Cadule, P.,  
1585 Devilliers, M., Ghattas, J., Lebas, N., Lurton, T., Mellul, L., Musat, I., Mignot, J., & Cheruy, F. (2018).  
1586 IPSL IPSL-CM6A-LR model output prepared for CMIP6 CMIP [Dataset]. Earth System Grid  
1587 Federation. <https://doi.org/10.22033/ESGF/CMIP6.1534>

1588 Boucher, O., Servonnat, J., Albright, A. L., Aumont, O., Balkanski, Y., Bastrikov, V., Bekki, S., Bonnet, R.,  
1589 Bony, S., Bopp, L., Braconnot, P., Brockmann, P., Cadule, P., Caubel, A., Cheruy, F., Codron, F., Cozic,  
1590 A., Cugnet, D., D'Andrea, F., ... Vuichard, N. (2020). Presentation and evaluation of the IPSL-CM6A-  
1591 LR climate model. *Journal of Advances in Modeling Earth Systems*, 12(7).  
1592 <https://doi.org/10.1029/2019ms002010>

1593 Büchner, M., & Reyer, C. (2022). ISIMIP3b atmospheric composition input data [Dataset]. ISIMIP  
1594 Repository. <https://doi.org/10.48364/ISIMIP.482153.1>

1595 Buck, A. L. (1981). New Equations for Computing Vapor Pressure and Enhancement Factor. *Journal of*  
1596 *Applied Meteorology and Climatology*, 20(12), 1527–1532. [https://doi.org/10.1175/1520-0450\(1981\)020<1527:NEFCVP>2.0.CO;2](https://doi.org/10.1175/1520-0450(1981)020<1527:NEFCVP>2.0.CO;2)

1598 Camargo, S. J., Tippett, M. K., Sobel, A. H., Vecchi, G. A., & Zhao, M. (2014). Testing the Performance of  
1599 Tropical Cyclone Genesis Indices in Future Climates Using the HiRAM Model. *Journal of Climate*,  
1600 27(24), 9171–9196. <https://doi.org/10.1175/JCLI-D-13-00505.1>

1601 Cannon, A. J. (2018). Multivariate quantile mapping bias correction: an N-dimensional probability  
1602 density function transform for climate model simulations of multiple variables. *Climate Dynamics*,  
1603 50(1), 31–49. <https://doi.org/10.1007/s00382-017-3580-6>

1604 Cecil, D. (2006). LIS/OTD 0.5 Degree High Resolution Monthly Climatology (HRMC) [Dataset]. NASA  
1605 Global Hydrometeorology Resource Center DAAC. <https://doi.org/10.5067/LIS/LIS-OTD/DATA303>

1606 Cucchi, M., Weedon, G. P., Amici, A., Bellouin, N., Lange, S., Müller Schmied, H., Hersbach, H., &  
1607 Buontempo, C. (2020). WFDE5: bias-adjusted ERA5 reanalysis data for impact studies. *Earth System  
1608 Science Data*, 12(3), 2097–2120. <https://doi.org/10.5194/essd-12-2097-2020>

1609 Dunne, J. P., Horowitz, L. W., Adcroft, A. J., Ginoux, P., Held, I. M., John, J. G., Krasting, J. P., Malyshev, S.,  
1610 Naik, V., Paulot, F., Shevliakova, E., Stock, C. A., Zadeh, N., Balaji, V., Blanton, C., Dunne, K. A.,  
1611 Dupuis, C., Durachta, J., Dussin, R., ... Zhao, M. (2020). The GFDL earth system model version 4.1  
1612 (GFDL-ESM 4.1): Overall coupled model description and simulation characteristics. *Journal of  
1613 Advances in Modeling Earth Systems*, 12(11). <https://doi.org/10.1029/2019ms002015>

1614 Durack, P. J. (n.d.). CMIP6 source\_id values. Retrieved January 16, 2023, from [https://wcrp-  
1615 cmip.github.io/CMIP6\\_CVs/docs/CMIP6\\_source\\_id.html](https://wcrp-cmip.github.io/CMIP6_CVs/docs/CMIP6_source_id.html)

1616 Eddy, T. D., Heneghan, R. F., Bryndum-Buchholz, A., Fulton, E. A., Harrison, C. S., Tittensor, D. P., Lotze,  
1617 H. K., Ortega-Cisneros, K., Novaglio, C., Bianchi, D., Büchner, M., Bulman, C., Cheung, W. W. L.,  
1618 Christensen, V., Coll, M., Everett, J. D., Fierro-Arcos, D., Galbraith, E. D., Gascuel, D., ... Blanchard, J.  
1619 L. (2025). Global and regional marine ecosystem models reveal key uncertainties in climate change  
1620 projections. *Earth's Future*, 13(3). <https://doi.org/10.1029/2024ef005537>

1621 Emanuel, K., DesAutels, C., Holloway, C., & Korty, R. (2004). Environmental Control of Tropical Cyclone  
1622 Intensity. *Journal of the Atmospheric Sciences*, 61(7), 843–858. [https://doi.org/10.1175/1520-  
0469\(2004\)061<0843:ECOTCI>2.0.CO;2](https://doi.org/10.1175/1520-<br/>1623 0469(2004)061<0843:ECOTCI>2.0.CO;2)

1624 Emanuel, K., Sundararajan, R., & Williams, J. (2008). Hurricanes and Global Warming: Results from  
1625 Downscaling IPCC AR4 Simulations. *Bulletin of the American Meteorological Society*, 89(3), 347–  
1626 368. <https://doi.org/10.1175/BAMS-89-3-347>

1627 Eyring, V., Bony, S., Meehl, G. A., Senior, C. A., Stevens, B., Stouffer, R. J., & Taylor, K. E. (2016). Overview  
1628 of the Coupled Model Intercomparison Project Phase 6 (CMIP6) experimental design and  
1629 organization. *Geoscientific Model Development*, 9(5), 1937–1958. <https://doi.org/10.5194/gmd-9->

1630 1937-2016

1631 Eyring, V., Gillett, N. P., Achuta Rao, K. M., Barimalala, R., Barreiro Parrillo, M., Bellouin, N., V. Masson-  
1632 Delmotte, P. Zhai, A. Pirani, S. L. Connors, C. Péan, S. Berger, & Intergovernmental Panel on Climate  
1633 Change (IPCC). (2023). Human Influence on the Climate System. In *Climate Change 2021 – The*  
1634 *Physical Science Basis: Working Group I Contribution to the Sixth Assessment Report of the*  
1635 *Intergovernmental Panel on Climate Change* (pp. 423–552). Cambridge University Press.  
1636 <https://doi.org/10.1017/9781009157896.005>

1637 Fosu, B., Sobel, A., Camargo, S., Tippett, M., Hemmati, M., Bowen, S., & Bloemendaal, N. (2024).  
1638 Assessing future tropical cyclone risk using downscaled 1 CMIP6 projections. *Journal of Catastrophe*  
1639 *Risk and Resilience*, 2(1). <https://doi.org/10.63024/dpva-2pa1>

1640 Frieler, K. (submitted 2023). Scenario Set-up and the new CMIP6-based climate-related forcings  
1641 provided within the third round of the Inter-Sectoral Model Intercomparison Project (ISIMIP3b,  
1642 group I and II). *Geoscientific Model Development*.

1643 Frieler, K., Lange, S., Piontek, F., Reyer, C. P. O., Schewe, J., Warszawski, L., Zhao, F., Chini, L., Denvil, S.,  
1644 Emanuel, K., Geiger, T., Halladay, K., Hurtt, G., Mengel, M., Murakami, D., Ostberg, S., Popp, A.,  
1645 Riva, R., Stevanovic, M., ... Yamagata, Y. (2017). Assessing the impacts of 1.5 °C global warming –  
1646 simulation protocol of the Inter-Sectoral Impact Model Intercomparison Project (ISIMIP2b).  
1647 *Geoscientific Model Development*, 10(12), 4321–4345. <https://doi.org/10.5194/gmd-10-4321-2017>

1648 Frieler, K., Volkholz, J., Lange, S., Schewe, J., Mengel, M., del Rocío Rivas López, M., Otto, C., Reyer, C. P.  
1649 O., Karger, D. N., & del Valle Gitta Lasslop Sarah Chadburn Eleanor Burke Angela Gallego-Sala Noah  
1650 Smith Jinfeng Chang Stijn Hantson Chantelle Burton Anne Gädeke Fang Li Simon N. Gosling Hannes  
1651 Müller Schmied Fred Hattermann Jida Wang Fangfang Yao Thomas Hickler Rafael Marcé Don  
1652 Pierson Wim Thiery Daniel Mercado-Bettín Robert Ladwig Ana Isabel Ayala-Zamora Matthew  
1653 Forrest and Michel Bechtold, J. T. M. S. T. C. M. J. L. B. C. S. H. C. M. P. T. D. E. K. O.-C. C. N. Y. R. R.

1654 A. W. C. S. X. L. R. H. D. T. O. M. M. B. T. V. T. W. F. S. I. J. S. J. K. I. V. J. J. C. M. S. R. J. K. I. D. V.  
1655 (2024, January 4). Scenario setup and forcing data for impact model evaluation and impact  
1656 attribution within the third round of the Inter-Sectoral Model Intercomparison Project (ISIMIP3a).  
1657 Geoscientific Model Development. [https://www.google.com/url?q=https://doi.org/10.5194/gmd-](https://www.google.com/url?q=https://doi.org/10.5194/gmd-17-1-2024&sa=D&source=docs&ust=1704377607845951&usg=AOvVaw3hFVXAV75ZSOClc8itQfEs)  
1658 [17-1-2024&sa=D&source=docs&ust=1704377607845951&usg=AOvVaw3hFVXAV75ZSOClc8itQfEs](https://www.google.com/url?q=https://doi.org/10.5194/gmd-17-1-2024&sa=D&source=docs&ust=1704377607845951&usg=AOvVaw3hFVXAV75ZSOClc8itQfEs)  
1659 Frieler, K., Volkholz, J., Lange, S., Schewe, J., Mengel, M., del Rocío Rivas López, M., Otto, C., Reyer, C. P.  
1660 O., Karger, D. N., Malle, J. T., Treu, S., Menz, C., Blanchard, J. L., Harrison, C. S., Petrik, C. M., Eddy,  
1661 T. D., Ortega-Cisneros, K., Novaglio, C., Rousseau, Y., ... Bechtold, M. (2024). Scenario setup and  
1662 forcing data for impact model evaluation and impact attribution within the third round of the Inter-  
1663 Sectoral Impact Model Intercomparison Project (ISIMIP3a). Geoscientific Model Development,  
1664 17(1), 1–51. <https://doi.org/10.5194/gmd-17-1-2024>  
1665 Frieler, K., Volkholz, J., Lange, S., Schewe, J., Mengel, M., Rivas López, M. del R., Otto, C., Reyer, C. P. O.,  
1666 Karger, D. N., Malle, J. T., Treu, S., Menz, C., Blanchard, J. L., Harrison, C. S., Petrik, C. M., Eddy, T.  
1667 D., Ortega-Cisneros, K., Novaglio, C., Rousseau, Y., ... Bechtold, M. (2023). Scenario set-up and  
1668 forcing data for impact model evaluation and impact attribution within the third round of the Inter-  
1669 Sectoral Model Intercomparison Project (ISIMIP3a). In EGU sphere.  
1670 <https://doi.org/10.5194/egusphere-2023-281>  
1671 Geiger, T., Gütschow, J., Bresch, D. N., Emanuel, K., & Frieler, K. (2021). Double benefit of limiting global  
1672 warming for tropical cyclone exposure. *Nature Climate Change*, 11(10), 861–866.  
1673 <https://doi.org/10.1038/s41558-021-01157-9>  
1674 Gennaretti, F., Sangelantoni, L., & Grenier, P. (2015). Toward daily climate scenarios for Canadian Arctic  
1675 coastal zones with more realistic temperature-precipitation interdependence. *JGR: Atmospheres*,  
1676 120(23), 11,862–11,877. <https://doi.org/10.1002/2015JD023890>  
1677 Gillett, N. P., Shiogama, H., Funke, B., Hegerl, G., Knutti, R., Matthes, K., Santer, B. D., Stone, D., &

1678 Tebaldi, C. (2016). The detection and Attribution Model Intercomparison Project (DAMIP v1.0)  
1679 contribution to CMIP6. *Geoscientific Model Development*, 9(10), 3685–3697.  
1680 <https://doi.org/10.5194/gmd-9-3685-2016>

1681 Good, P., Sellar, A., Tang, Y., Rumbold, S., Ellis, R., Kelley, D., Kuhlbrodt, T., & Walton, J. (2019). MOHC  
1682 UKESM1.0-LL model output prepared for CMIP6 ScenarioMIP [Dataset]. Earth System Grid  
1683 Federation. <https://doi.org/10.22033/ESGF/CMIP6.1567>

1684 Grenier, P. (2018). Two Types of Physical Inconsistency to Avoid with Univariate Quantile Mapping: A  
1685 Case Study over North America Concerning Relative Humidity and Its Parent Variables. *Journal of*  
1686 *Applied Meteorology and Climatology*, 57(2), 347–364. <https://doi.org/10.1175/JAMC-D-17-0177.1>

1687 Haerter, J. O., Hagemann, S., Moseley, C., & Piani, C. (2011). Climate model bias correction and the role  
1688 of timescales. *Hydrology and Earth System Sciences*, 15(3), 1065–1079.  
1689 <https://doi.org/10.5194/hess-15-1065-2011>

1690 Hausfather, Z., & Peters, G. P. (2020, January 29). Emissions – the “business as usual” story is misleading.  
1691 Nature Publishing Group UK. <https://doi.org/10.1038/d41586-020-00177-3>

1692 Hersbach, H., Bell, B., Berrisford, P., Hirahara, S., Horányi, A., Muñoz-Sabater, J., Nicolas, J., Peubey, C.,  
1693 Radu, R., Schepers, D., Simmons, A., Soci, C., Abdalla, S., Abellan, X., Balsamo, G., Bechtold, P.,  
1694 Biavati, G., Bidlot, J., Bonavita, M., ... Jean-Noël Thépaut. (2020). The ERA5 global reanalysis.  
1695 *Quarterly Journal of the Royal Meteorological Society*, 146(730), 1999–2049.  
1696 <https://doi.org/10.1002/qj.3803>

1697 Holland. (1980). An Analytic Model of the Wind and Pressure Profiles in Hurricanes, *Mon. Mon. Weather*  
1698 *Rev*, 108, 1212–1218.

1699 Holland. (2008). A revised hurricane pressure–wind model. *Monthly Weather Review*, 136(9), 3432–  
1700 3445. <https://doi.org/10.1175/2008mwr2395.1>

1701 ISIMIP3b simulation protocol. (2023). <https://protocol.isimip.org/>

1702 Jägermeyr, J., Müller, C., Ruane, A. C., Elliott, J., Balkovic, J., Castillo, O., Faye, B., Foster, I., Folberth, C.,  
1703 Franke, J. A., Fuchs, K., Guarin, J. R., Heinke, J., Hoogenboom, G., Iizumi, T., Jain, A. K., Kelly, D.,  
1704 Khabarov, N., Lange, S., ... Rosenzweig, C. (2021). Climate impacts on global agriculture emerge  
1705 earlier in new generation of climate and crop models. *Nature Food*, 2(11), 873–885.  
1706 <https://doi.org/10.1038/s43016-021-00400-y>

1707 John, J. G., Blanton, C., McHugh, C., Radhakrishnan, A., Rand, K., Vahlenkamp, H., Wilson, C., Zadeh, N.  
1708 T., Dunne, J. P., Dussin, R., Horowitz, L. W., Krasting, J. P., Lin, P., Malyshev, S., Naik, V., Ploshay, J.,  
1709 Shevliakova, E., Silvers, L., Stock, C., ... Zeng, Y. (2018). NOAA-GFDL GFDL-ESM4 model output  
1710 prepared for CMIP6 ScenarioMIP [Dataset]. Earth System Grid Federation.  
1711 <https://doi.org/10.22033/ESGF/CMIP6.1414>

1712 Jungclaus, J., Bittner, M., Wieners, K.-H., Wachsmann, F., Schupfner, M., Legutke, S., Giorgetta, M.,  
1713 Reick, C., Gayler, V., Haak, H., de Vrese, P., Raddatz, T., Esch, M., Mauritsen, T., von Storch, J.-S.,  
1714 Behrens, J., Brovkin, V., Claussen, M., Crueger, T., ... Roeckner, E. (2019). MPI-M MPIESM1.2-HR  
1715 model output prepared for CMIP6 CMIP [Dataset]. Earth System Grid Federation.  
1716 <https://doi.org/10.22033/ESGF/CMIP6.741>

1717 Kaplan, J. O., Koch, A., & Lau, K. H.-K. (2023). Estimated future global lightning strokes (2010-2100).  
1718 <https://doi.org/10.5281/zenodo.7511843>

1719 Kaplan, J. O., & Lau, K. H.-K. (2021). The WGLC global gridded lightning climatology and time series.  
1720 *Earth System Science Data*, 13(7), 3219–3237. <https://doi.org/10.5194/essd-13-3219-2021>

1721 Kaplan, J. O., & Lau, K. H.-K. (2022). World Wide Lightning Location Network (WWLLN) Global Lightning  
1722 Climatology (WGLC) and time series, 2022 update. *Earth System Science Data*, 14(12), 5665–5670.  
1723 <https://doi.org/10.5194/essd-14-5665-2022>

1724 Krasting, J. P., John, J. G., Blanton, C., McHugh, C., Nikonov, S., Radhakrishnan, A., Rand, K., Zadeh, N. T.,  
1725 Balaji, V., Durachta, J., Dupuis, C., Menzel, R., Robinson, T., Underwood, S., Vahlenkamp, H., Dunne,

1726 K. A., Gauthier, P. P. G., Ginoux, P., Griffies, S. M., ... Zhao, M. (2018). NOAA-GFDL GFDL-ESM4  
1727 model output prepared for CMIP6 CMIP [Dataset]. Earth System Grid Federation.  
1728 <https://doi.org/10.22033/ESGF/CMIP6.1407>

1729 Lange, S. (2017). ISIMIP2b Bias-Correction Code. <https://doi.org/10.5281/zenodo.1069050>

1730 Lange, S. (2018). Bias correction of surface downwelling longwave and shortwave radiation for the  
1731 EWEMBI dataset. *Earth System Dynamics*, 9(2), 627–645. <https://doi.org/10.5194/esd-9-627-2018>

1732 Lange, S. (2019a). Earth2Observe, WFDEI and ERA-interim data merged and bias-corrected for ISIMIP  
1733 (EWEMBI) [Dataset]. <https://doi.org/10.5880/pik.2019.004>

1734 Lange, S. (2019b). Trend-preserving bias adjustment and statistical downscaling with ISIMIP3BASD  
1735 (v1.0). *Geoscientific Model Development*, 12(7), 3055–3070. [https://doi.org/10.5194/gmd-12-](https://doi.org/10.5194/gmd-12-3055-2019)  
1736 [3055-2019](https://doi.org/10.5194/gmd-12-3055-2019)

1737 Lange, S. (2021a). ISIMIP3BASD. <https://doi.org/10.5281/zenodo.4686991>

1738 Lange, S. (2021b). ISIMIP3b bias adjustment fact sheet.  
1739 [https://www.isimip.org/documents/413/ISIMIP3b\\_bias\\_adjustment\\_fact\\_sheet\\_Gnsz7CO.pdf](https://www.isimip.org/documents/413/ISIMIP3b_bias_adjustment_fact_sheet_Gnsz7CO.pdf)

1740 Lange, S., Menz, C., Gleixner, S., Cucchi, M., Weedon, G. P., Amici, A., Bellouin, N., Schmied, H. M.,  
1741 Hersbach, H., Buontempo, C., & Cagnazzo, C. (2021). WFDE5 over land merged with ERA5 over the  
1742 ocean (W5E5 v2.0) [Dataset]. ISIMIP Repository. <https://doi.org/10.48364/ISIMIP.342217>

1743 Lange, S., Quesada-Chacón, D., & Büchner, M. (2023). Secondary ISIMIP3b bias-adjusted atmospheric  
1744 climate input data [Dataset]. ISIMIP Repository. <https://doi.org/10.48364/ISIMIP.581124.3>

1745 Lan, X., Tans, P., & Thoning, K. W. (2023). Trends in globally-averaged CO2 determined from NOAA  
1746 Global Monitoring Laboratory measurements. Version 2023-01 NOAA/GML [Dataset].  
1747 <https://gml.noaa.gov/ccgg/trends/>

1748 Large W. G., A. S. G. Y. (2004). Diurnal to decadal global forcing for ocean and sea ice models: the data  
1749 sets and flux climatologies (No. NCAR/TN460+STR). CGD Division of the National Centre for

1750 Atmospheric Research (NCAR). <https://www.researchgate.net/profile/Stephen->  
1751 [Yeager/publication/281588002\\_Diurnal\\_to\\_Decadal\\_Global\\_Forcing\\_for\\_Ocean\\_and\\_Sea-](https://www.researchgate.net/publication/281588002_Diurnal_to_Decadal_Global_Forcing_for_Ocean_and_Sea-)  
1752 [Ice\\_Models\\_The\\_Data\\_Sets\\_and\\_Flux\\_Climatologies/links/55eede7108ae199d47bfaf41/Diurnal-](https://www.researchgate.net/publication/281588002_Diurnal_to_Decadal_Global_Forcing_for_Ocean_and_Sea-Ice_Models_The_Data_Sets_and_Flux_Climatologies/links/55eede7108ae199d47bfaf41/Diurnal-)  
1753 [to-Decadal-Global-Forcing-for-Ocean-and-Sea-Ice-Models-The-Data-Sets-and-Flux-](https://www.researchgate.net/publication/281588002_Diurnal_to_Decadal_Global_Forcing_for_Ocean_and_Sea-Ice_Models_The_Data_Sets_and_Flux-)  
1754 [Climatologies.pdf](https://www.researchgate.net/publication/281588002_Diurnal_to_Decadal_Global_Forcing_for_Ocean_and_Sea-Ice_Models_The_Data_Sets_and_Flux-)

1755 Lee, C.-Y., Camargo, S. J., Sobel, A. H., & Tippett, M. K. (2020). Statistical–Dynamical Downscaling  
1756 Projections of Tropical Cyclone Activity in a Warming Climate: Two Diverging Genesis Scenarios.  
1757 *Journal of Climate*, 33(11), 4815–4834. <https://doi.org/10.1175/JCLI-D-19-0452.1>

1758 Lee, C.-Y., Tippett, M. K., Camargo, S. J., & Sobel, A. H. (2015). Probabilistic Multiple Linear Regression  
1759 Modeling for Tropical Cyclone Intensity. *Monthly Weather Review*, 143(3), 933–954.  
1760 <https://doi.org/10.1175/MWR-D-14-00171.1>

1761 Lee, C.-Y., Tippett, M. K., Sobel, A. H., & Camargo, S. J. (2016). Rapid intensification and the bimodal  
1762 distribution of tropical cyclone intensity. *Nature Communications*, 7, 10625.  
1763 <https://doi.org/10.1038/ncomms10625>

1764 Lee, C.-Y., Tippett, M. K., Sobel, A. H., & Camargo, S. J. (2018). An environmentally forced tropical  
1765 cyclone hazard model. *Journal of Advances in Modeling Earth Systems*, 10(1), 223–241.  
1766 <https://doi.org/10.1002/2017ms001186>

1767 Lengaigne, M., Pang, S., Silvy, Y., Danielli, V., Gopika, S., Sadhvi, K., Dutheil, C., Rousset, C., Ethé, C.,  
1768 Person, R., Madec, G., Barrier, N., Maury, O., Dalaut, L., Menkes, C., Nicol, S., Gorgues, T., Melet, A.,  
1769 & Guihou, K. (2025). Vialard: An ocean modelling framework for mitigating oceanic projections  
1770 from global climate models present-day biases. In *Earth future*.

1771 Li, G., Xie, S.-P., Du, Y., & Luo, Y. (2016). Effects of excessive equatorial cold tongue bias on the  
1772 projections of tropical Pacific climate change. Part I: the warming pattern in CMIP5 multi-model  
1773 ensemble. *Climate Dynamics*, 47(12), 3817–3831. <https://doi.org/10.1007/s00382-016-3043-5>

1774 Madec, G. (2015). NEMO ocean engine, Version 3.6 stable Note du Pole de modelisation de l'Institut  
1775 Pierre-Simon Laplace, vol. 27. IPSL, Paris: France.

1776 Maraun, D. (2013). Bias Correction, Quantile Mapping, and Downscaling: Revisiting the Inflation Issue.  
1777 Journal of Climate, 26(6), 2137–2143. <https://doi.org/10.1175/JCLI-D-12-00821.1>

1778 Mauritsen, T., Bader, J., Becker, T., Behrens, J., Bittner, M., Brokopf, R., Brovkin, V., Claussen, M.,  
1779 Crueger, T., Esch, M., Fast, I., Fiedler, S., Fläschner, D., Gayler, V., Giorgetta, M., Goll, D. S., Haak, H.,  
1780 Hagemann, S., Hedemann, C., ... Roeckner, E. (2019). Developments in the MPI-M Earth System  
1781 Model version 1.2 (MPI-ESM1.2) and Its Response to Increasing CO<sub>2</sub>. Journal of Advances in  
1782 Modeling Earth Systems, 11(4), 998–1038. <https://doi.org/10.1029/2018MS001400>

1783 Meehl, G. A., Senior, C. A., Eyring, V., Flato, G., Lamarque, J.-F., Stouffer, R. J., Taylor, K. E., & Schlund, M.  
1784 (2020). Context for interpreting equilibrium climate sensitivity and transient climate response from  
1785 the CMIP6 Earth system models. Science Advances, 6(26), eaba1981.  
1786 <https://doi.org/10.1126/sciadv.aba1981>

1787 Meiler, S., Vogt, T., Bloemendaal, N., Ciullo, A., Lee, C.-Y., Camargo, S. J., Emanuel, K., & Bresch, D. N.  
1788 (2022). Intercomparison of regional loss estimates from global synthetic tropical cyclone models.  
1789 Nature Communications, 13(1), 6156. <https://doi.org/10.1038/s41467-022-33918-1>

1790 Meinshausen, M., Nicholls, Z. R. J., Lewis, J., Gidden, M. J., Vogel, E., Freund, M., Beyerle, U., Gessner, C.,  
1791 Nauels, A., Bauer, N., Canadell, J. G., Daniel, J. S., John, A., Krummel, P. B., Luderer, G.,  
1792 Meinshausen, N., Montzka, S. A., Rayner, P. J., Reimann, S., ... Wang, R. H. J. (2020). The shared  
1793 socio-economic pathway (SSP) greenhouse gas concentrations and their extensions to 2500.  
1794 Geoscientific Model Development, 13(8), 3571–3605. <https://doi.org/10.5194/gmd-13-3571-2020>

1795 Meinshausen, M., Smith, S. J., Calvin, K., Daniel, J. S., Kainuma, M. L. T., Lamarque, J.-F., Matsumoto, K.,  
1796 Montzka, S. A., Raper, S. C. B., Riahi, K., Thomson, A., Velders, G. J. M., & van Vuuren, D. P. P.  
1797 (2011). The RCP greenhouse gas concentrations and their extensions from 1765 to 2300. Climatic

1798 Change, 109(1), 213. <https://doi.org/10.1007/s10584-011-0156-z>

1799 Meinshausen, M., Vogel, E., Nauels, A., Lorbacher, K., Meinshausen, N., Etheridge, D. M., Fraser, P. J.,  
1800 Montzka, S. A., Rayner, P. J., Trudinger, C. M., Krummel, P. B., Beyerle, U., Canadell, J. G., Daniel, J.  
1801 S., Enting, I. G., Law, R. M., Lunder, C. R., O'Doherty, S., Prinn, R. G., ... Weiss, R. (2017). Historical  
1802 greenhouse gas concentrations for climate modelling (CMIP6). *Geoscientific Model Development*,  
1803 10(5), 2057–2116. <https://doi.org/10.5194/gmd-10-2057-2017>

1804 Muis, S., Aerts, J. C. J. H., Á. Antolínez, J. A., Dullaart, J. C., Duong, T. M., Erikson, L., Haarsma, R. J.,  
1805 Apecechea, M. I., Mengel, M., Le Bars, D., O'Neill, A., Ranasinghe, R., Roberts, M. J., Verlaan, M.,  
1806 Ward, P. J., & Yan, K. (2023). Global projections of storm surges using high-resolution CMIP6  
1807 climate models. *Earth's Future*, 11(9). <https://doi.org/10.1029/2023ef003479>

1808 Muis, S., Apecechea, M. I., Dullaart, J., de Lima Rego, J., Madsen, K. S., Su, J., Yan, K., & Verlaan, M.  
1809 (2020). A High-Resolution Global Dataset of Extreme Sea Levels, Tides, and Storm Surges, Including  
1810 Future Projections. *Frontiers in Marine Science*, 7. <https://doi.org/10.3389/fmars.2020.00263>

1811 Perrette, M., & Mengel, M. (submitted 2024). Relative sea level projections constrained by historical  
1812 trends at tide gauge sites.

1813 Righi, M., Andela, B., Eyring, V., Lauer, A., Predoi, V., Schlund, M., Vegas-Regidor, J., Bock, L., Brötz, B., de  
1814 Mora, L., Diblen, F., Dreyer, L., Drost, N., Earnshaw, P., Hassler, B., Koldunov, N., Little, B., Loosveldt  
1815 Tomas, S., & Zimmermann, K. (2020). Earth System Model Evaluation Tool (ESMValTool) v2.0 –  
1816 technical overview. *Geoscientific Model Development*, 13(3), 1179–1199.  
1817 <https://doi.org/10.5194/gmd-13-1179-2020>

1818 Ruosteenoja, K., Jylhä, K., Räisänen, J., & Mäkelä, A. (2017). Surface air relative humidities spuriously  
1819 exceeding 100% in CMIP5 model output and their impact on future projections. *JGR Atmospheres*,  
1820 122(18), 9557–9568. <https://doi.org/10.1002/2017JD026909>

1821 Ruosteenoja, K., Jylhä, K., Räisänen, J., & Mäkelä, A. (2018). Reply to comment by genthon et al. On

1822 “surface air relative humidities spuriously exceeding 100% in CMIP5 model output and their impact  
1823 on future projections.” *Journal of Geophysical Research*, 123(16), 8728–8734.  
1824 <https://doi.org/10.1029/2018jd028680>

1825 Schupfner, M., Wieners, K.-H., Wachsmann, F., Steger, C., Bittner, M., Jungclaus, J., Früh, B., Pankatz, K.,  
1826 Giorgetta, M., Reick, C., Legutke, S., Esch, M., Gayler, V., Haak, H., de Vrese, P., Raddatz, T.,  
1827 Mauritsen, T., von Storch, J.-S., Behrens, J., ... Roeckner, E. (2019). DKRZ MPI-ESM1.2-HR model  
1828 output prepared for CMIP6 ScenarioMIP [Dataset]. Earth System Grid Federation.  
1829 <https://doi.org/10.22033/ESGF/CMIP6.2450>

1830 Séférian, R., Berthet, S., Yool, A., Palmiéri, J., Bopp, L., Tagliabue, A., Kwiatkowski, L., Aumont, O.,  
1831 Christian, J., Dunne, J., Gehlen, M., Ilyina, T., John, J. G., Li, H., Long, M. C., Luo, J. Y., Nakano, H.,  
1832 Romanou, A., Schwinger, J., ... Yamamoto, A. (2020). Tracking Improvement in Simulated Marine  
1833 Biogeochemistry Between CMIP5 and CMIP6. *Current Climate Change Reports*, 6(3), 95–119.  
1834 <https://doi.org/10.1007/s40641-020-00160-0>

1835 Sellar, A. A., Jones, C. G., Mulcahy, J. P., Tang, Y., Yool, A., Wiltshire, A., O’Connor, F. M., Stringer, M.,  
1836 Hill, R., Palmieri, J., Woodward, S., Mora, L., Kuhlbrodt, T., Rumbold, S. T., Kelley, D. I., Ellis, R.,  
1837 Johnson, C. E., Walton, J., Abraham, N. L., ... Zerroukat, M. (2019). UKESM1: Description and  
1838 evaluation of the U.k. earth system model. *Journal of Advances in Modeling Earth Systems*, 11(12),  
1839 4513–4558. <https://doi.org/10.1029/2019ms001739>

1840 Shiogama, H., Fujimori, S., Hasegawa, T., Hayashi, M., Hirabayashi, Y., Ogura, T., Iizumi, T., Takahashi, K.,  
1841 & Takemura, T. (2023). Important distinctiveness of SSP3–7.0 for use in impact assessments. *Nature*  
1842 *Climate Change*, 13(12), 1276–1278. <https://doi.org/10.1038/s41558-023-01883-2>

1843 Sobel, A. H., Lee, C.-Y., Bowen, S. G., Camargo, S. J., Cane, M. A., Clement, A., Fosu, B., Hart, M., Reed, K.  
1844 A., Seager, R., & Tippett, M. K. (2021). Near-term tropical cyclone risk and coupled Earth system  
1845 model biases. *Proceedings of the National Academy of Sciences of the United States of America*,

1846 120(33), e2209631120. <https://doi.org/10.1073/pnas.2209631120>

1847 Sobel, A. H., Lee, C.-Y., Camargo, S. J., Mandli, K. T., Emanuel, K. A., Mukhopadhyay, P., & Mahakur, M.  
1848 (2019). Tropical Cyclone Hazard to Mumbai in the Recent Historical Climate. *Monthly Weather*  
1849 *Review*, 147(7), 2355–2366. <https://doi.org/10.1175/MWR-D-18-0419.1>

1850 Stewart, K. D., Kim, W. M., Urakawa, S., Hogg, A. M., Yeager, S., Tsujino, H., Nakano, H., Kiss, A. E., &  
1851 Danabasoglu, G. (2020). JRA55-do-based repeat year forcing datasets for driving ocean–sea-ice  
1852 models. *Ocean Modelling*, 147, 101557. <https://doi.org/10.1016/j.ocemod.2019.101557>

1853 Switanek, M. B., Troch, P. A., Castro, C. L., Leuprecht, A., Chang, H.-I., Mukherjee, R., & Demaria, E. M. C.  
1854 (2017). Scaled distribution mapping: a bias correction method that preserves raw climate model  
1855 projected changes. *Hydrology and Earth System Sciences*, 21(6), 2649–2666.  
1856 <https://doi.org/10.5194/hess-21-2649-2017>

1857 Tagliabue, A., Kwiatkowski, L., Bopp, L., Butenschön, M., Cheung, W., Lengaigne, M., & Vialard, J. (2021).  
1858 Persistent Uncertainties in Ocean Net Primary Production Climate Change Projections at Regional  
1859 Scales Raise Challenges for Assessing Impacts on Ecosystem Services. *Frontiers in Climate*, 3.  
1860 <https://doi.org/10.3389/fclim.2021.738224>

1861 Tang, Y., Rumbold, S., Ellis, R., Kelley, D., Mulcahy, J., Sellar, A., Walton, J., & Jones, C. (2019). MOHC  
1862 UKESM1.0-LL model output prepared for CMIP6 CMIP [Dataset]. Earth System Grid Federation.  
1863 <https://doi.org/10.22033/ESGF/CMIP6.1569>

1864 Themeßl, M. J., Gobiet, A., & Heinrich, G. (2012). Empirical-statistical downscaling and error correction  
1865 of regional climate models and its impact on the climate change signal. *Climatic Change*, 112(2),  
1866 449–468. <https://doi.org/10.1007/s10584-011-0224-4>

1867 Thrasher, B., Maurer, E. P., McKellar, C., & Duffy, P. B. (2012). Technical Note: Bias correcting climate  
1868 model simulated daily temperature extremes with quantile mapping. *Hydrology and Earth System*  
1869 *Sciences*, 16(9), 3309–3314. <https://doi.org/10.5194/hess-16-3309-2012>

1870 Tippett, M. K., Camargo, S. J., & Sobel, A. H. (2011). A Poisson Regression Index for Tropical Cyclone  
1871 Genesis and the Role of Large-Scale Vorticity in Genesis. *Journal of Climate*, 24(9), 2335–2357.  
1872 <https://doi.org/10.1175/2010JCLI3811.1>

1873 Treu, S., Muis, S., Dangendorf, S., Wahl, T., Oelsmann, J., Heinicke, S., Frieler, K., & Mengel, M. (2023).  
1874 Reconstruction of hourly coastal water levels and counterfactuals without sea level rise for impact  
1875 attribution. In *Earth System Science Data Discussions*. <https://doi.org/10.5194/essd-2023-112>

1876 Tsujino, H., Urakawa, L. S., Griffies, S. M., Danabasoglu, G., Adcroft, A. J., Amaral, A. E., Arsouze, T.,  
1877 Bentsen, M., Bernardello, R., Böning, C. W., Bozec, A., Chassignet, E. P., Danilov, S., Dussin, R.,  
1878 Exarchou, E., Fogli, P. G., Fox-Kemper, B., Guo, C., Ilicak, M., ... Yu, Z. (2020). Evaluation of global  
1879 ocean–sea-ice model simulations based on the experimental protocols of the Ocean Model  
1880 Intercomparison Project phase 2 (OMIP-2). *Geoscientific Model Development*, 13(8), 3643–3708.  
1881 <https://doi.org/10.5194/gmd-13-3643-2020>

1882 Weedon, G. P., Gomes, S., Viterbo, P., Österle, H., Adam, J. C., Bellouin, N., Boucher, O., & Best, M.  
1883 (2010). The watch forcing data 1958-2001: a meteorological forcing data set for land surface- and  
1884 hydrological-models. 41. [https://publications.pik-potsdam.de/pubman/item/item\\_16400](https://publications.pik-potsdam.de/pubman/item/item_16400)

1885 Woodworth-Jefcoats, P. (2022). therMizer-FishMIP-2022-HI: Code and data for FishMIP 2022 ISIMIP 3a -  
1886 Hawaii longline fishing ground regional model. Github. [https://github.com/pwoodworth-](https://github.com/pwoodworth-jefcoats/therMizer-FishMIP-2022-HI)  
1887 [jefcoats/therMizer-FishMIP-2022-HI](https://github.com/pwoodworth-jefcoats/therMizer-FishMIP-2022-HI)

1888 Yukimoto, S., Kawai, H., Koshiro, T., Oshima, N., Yoshida, K., Urakawa, S., Tsujino, H., Deushi, M., Tanaka,  
1889 T., Hosaka, M., Yabu, S., Yoshimura, H., Shindo, E., Mizuta, R., Obata, A., Adachi, Y., & Ishii, M.  
1890 (2019). The Meteorological Research Institute Earth System Model Version 2.0, MRI-ESM2.0:  
1891 Description and Basic Evaluation of the Physical Component. *Journal of the Meteorological Society*  
1892 of Japan. Ser. II, 97(5), 931–965. <https://doi.org/10.2151/jmsj.2019-051>

1893 Yukimoto, S., Koshiro, T., Kawai, H., Oshima, N., Yoshida, K., Urakawa, S., Tsujino, H., Deushi, M., Tanaka,

1894 T., Hosaka, M., Yoshimura, H., Shindo, E., Mizuta, R., Ishii, M., Obata, A., & Adachi, Y. (2019a). MRI  
1895 MRI-ESM2.0 model output prepared for CMIP6 CMIP [Dataset]. Earth System Grid Federation.  
1896 <https://doi.org/10.22033/ESGF/CMIP6.621>

1897 Yukimoto, S., Koshiro, T., Kawai, H., Oshima, N., Yoshida, K., Urakawa, S., Tsujino, H., Deushi, M., Tanaka,  
1898 T., Hosaka, M., Yoshimura, H., Shindo, E., Mizuta, R., Ishii, M., Obata, A., & Adachi, Y. (2019b). MRI  
1899 MRI-ESM2.0 model output prepared for CMIP6 ScenarioMIP [Dataset]. Earth System Grid  
1900 Federation. <https://doi.org/10.22033/ESGF/CMIP6.638>

1901 Zhu, L., Quiring, S. M., & Emanuel, K. A. (2013). Estimating tropical cyclone precipitation risk in Texas.  
1902 *Geophysical Research Letters*, 40(23), 6225–6230. <https://doi.org/10.1002/2013gl058284>

1903 ISIMIP data repository: ISIMIP [data set], <https://data.isimip.org/>, last access: 28 April 2025.  
1904 ISIMIP Input data table: ISIMIP [data set], [https://www.isimip.org/gettingstarted/input-data-bias-  
1905 adjustment/](https://www.isimip.org/gettingstarted/input-data-bias-adjustment/), last access: 28 April 2025.  
1906 ISIMIP terms of use: <https://www.isimip.org/gettingstarted/terms-of-use/>, last access: 28 April  
1907 2025.  
1908